1. INTRODUCTION

1.1 Free Radical Polymerization

The free radical polymerization process consists of a sequence of three steps: initiation, propagation, and termination. The initiation step is considered to proceed via two reactions. The first is the production of free radicals. The usual case is the homolytic dissociation of an initiator or a catalyst *I* to yield a pair of radicals $R\bullet$

$$I \xrightarrow{k_d} 2R\bullet \tag{1.1}$$

where k_d is the rate constant for the catalyst dissociation. The second part of the initiation involves the addition of this radical to the first monomer molecule to produce the chain initiating species $M_1\bullet$

$$R_1\bullet + M \xrightarrow{k_i} M_1\bullet \tag{1.2}$$

where M represents a monomer molecule and k_i is the rate constant for the initiation step (Eq. 1.2). For the polymerization of $CH_2=CHY$, Eq. 1.2 takes the form

$$R\bullet + CH_2 = CHY \longrightarrow R - CH_2 - CHY\bullet \tag{1.3}$$

(The radical $R\bullet$ is often referred to as an initiator radical or a primary radical.)

The propagation consists of the growth of $M_1\bullet$ by the successive additions of large numbers (hundreds, and perhaps, thousands) of monomer molecules. Each addition creates a new radical which has the same identity as the previous one, except that it is larger by one monomer unit. The successive additions may be represented by

$$M_1 \bullet + M \xrightarrow{k_p} M_2 \bullet \tag{1.3}$$

$$M_2 \bullet + M \xrightarrow{k_p} M_3 \bullet \tag{1.4}$$

$$M_3 \bullet + M \xrightarrow{k_p} M_4 \bullet \tag{1.5}$$

etc., etc.

or in general terms

$$M_n \bullet + M \xrightarrow{k_p} M_{n+1} \bullet \tag{1.6}$$

where k_p is the rate constant for propagation. Propagation with growth of the chain to high polymer proportions takes place very rapidly. The value of k_p for most monomers is in the range 10^2-10^4 liter/mole-sec.

At some point, the propagation polymer chain stops growing and terminates. The termination with the annihilation of the radical centers occurs by bimolecular reaction between radicals. Two radicals react with each other by *combination* (*coupling* (k_{tc})),

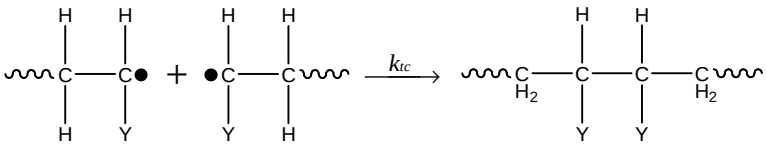

(1.7)

or, more rarely, by *disproportionation* in which a hydrogen radical that is *beta* to a radical center is transferred to another radical center (k_{td}). This results in the formation of two polymer molecules-one saturated and one unsaturated.

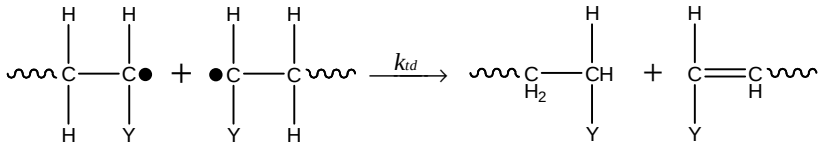

(1.8)

Termination can also occur by a combination of coupling and disproportionation. The two different modes of termination can be represented in general terms by

$$M_n\bullet + M_m\bullet \xrightarrow{k_{tc}} M_{n+m} \tag{1.9}$$

$$M_n\bullet + M_m\bullet \xrightarrow{k_{td}} M_n + M_m \tag{1.10}$$

where k_{tc} and k_{td} are the rate constants for termination by coupling and disproportionation, respectively. One can also express the termination step by

$$M_n\bullet + M_m\bullet \xrightarrow{k_t} \text{dead polymer} \tag{1.11}$$

where the particular mode of termination is not specified

$$k_t = k_{tc} + k_{td} \tag{1.12}$$

The term *dead polymer* signifies the cessation of growth for the propagating radical. The propagation reaction would proceed indefinitely until all the monomers in a reaction system are exhausted. Typical termination rate constants are in the range of 10^6-10^8 liter/mole-sec or orders of magnitude greater than the propagation rate constants. The much greater value of k_t (whether k_{tc} or k_{td}) compared to k_p does not prevent propagation because the radical species are present in very low concentrations and because the polymerization rate is dependent on only the one-half power of k_t.

1.2. Free Radical Polymerization Kinetics

When the reaction kinetics is considered, the rate of initiation (υ_i) according to the initiation reaction may be given as

$$\upsilon_i = 2fk_d[I] \tag{1.13}$$

where f, k_d and I denote the initiator efficiency, the rate constant for the decomposition of the initiator, and the concentration of the initiator, respectively. The initiator efficiency factor is used since all the generated free radicals are not able to initiate polymer growth. Sometimes recombination between radicals may take place. Initiator efficiency may take values between zero and one.

The rate of termination (υ_t) is a bimolecular process so that

$$\upsilon_t = 2k_t[M^\bullet]^2 \tag{1.14}$$

where k_t and M stand for the termination rate constant and the concentration of the monomer respectively. The rate constant $2k_t$ is actually ($k_{tc} + k_{td}$).

According to the steady state approximation, the initiation is relatively small but continuous. The termination speeds up as the active radical concentration builds and the

termination removes (kills) active radicals. Therefore it is an excellent approximation to assume that rate of initiation of radicals is equal to the rate of termination of radicals.

$$\upsilon_i = \upsilon_t \tag{1.15}$$

$$2 f k_d [I] = 2 k_t [M^\bullet]^2 \tag{1.16}$$

$$[M^\bullet] = \left(\frac{f k_d [I]}{k_t} \right)^{1/2} \tag{1.17}$$

Thus, rate of propagation (υ_p) may be given as

$$\upsilon_p = k_p [M][M^\bullet] = k_p [M] \left(\frac{f k_d [I]}{k_t} \right)^{1/2} \tag{1.18}$$

where k_p stands for the propagation rate constant. In the derivation of polymerization rate, the propagation (k_p) and termination (k_t) rate coefficients are assumed to be chain length and conversion independent [1, 2].

The overall homopolymerization rate constant, k, is based on the kinetic expression for homopolymerization [3]

$$R_p = k[I]^{1/2}[M] \tag{1.19}$$

Then, the expression for k is

$$k = \frac{k_p}{k_t^{1/2}} (f k_d)^{1/2} \tag{1.20}$$

1.3. Experimental Behavior of the Monomers Modeled

The relationship between the monomer structure and the reactivity was investigated extensively by Decker et al. using several model monofunctional acrylates with various pendant groups ranging from cyclic carbonates and oxazolidones to dioxolanes and oxetanes [4-8]. Each of these modified acrylates exhibited much greater polymerization rates than observed for conventional alkyl acrylates. Three pathways for the enhanced reactivity of these monoacrylates have been hypothesized; they include hydrogen abstraction and subsequent chain transfer, hydrogen bonding, and electronic and resonance effects. Decker et al. first proposed a highly efficient hydrogen abstraction mechanism and subsequent chain transfer reaction to account for the increased reactivity and cross-linked polymer formation [9].

Introduction of a heteroatom into the α-position of acrylates is known to influence the polymerization behavior of the monomer. An electronegative heteroatom is known to withdraw a singlet electron from the propagating radical inductively and to stabilize the propagating radicals. The polymerization of α-hydroxymethylacrylate (MHMA = M1) is known to be under the influence of chain transfer to monomer, however MHMA is more successful for producing high molecular weight polymers than methyl methacrylate (MMA) [14,15]. In industry, the most favoured monomers include 2-hydoxyethyl methacrylate (EHMA = M2) and acrylate – both can provide hydrophilicity, crosslinking sites and/or functionality for subsequent reaction. EHMA is of interest because of its potential as a functional monomer in coatings and it has been used previously as a precursor to a number of ‘hindered’ acrylic monomers via reactions with the hydroxy groups [16]. Another factor that attracted industry is its unusual reactivity in catalytic chain transfer polymerization.

The monomers tabulated in Table 1.1 are modeled in order to understand the effect of the structure and substituents on their polymerizability behavior.

Table 1.1 Monomers modeled

No	Structure	Name	R_p (mol $L^{-1}s^{-1}$)	Dipole (Debye)	Reference
M1	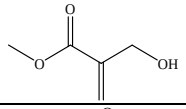	Methyl (α -hydroxymethyl) acrylate	3.70E-02	2.97	[10]
M2	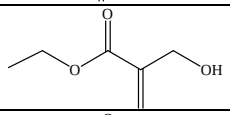	Ethyl (α -hydroxymethyl) acrylate	3.00E-02	3.23	[10, 11]
M3	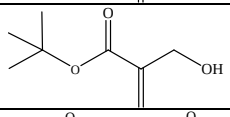	t-Butyl (α -hydroxymethyl) acrylate	1.60E-02	3.30	[11]
M4	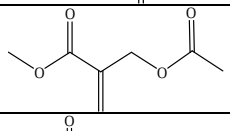	Methyl α-acetoxymethyl acrylate	2.42E-01	1.88	[12]
M5	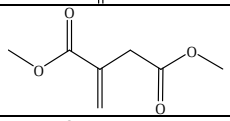	Dimethyl itaconate-methacrylic acid	8.67E-03	1.46	[12]
M6	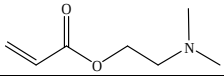	2-(dimethylamino) ethyl acrylate	1.04	2.01	[13]
M7	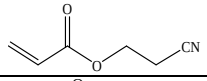	2-(cyano)ethyl acrylate	13.9	3.70	[13]
M8	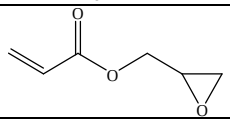	2,3-epoxypropyl acrylate	4.11	2.59	[13]
M9	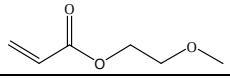	2-(methoxy) ethyl acrylate	2.67	2.50	[13]

During the polymerization of M1 and M2, the viscosity of a polymerizing solution increases rapidly, and this may autoaccelerate the polymerization due to gel effect [17]. Gel effect (also called as Tromsdorff Effect, Norrish-Smith Effect or autoacceleration) only occurs during polymerizations with high concentrations of monomer (i. e., little or no solvent). The reaction proceeds normally for a while, and then suddenly the rate of polymerization goes up dramatically. The molecular weight of chains that grow during the accelerated period is substantially higher than that of the chains that grew earlier. To explain the effect, it is important to note that initiation, propagation, and termination are completely different chemical reactions with different responses to conditions. Termination involves the reaction between two chain ends. However, in concentrated solutions, the viscosity of the reaction, mixture becomes high as the polymer chains form. This high viscosity hinders the diffusion of chains because of entanglements, so the rate of

termination slows considerably. However, viscosity hardly affects the diffusion of small molecular monomers, therefore propagation proceeds as before. Furthermore, initiator continues to add more free radicals to the system. The rates of initiation and propagation come out of balance. What was once a low, steady state concentration of radicals gives way to increasing concentration. The conversion is rapid and the molecular weight is high because chains grow without termination [1]. The electronic effect of hydroxymethyl ester group is clearly important in facilitating polymerization. This effect can overcome even the steric effect of an acrylic t-butyl ester group (TBHMA = M3). T-butyl α-alkyloxymethylacrylates do not give high molecular weight polymers [18]. On the other hand, t-butyl α-acetoxymethylacrylate gives higher molecular weight when polymerized under identical conditions. It is clear that better polymerizability occurs for monomers with ester attached to the α-methyl group (methyl α-acetoxymethylacrylate = M4).

The steric factors do not seem to be the only reason for reduced termination since methyl α-isopropoxymethylacrylate has essentially the same three dimensional shape around the vinyl group as α-acetoxymethylacrylate (Figure 1.1), yet the ether-linked monomer does not give high molecular weight [19, 20].

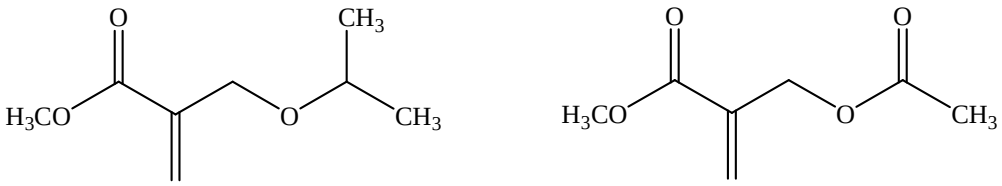

(a) (b)

Figure 1.1 Monomer structures of (a) methyl α-isopropoxymethyl acrylate and (b) methyl α-acetoxymethyl acrylate

The dialkyl esters of itaconic acid can be radically polymerized to relatively high molar mass polymers. The molar masses of the resulting polymers were, however; significantly lower than those obtainable from the structurally similar esters of methacrylic acid. The polymerization rate, R_p, increases with increasing length of the alkyl groups and suggested that degradative chain transfer to monomer could be the cause of this trend. As there is less chain transfer to monomer with increasing size of alkyl substituent, the rate of

polymerization increases with the increasing length of the ester substituent. It was shown that the rate constant of propagation, k_p, and termination k_t, both decrease when going from dimethyl itaconate (DMI = M5) to di-2-ethylhexyl itaconate (D2EHI) (Figure 1.2) but that the k_t for DMI was 590 times higher than that of D2EHI, whereas the value of k_p was only 3.3 times higher [21].

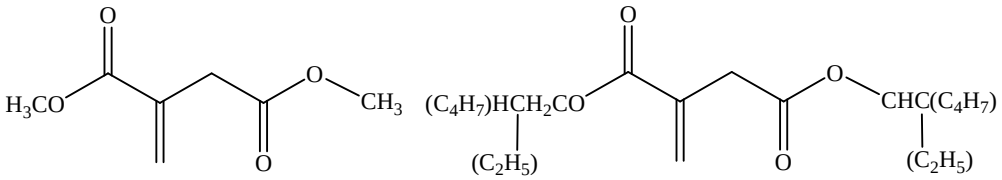

Figure 1.2 Monomer structures of (a) dimethyl itaconate (DMI = M5), (b) di-2-ethylhexyl itaconate (D2EHI)

These decreases in the rate constants are believed to result from steric hindrance as the size of the ester group increases. The influence of steric hindrance is felt more strongly during termination, when two tertiary carbon radicals must approach one another, than during propagation when tertiary carbon atom reacts with a primary one. This results in an increase in the overall rate constant, k, with increasing size of the alkyl group.

The monomers which make hydrogen bonding exhibite 3-6 times higher polymerization rates compared to their non-hydrogen bonding analogues possessing ester and carbonate groups [22]. Furthermore, hydrogen bonding will increase the overall viscosity of the bulk monomer solution. Thus, hindering radical termination causes an increase in radical concentration. This increase in radical concentration increases the polymerization rate.

Finally, electronic and resonance effects may also have an impact on the reactivity of these monoacrylate monomers (M6 and M7). Jansen et al. have reported that the polymerization rate increases as the dipole moment increas [23]. However, this consequence is possible when the overall dipole moment of the solution exceeds a threshold value of 3.5 D (M6, M7, M8, and M9).

2. AIM OF THE STUDY

The aim of this work is to understand the relationship between the structure of the monomers and their polymerizability behavior by using the quantum chemical tools.

The factors which play an important role in the polymerization of acrylates will be discussed by modeling the experimentally synthesized and polymerized compounds.

Another task of this study is to identify the relationship between the propagation, chain transfer and disproportionation reactions in order to predict the polymerization behavior of the acrylates.

3. METHODOLOGY

All the geometry optimizations have been carried out by using the density functional theory (B3LYP/6-31G*) [24, 25]. Harmonic frequencies have been computed in order to identify the stationary points as minima (with all real frequencies) or transition states (with only one imaginary frequency) and to obtain thermal energy and entropy contributions. All radicals and transition states have been treated with the spin-unrestricted formalism. All computations have been carried out by using the Gaussian 98 program [26].

The energetic results are reported as the change in the electronic energy at 298 K (ΔE_{298}), sum of the electronic energy and zero point energy at 298 K ($\Delta E_{298+ZPE}$).

The reaction rate constants are calculated by using the conventional Transition State Theory (TST) [27, 28]. In the conventional TST formalism, the zero point energy contributions are included by direct addition to the energies on the minimum potential energy surface [29, 30]. Such formalism preassumes that, contributions of the zero point energies added to the electronic energies do not vary the position of the maxima along the zero point energy contributions of the stationary points [31]. The rate constant in the conventional TST is given by

$$k(T) = Ae^{-\Delta G^{\neq}/RT} \tag{3.1}$$

Since $\Delta G^{\neq} = \Delta H^{\neq} - T\Delta S^{\neq}$

$$k(T) = Ae^{-(\Delta H^{\neq} - T\Delta S^{\neq})/RT} \tag{3.2}$$

where

$$k(T) = Ae^{\Delta S^{\neq}/R} e^{-\Delta H^{\neq}/RT} \tag{3.3}$$

and the rate expression for the reaction $A + B \rightarrow C$ may be written as

$$k(T) = \frac{k_B T}{h} \frac{q_{TS}}{q_A q_B} e^{-\Delta E_0 / RT} \tag{3.4}$$

where k_B represents Boltzman's constant, T is the temperature, h is the Planck's constant, ΔE_0 represents the molecular energy difference between the activated complex and the reactants (with inclusion of zero point vibrational energies), and q_{TS}, q_A and q_B are the molecular partition functions of the transition state and reactants, respectively. Effects of tunneling on the rate constants are neglected. The activation energies, ΔE_0, are calculated at 298 K. The partition functions are obtained from the Gaussian output and are evaluated at 298 K.

The activation energy can be calculated as the difference between the energy of the transition state and the reactants.

The rate constant may be expressed in terms of the partition functions of the reactants and the transition states. Applying basic statistical thermodynamic principles and the classical TST formula, the overall rate constant may be obtained as

$$k = \frac{k_B T}{h} \frac{q_{TS}}{q_A q_B} e^{-[E_{TS} - (E_A + E_B)]/RT} \tag{3.5}$$

3.1 Density Functional Theory

The DFT functional used is the Becke 3-parameter-Lee-Yang-Parr exchange-correlation functional (B3LYP) [32, 33] as implemented in the Gaussian 98 package. This functional has been successfully applied to the radical addition reactions to the unsaturated carbon atom and hydrogen abstraction reactions [34-39].

The density functional theory is based on the Kohn-Hohenberg theorems proposed in 1964 [40, 41]. The first theorem states that the electron density $\rho(r)$ determines the external potential $v(r)$, i. e. the potential due to the nuclei. The second theorem introduces the variational principle. Hence, the electron density can be computed variationally and the

position of nuclei, energy, wave function and other related parameters can be calculated [40, 41].

The electron density is defined as:

$$\rho(x) = N\int\ldots\int|\Psi(x_1, x_2, \ldots x_n)|^2 dx_1 dx_2 \ldots dx_n \tag{3.11}$$

where x represents both spin and spatial coordinates of electrons.

The electronic energy can be expressed as a functional of the electron density:

$$E[\rho] = \int v(r)\rho(r)dr + T[\rho] + V_{ee}[\rho] \tag{3.12}$$

where $T[\rho]$ is the kinetic energy of the interacting electrons and $V_{ee}[\rho]$ is the interelectronic interaction energy. The electronic energy may be rewritten as

$$E[\rho] = \int v(r)\rho(r)dr + T_s[\rho] + J[\rho] + E_{xc}[\rho] \tag{3.13}$$

with $J[\rho]$ being the coulomb energy, $T_s[\rho]$ being the kinetic energy of the non-interacting electrons and $E_{xc}[\rho]$ being the exchange-correlation energy functional. The exchange-correlation functional is expressed as the sum of an exchange functional $E_x[\rho]$ and a correlation functional $E_c[\rho]$, although it contains also a kinetic energy term arising from the kinetic energy difference between the interacting and non-interacting electron systems. The kinetic energy term, being the measure of the freedom, and exchange-correlation energy, describing the change of opposite spin electrons (defining extra freedom to an electron), are the favorable energy contributions. The Coulomb energy term describes the unfavorable electron-electron repulsion energy and therefore disfavors the total electronic energy [42].

In Kohn-Sham density functional theory, a reference system of independent non-interacting electrons in a common, one-body potential V_{KS} yielding the same density as the real fully-interacting system is considered. More specifically, a set of independent

reference orbitals ψ_i satisfying the following independent particle Schrödinger equation are imagined.

$$\left[-\frac{1}{2}\nabla^2 + V_{KS}\right]\psi_i = \varepsilon_i\psi_i \tag{3.14}$$

with the one-body potential V_{KS} defined as

$$V_{KS} = v(r) + \frac{\partial J[\rho]}{\partial \rho(r)} + \frac{\partial E_{xc}[\rho]}{\partial \rho(r)} \tag{3.15}$$

$$V_{KS} = v(r) + \frac{\rho(r')}{|r - r'|}dr' + v_{xc}(r) \tag{3.16}$$

where $v_{xc}(r)$ is the exchange-correlation potential. The independent orbitals ψ_i are known as Kohn-Sham orbitals and give the exact density by

$$\rho(r) = \sum_i^N |\psi_i|^2 \tag{3.17}$$

if the exact form of the exchange-correlation functional is known. However, the exact form of this functional is not known and approximate forms are developed starting with the local density approximation (LDA). This approximation gives the energy of a uniform electron gas, i. e. a large number of electrons uniformly spread out in a cube accompanied with a uniform distribution of the positive charge to make the system neutral. The energy expression is

$$E[\rho] = T_s[\rho] + \int \rho(r)v(r)dr + J[\rho] + E_{xc}[\rho] + E_b \tag{3.18}$$

where E_b is the electrostatic energy of the positive background. Since the positive charge density is the negative of the electron density due to uniform distribution of particles, the energy expression is reduced to

$$E[\rho] = T_s[\rho] + E_{xc}[\rho] \tag{3.19}$$

$$E[\rho] = T_s[\rho] + E_x[\rho] + E_c[\rho] \tag{3.20}$$

The kinetic energy functional can be written as

$$T_s[\rho] = C_F \int \rho(r)^{5/3} dr \tag{3.21}$$

where C_F is a constant equal to 2.8712. The exchange functional is given by

$$E_x[\rho] = -C_x \int \rho(r)^{4/3} dr \tag{3.22}$$

with C_x being a constant equal to 0.7386. The correlation energy, $E_c[\rho]$, for a homogeneous electron gas comes from the parametrization of the results of a set of quantum Monte Carlo calculations.

The LDA method underestimates the exchange energy by about 10 per cent and does not have the correct asymptotic behavior. The exact asymptotic behavior of the exchange energy density of any finite many-electron system is given by

$$\lim_{x\to\infty} U_x^{\sigma} = -\frac{1}{r} \tag{3.23}$$

U_x^{σ} being related to $E_x[\rho]$ by

$$E_x[\rho] = \frac{1}{2}\sum_{\sigma} \int \rho_{\sigma} U_x^{\sigma} dr \tag{3.24}$$

A gradient-corrected functional is proposed by Becke

$$E_x = E_x^{LDA} - \beta \sum_{\sigma} \int \rho_{\sigma}^{4/3} \frac{x_{\sigma}^2}{1 + 6\beta x_{\sigma} \sinh^{-1} x_{\sigma}} dr \tag{3.25}$$

where σ denotes the electron spin, $x_\sigma = \frac{|\nabla \rho_\sigma|}{\rho_\sigma^{4/3}}$ and β is an empirical constant (β=0.0042). This functional is known as Becke88 (B88) functional [43].

The adiabatic connection formula connects the non-interacting Kohn-Sham reference system (λ=0) to the fully-interacting real system (λ=1) and is given by

$$E_{xc} = \int_0^1 U_{xc}^{\lambda} d\lambda \tag{3.26}$$

where λ is the interelectronic coupling-strength parameter and U_{xc}^{λ} is the potential energy of exchange-correlation at intermediate coupling strength. The adiabatic connection formula can be approximated by

$$E_{xc} = \frac{1}{2} E_x^{exact} + \frac{1}{2} U_{xc}^{LDA} \tag{3.27}$$

since $U_{xc}^{0} = E_x^{exact}$, the exact exchange energy of the Slater determinant of the Kohn-Sham orbitals, and $U_{xc}^{1} = U_{xc}^{LDA}$ [44].

The closed shell Lee-Yang-Parr (LYP) correlation functional [45] is given by

$$E_c = -a \int \frac{1}{1 + d\rho^{-1/3}} \left\{ \rho + b\rho^{-2/3} \left[C_F \rho^{5/3} - 2t_w + \left(\frac{1}{9} t_w + \frac{1}{18} \nabla^2 \rho \right) \right] e^{-c\rho^{-1/3}} \right\} dr \tag{3.28}$$

where

$$t_w = \frac{1}{8} \frac{|\nabla \rho(r)|^2}{\rho(r)} - \frac{1}{8} \nabla^2 \rho \tag{3.29}$$

The mixing of LDA, B88, E_x^{exact} and the gradient-corrected correlation functionals to give the hybrid functionals [46] involves three parameters.

$$E_{xc} = E_{xc}^{LDA} + a_0\left(E_x^{exact} - E_x^{LDA}\right) + a_x \Delta E_x^{B88} + a_c \Delta E_c^{non-local} \quad (3.30)$$

where ΔE_x^{B88} is the Becke's gradient correction to the exchange functional. In the B3LYP functional, the gradient-correction ($\Delta E_c^{non-local}$) to the correlation functional is included in LYP. However, LYP contains also a local correlation term which must be subtracted to yield the correction term only.

$$\Delta E_c^{non-local} = E_c^{LYP} - E_c^{VWN} \quad (3.31)$$

where E_c^{VWN} is the Vosko-Wilk-Nusair correlation functional, a parametrized form of the LDA correlation energy based on Monte Carlo calculations. The empirical coefficients are a_0=0.20, a_x=0.72 and a_c=0.81 [47].

3.2 Basis Set

It has been shown in the literature that the 6-31G* basis set may be used in conjunction with the B3LYP method in order to obtain the activation barriers for the radical addition to the double bond [48]. In the present study, the 6-31G* basis set is used in the determination of the structural parameters of acrylates, and the reactions of polymerization.

For the first row atoms, the 6-31G* basis set describes the core orbitals by a combination of six primitive Gaussian functions and the valence shell is split into two orbitals consisting of three and one primitive Gaussian functions. This set is augmented by a set of diffuse functions and a set of d orbitals. For the hydrogen atoms, this basis set uses two sets of s orbitals containing three and one primitive Gaussian functions, and a set of p orbitals.

3.3. Local Softness and Hardness Based Reactivity Descriptors

The concepts of chemical hardness (η) and its inverse, the chemical softness (S) were introduced by Pearson [49] in the early sixties when comparing the stabilities of reaction products of Lewis acid-base reactions. On the basis of these data, a classification of Lewis acids and bases as hard and soft were presented in terms of polarizability, easiness to oxidize, etc. Pearson then formulated his famous hard and soft acids and bases (HSAB) principle stating that the hard acids prefer to interact with hard bases and similarly for soft acids and soft bases [49-51].

3.3.1. Global Hardness and Softness

Parr and Pearson first provided the analytical definition of global hardness of any chemical species as

$$\eta = \left(\frac{\partial^2 E}{\partial N^2} \right)_{v(r)} = \left(\frac{\partial \mu}{\partial N} \right)_{v(r)} \tag{3.32}$$

where E is the total energy, N is the number of electrons of the chemical species and μ is the chemical potential, which is identified as the negative of the electronegativity (χ).

The corresponding global softness is expressed as

$$S = \frac{1}{2\eta} = \left(\frac{\partial^2 N}{\partial E^2} \right)_{v(r)} = \left(\frac{\partial N}{\partial \mu} \right)_{v(r)} \tag{3.33}$$

By applying the finite difference approximation to equation 3.32, the operational definition of η and S can be obtained as

$$\eta = \frac{IP - EA}{2} \tag{3.34}$$

$$S = \frac{1}{IP - EA} \tag{3.35}$$

where *IP* and *EA* are the ionization potential and electron affinity of the chemical species.

According to Koopman's theorem, the ionization energy is simply the orbital energy of the HOMO, with change in sign. For spin paired molecules, the electron affinity is the negative of the orbital energy of the LUMO.

3.3.2. Local Softness and Fukui Functions

The local softness $s(r)$ can be defined as

$$s(r) = \left(\frac{\partial \rho(r)}{\partial \mu} \right)_{v(r)} \tag{3.36}$$

so that

$$\int s(r) dr = S \tag{3.37}$$

Combining Equations 3.36 and 3.33, s(r) can be written as

$$s(r) = \left(\frac{\partial \rho(r)}{\partial N} \right)_{v(r)} \left(\frac{\partial N}{\partial \mu} \right)_{v(r)} = f(r) S = \left(\frac{\partial \mu}{\partial v(r)} \right)_{N} S \tag{3.38}$$

where $f(r)$ is defined as as the Fukui function. Local softness contains the same information as Fukui functions (Eqn. 3.38) plus additional information about the total molecular softness. Therefore either the Fukui function or local softness can be used in studies of intramolecular reactivity sequences (i. e., relative site reactivity in a molecule). But only s(r) (not $f(r)$) should be a better descriptor of the global reactivity with respect to a reaction partner with a given hardness (or softness), as stated in the HSAB principle.

As $\rho(r)$ is a discontinuous function of *N*, three types of $f(r)$ can be defined which, when multiplied by *S*, result in three different local softness. Within a finite difference approximation the condensed form of these three local softness for any particular atom (*k*) can be written as

$$s_k^{+} = [\rho_k(N_0+1) - \rho_k(N_0)]S \tag{3.39}$$

which is suited for studies of nucleophilic attack.

$$s_k^{-} = [\rho_k(N_0) - \rho_k(N_0-1)]S \tag{3.40}$$

which is suited for studies of electrophilic attack.

$$s_k^{0} = \frac{1}{2}[\rho_k(N_0+1) - \rho_k(N_0-1)]S \tag{3.41}$$

which is suited for studies of radical attack.

Here, $\rho_k(N_0)$ represents the electronic population (Mulliken) on atom *k* for the N_0 electron system.

4. RESULTS AND DISCUSSION

4.1. The Effect of Pendant Groups Size on the Polymerization Rate

Photoinitiated polymerization of acrylates and methacrylates is one of the most efficient processes for the rapid production of polymeric cross-linked materials with defined properties. This efficiency is the reason why photoinitiated polymerization is widely employed in applications where emphasis is put on the mechanical as well as optical properties of the material. These applications are typically dental restorative fillers, fiber-optic coatings, optical adhesives, aspherical lenses for CD applications, and contact lenses [13]. α - (hydroxymethyl) acrylate (HMA) derivatives show fast polymerizations both alone, and in the presence of acrylate or methacrylate crosslinkers [10]. Alkyl (α-hydroxylmethyl) acrylates (RHMA) derivatives give faster photopolymerization rates than typical methacrylates [52]. In this study, the free radical polymerizability of a series of alkyl (α-hydroxylmethyl) methacrylates (MHMA, EHMA, and TBHMA) is investigated in an attempt to analyze in detail the effects exerted by the bulky groups on the polymerizability (Table 4.1.). The experimental photopolymerization behavior of various alkyl (α-hydroxylmethyl) methacrylates is shown in Table 4.2. The monomer itself is used as the attacking radical to model the propagation, the chain transfer, and the disproportionation reactions. After locating all the ground state and transition state geometries on the potential energy surface, the kinetic parameters are evaluated. The overall polymerization rate coefficient ($k_p/k_d^{½}$) is used to compare the polymerization behavior of the monomers under study.

Table 4.1. α-(hydroxylmethyl) acrylate monomers modeled.

No	Structure	Name
M1	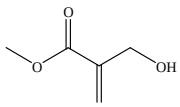	Methyl (α-hydroxymethyl)acrylate (MHMA)
M2	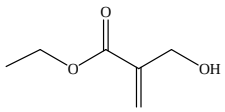	Ethyl (α-hydroxymethyl)acrylate (EHMA)
M3	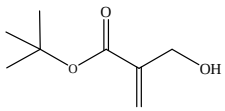	t-Butyl (α-hydroxymethyl)acrylate (TBHMA)

Table 4.2. Photopolymerization results for monomers M1, M2 and M3

Monomer	R_p (mol L^{-1} s^{-1})	Dipole (Debye)	Reference
M1	3.70E-02	2.97	[10]
M2	3.00E-02	3.23	[10, 11]
M3	1.60E-02	3.3	[11]

4.1.1 3D-structures of MHMA, EHMA, and TBHMA

The numbering system used in alkyl (α-hydroxymethyl) acrylates is shown in Figures 4.1. – 4.3.

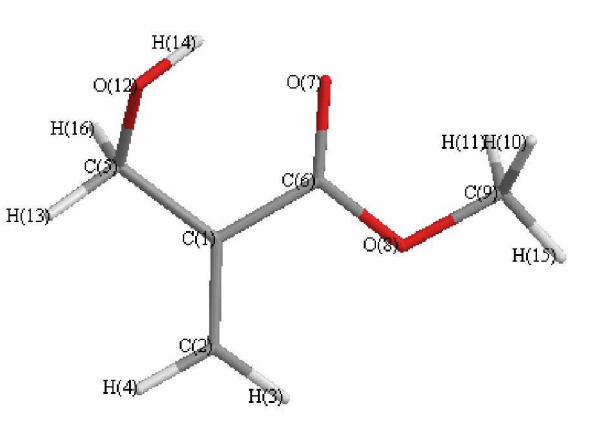

Figure 4.1. Numbering system used for MHMA

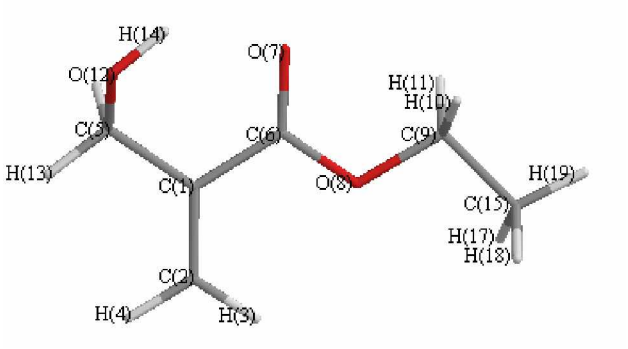

Figure 4.2. Numbering system of used for EHMA

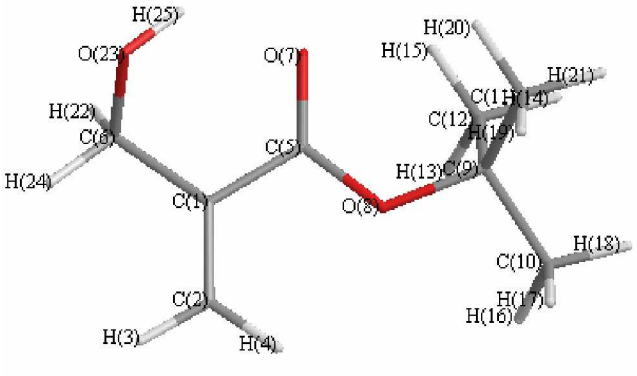

Figure 4.3. Numbering system used for TBHMA

In alkyl (α-hydroxymethyl)acrylates there is free rotation around the C_1-C_6 and C_6-O_8 bonds (C_1-C_5 and C_5-C_8 bonds for TBHMA) and various conformers exist. Based on B3LYP/6-31G* calculations, the anti conformer with respect to C1-C6 (C1-C5 for TBHMA) bond is more stable than the syn conformer (Table 4.3). Two factors have to be considered in analyzing the conformers of RHMA derivatives. The first one is the hydrogen-bond between the –OH group and O_7. The energy difference between linear-MHMA and anti-MHMA is 1.83kcal/mol. Therefore the monomer structure prefers to have an intramolecular H-bond. The second factor of importance is the electron delocalization between the double bonds C_2-C_1 and the C_6-O_7 (C_5-C_7 for the TBHMA) bonds. There are two H-bond possibilities in the monomer structure. One of them is in the anti-MHMA between –OH and O_7 and the other one is in syn-MHMA between –OH and O_8. Figure 4.5 and Figure 4.6 illustrate these different geometries. The energy difference between these

two structures is 1.33kcal/mol in favor of anti-MHMA. Table 4.3 illustrates the relative energies of the conformers of MHMA, EHMA, and TBHMA. EHMA and TBHMA show the same qualitative trend with MHMA and the most stable conformer is the anti conformer for these monomers.

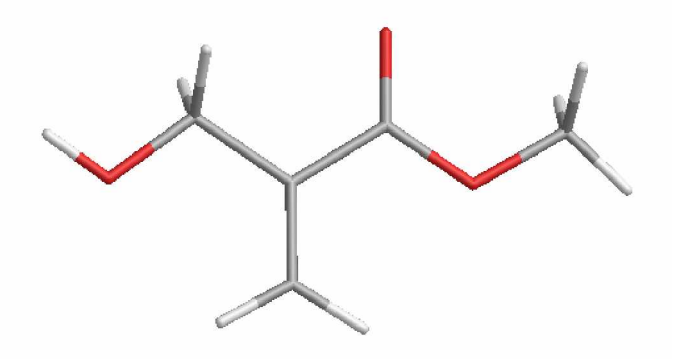

Figure 4.4. The linear structure of MHMA (linear-MHMA)

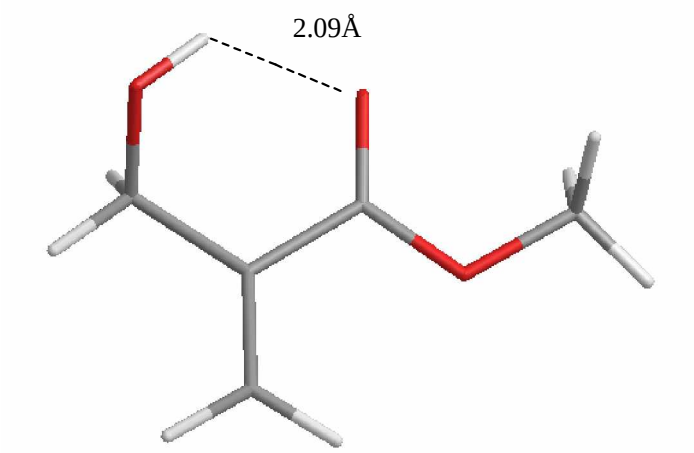

Figure 4.5. The intramolecular H-bonding of MHMA (anti-MHMA)

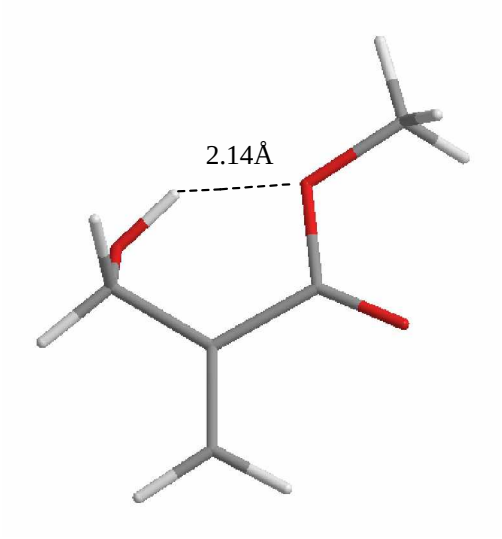

Figure 4.6. The intramolecular H-bonding of MHMA (syn-MHMA)

Table 4.3. Relative energies (kcal/mol) for the conformers of MHMA, EHMA, and TBHMA

Monomer	**MHMA**	**EHMA**	**TBHMA**
anti	0.00	0.00	0.00
syn	1.33	1.38	1.33
planar	1.83	1.9	1.99

Table 4.4. Internal coordinates of monomers M1-M3.

Internal Coordinates	**Monomer**		
	M1	**M2**	**M3**
$H_{14}O_{12}C_5C_1(H_{25}O_{23}C_6C_1)^*$	61.97	61.56	61.75
$O_{12}C_5C_1C_2\,(O_{23}C_6C_1C_2)^*$	123.18	123.04	122.68
$C_2C_1C_6O_7\,(C_2C_1C_5O_7)^*$	-174.81	-174.24	-174.98
$O_7C_6O_8C_9\,(O_7C_5O_8C_9)^*$	-1.10	1.35	1.78
$C_6O_8C_9C_{15}\,(C_5O_8C_9C_{10})^*$	-	-180	179
$H_{14}....O_7\,(H_{25}....O_7)^{**}$	2.085 Å	2.077 Å	2.071 Å

* The numbering system used for TBHMA

** Hydrogen bonding distance

The RHMA monomers prefer to be planar except for the –OH moiety. This group prefers to be out of plane as seen from the dihedral angle $O_{12}C_5C_1C_2$ which is 123.18˚ (Table 4.4).

4.1.2. Methyl radical addition to the monomer

The methyl radical is used as the attacking radical to understand the side on which the C-C double bond of the monomer is being attacked. Schematic representation of the methyl addition reaction is given in Figure 4.7.

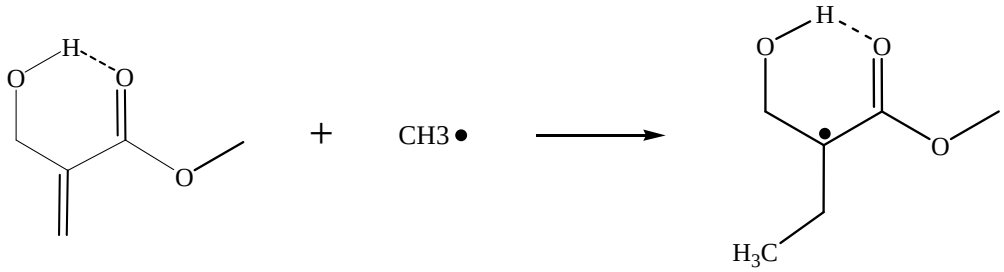

Figure 4.7. Schematic representation of the methyl addition reaction

The face which possesses the –OH group of the monomer is named as the α-face and the other face is the β face. Figures 4.8-4.10 show the way the methyl radical attacks the monomers **M1**, **M2**, and **M3** (α versus β faces).

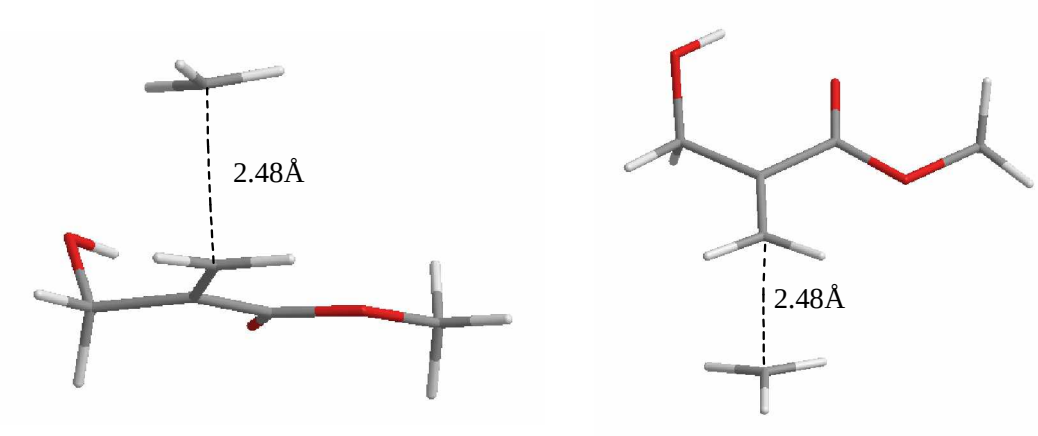

Figure 4.8. Radical addition to **M1** from the α and β faces

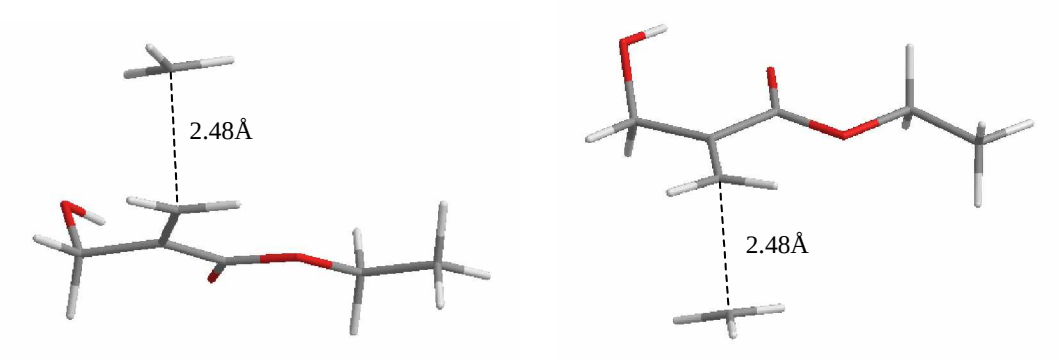

Figure 4.9. Radical addition to **M2** from the α and β faces

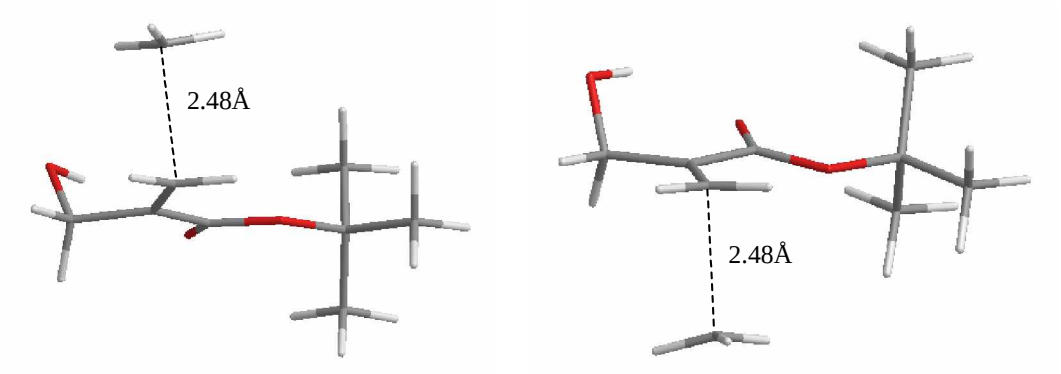

Figure 4.10. Radical addition to **M3** from the α and β faces

Table 4.5. Relative energies (kcal/mol) of the radicals attacking the C-C double bond of alkyl (α-hydroxylmethyl) methacrylates from the α and β faces

	M1	**M2**	**M3**
α face	0.00	0.00	0.00
β face	0.29	0.39	0.36

B3LYP/6-31G* calculations show that the radical prefers to attack the C-C double bond of the monomer from the α face (Table 4.5). The product of methyl (CH_3) radical addition to the C-C double bond of the monomer is used as a radical for all transition state searches in this study.

4.1.3. 3D-structures of the radical derivatives of MHMA, EHMA, and TBHMA

The numbering system of the atoms of radical derivatives of the alkyl (α-hydroxylmethyl) acrylates is shown in Figures 4.11-4.13. All the dihedral angles of the radical derivative of monomers M1, M2, and M3 are given in Table 4.6.

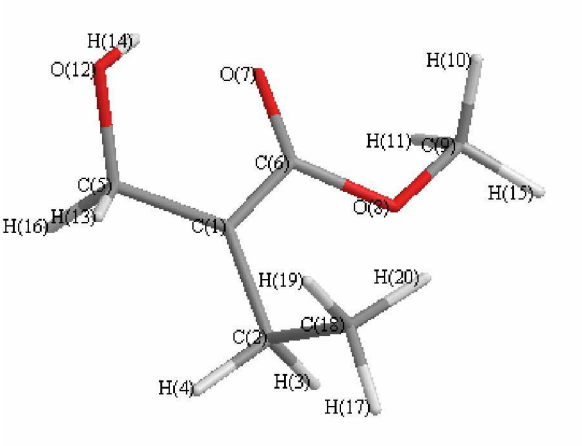

Figure 4.11. Numbering system used for the radical derivative of methyl (α-hydroxylmethyl) methacrylate (MHMA)

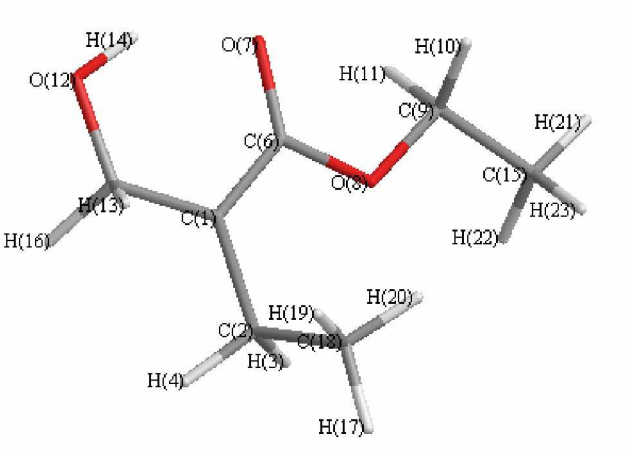

Figure 4.12. Numbering system used for the radical derivative of ethyl (α-hydroxylmethyl) methacrylate (EHMA)

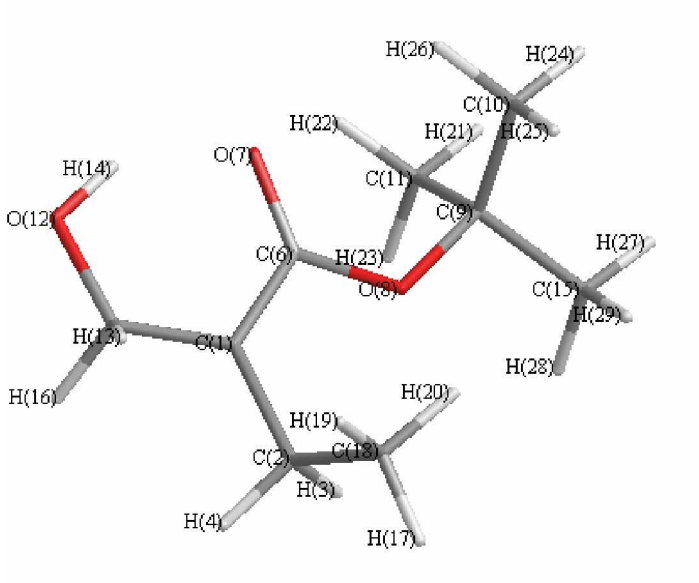

Figure 4.13. Numbering system used for the radical derivative of t-butyl (α-hydroxylmethyl) methacrylates (TBHMA)

There is a geometry change about the –OH moiety that depend on the size of the substituent on the radical. While the –OH group prefers to be out of plane in the monomers **M1**-**M3**, it prefers to be in the same plane for the radical with increasing alkyl group size (Figures from 4.11 to 4.13). On the other hand, the methyl group (-CH_3) which comes from methyl radical attached to the C-C double bond of the monomer prefers to be out of face of the radical structure as seen from the dihedral angle $C_6C_1C_2C_{18}$ to be 86.42˚ (Table 4.6).

Table 4.6. Internal coordinates for the radicals.**M1R**, **M2R** and **M3R**

Internal Coordinates	Radical		
	M1R	**M2R**	**M3R**
$H_{14}O_{12}C_5C_1$	41.82	-7.52	-8.36
$O_{12}C_5C_1C_2$	152.55	-179.59	-179.28
$C_2C_1C_6O_7$	174.52	-175.3	-175.01
$O_7C_6O_8C_9$	0.47	-0.41	-0.93
$C_6O_8C_9C_{15}$	-	-179.3	-179.5
$C_6C_1C_2C_{18}$	86.42	76.67	77.33
$\mathbf{H_{14}....O_7}^*$	1.907 Å	1.812 Å	1.803Å

*Hydrogen bonding distance.

4.1.4 Propagation reaction of M1, M2 and M3

In order to model this reaction, radical derivatives of monomers are used. Radicals are produced by attaching the methyl radical to the less substituted C-C double bond of the monomers. The radical derivatives of the monomers are used to model the transition structures (Figure 4.14).

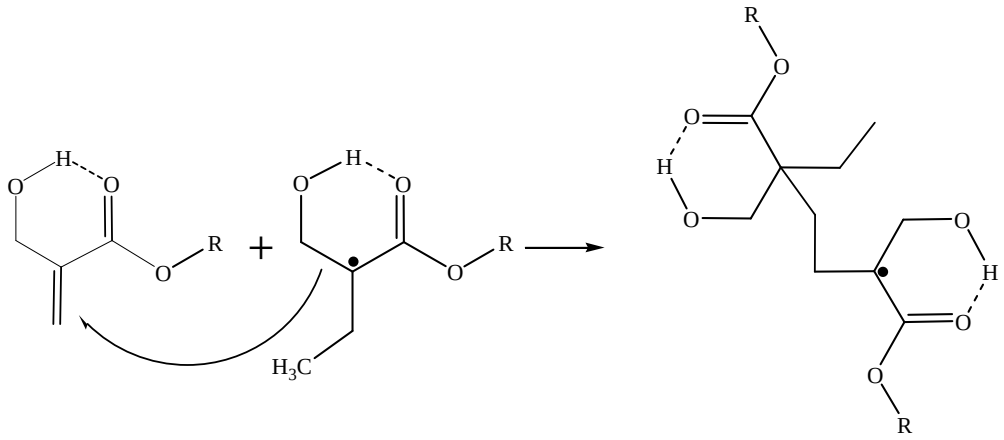

Figure 4.14. Schematic representation of the propagation reaction

Figures 4.15 – 4.17 illustrate the propagation reaction transition states of monomers **M1**, **M2**, and **M3**.

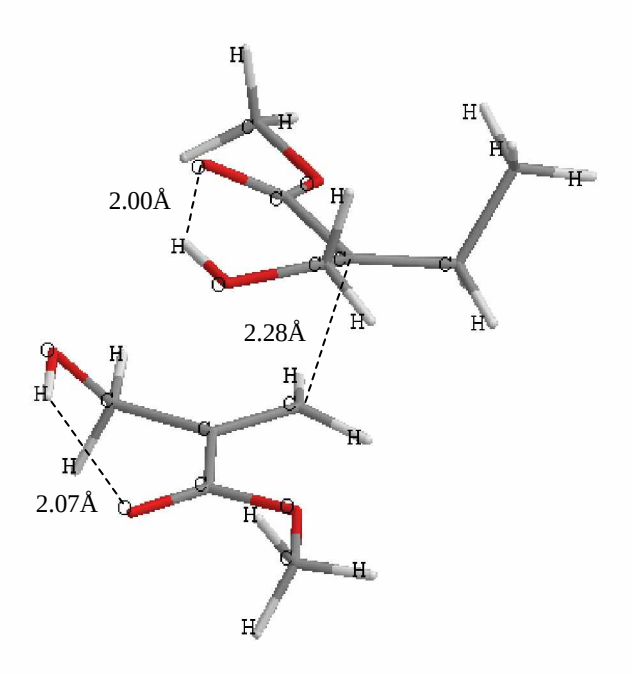

Figure 4.15. Radical addition to **M1**

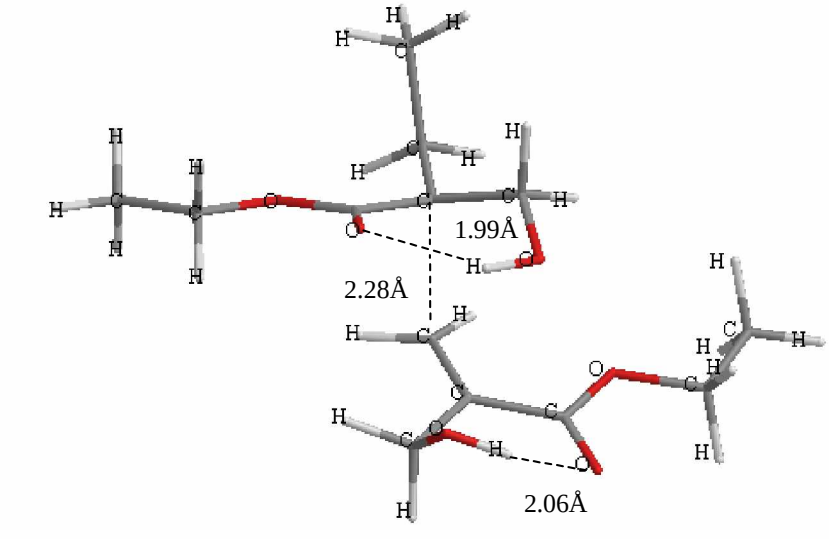

Figure 4.16. Radical addition to **M2**

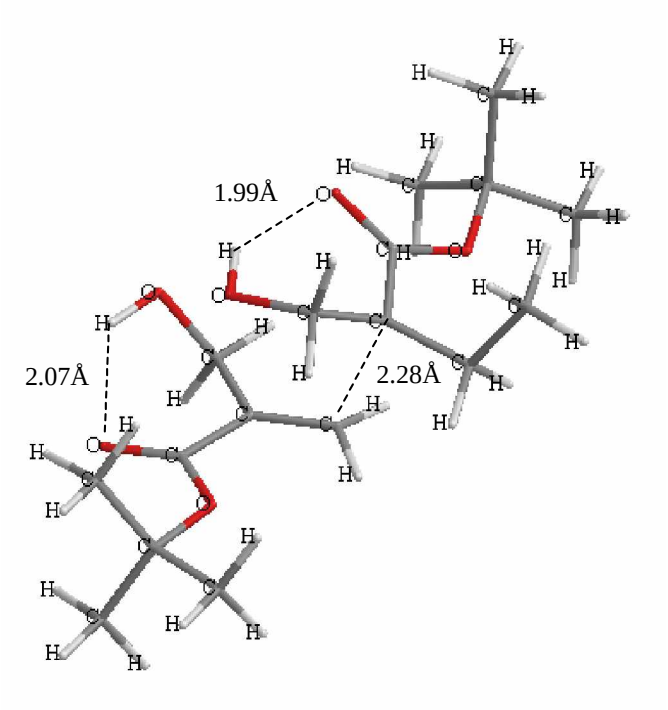

Figure 4.17. Radical addition to **M3**

4.1.5 Lability of hydrogen atoms on M1, M2 and M3 for modeling the chain transfer reaction

Monomers **M1**, **M2** and **M3** have two hydrogen atoms which can contribute to chain transfer reactions (Figure 4.18).

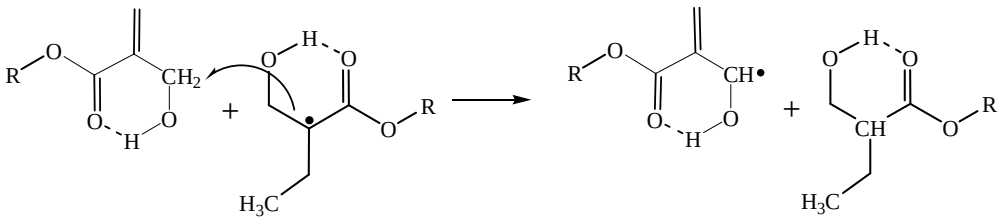

Figure 4.18. Schematic representation of the chain transfer reaction

First of all we try to understand which hydrogen atom is more labile in order to model the chain transfer reactions. Mulliken charges of labile hydrogen atoms on

monomers show that H_{16} (H_{24} for monomer **M3**) is more labile because it is positively charged (Figures 4.19 – 4.21).

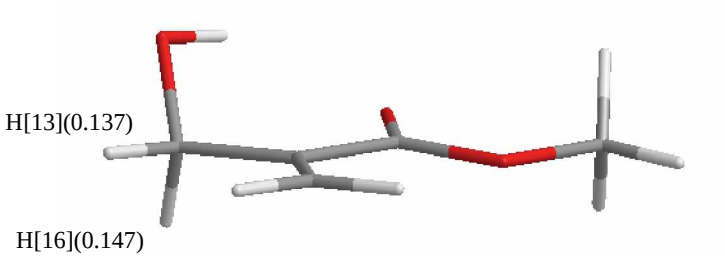

Figure 4.19. Mulliken charges of the labile hydrogen atoms on the monomer **M1**

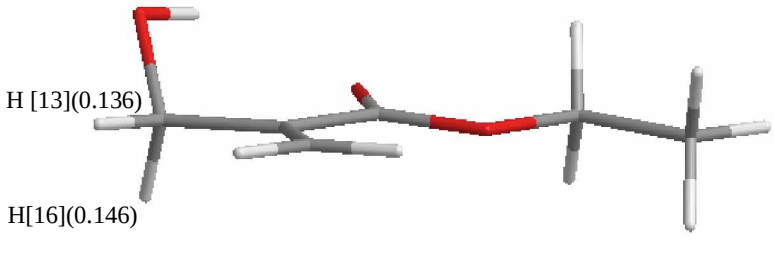

Figure 4.20. Mulliken charges of the labile hydrogen atoms on the monomer **M2**

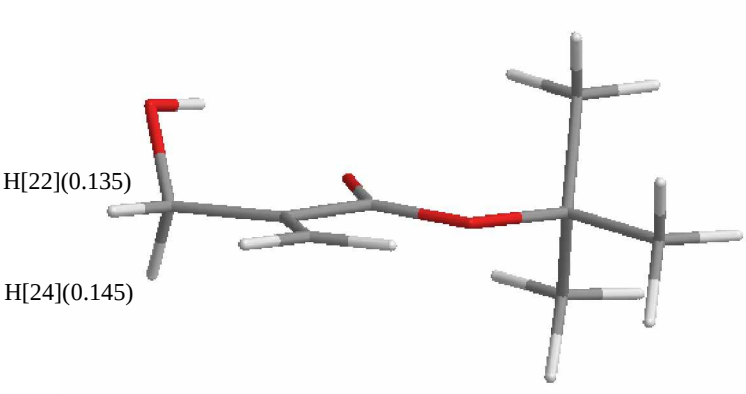

Figure 4.21. Mulliken charges of the labile hydrogen atoms on the monomer **M3**

On the other hand, hydrogen abstraction barriers show that there is no difference between abstractions of hydrogen atoms on the α-C atom of monomer (Table 4.7) because monomers show symmetry according to the monomer plane (Figures 4.22 – 4.24).

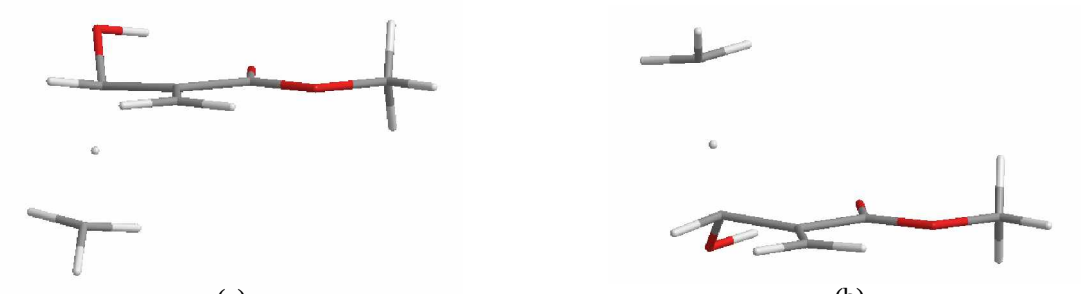

(a) (b)

Figure 4.22. Hydrogen abstraction transition state structures for **M1**

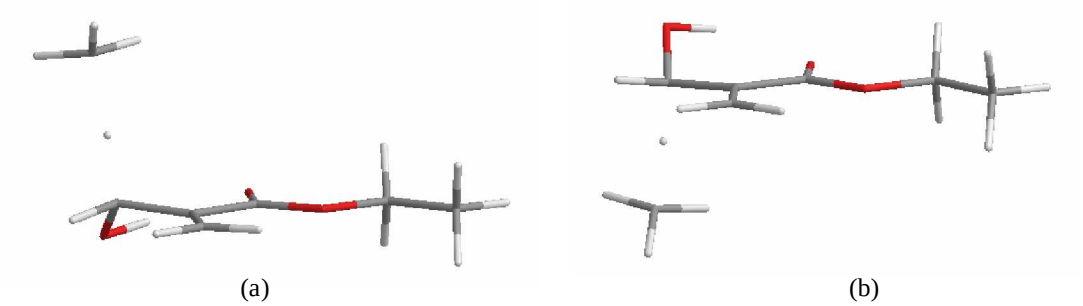

(a) (b)

Figure 4.23. Hydrogen abstraction transition state structures for **M2**

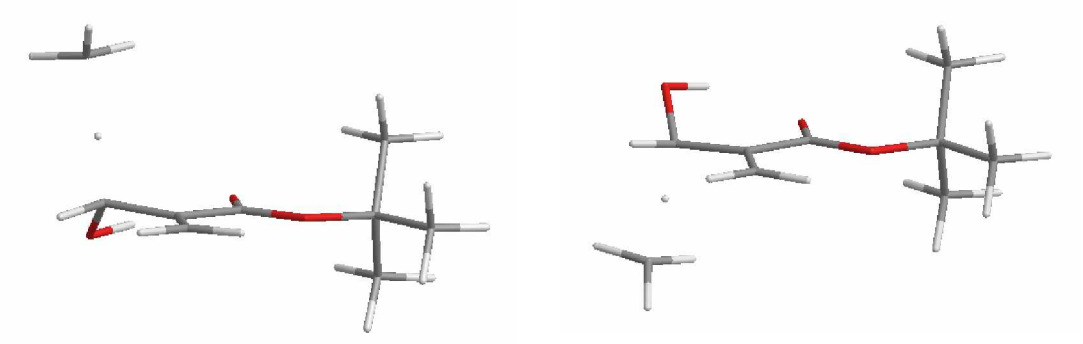

(a) (b)

Figure 4.24. Hydrogen abstraction transition state structures for **M3**

Table 4.7. Hydrogen abstraction barriers (Ea (kcal/mol)) for **M1**, **M2** and **M3**

	a	**b**
M1	4.30	4.30
M2	4.88	4.88
M3	4.88	4.88

Table 4.8. Reactivity descriptors of hydrogen atoms on the α-C atom of the monomers **M1**, **M2** and **M3**

	k	$\rho_k(N_0)$	$\rho_k(N_o+1)$	$\rho_k(N_o-1)$	S	s_k^0	$s_k^0(CH_3)-s_k^0$
M1	H_{13}	0.146973	0.082918	0.240309	4.821601	0.379438	0.998260
	H_{16}	0.137227	0.071870	0.240551	4.821601	0.406626	0.971062
M2	H_{13}	0.163834	0.141133	0.188369	4.814400	0.113706	1.263982
	H_{16}	0.136493	0.071848	0.237688	4.814400	0.399210	0.978478
M3	H_{22}	0.135370	0.073268	0.227960	4.812320	0.372214	1.005474
	H_{24}	0.145086	0.084022	0.229439	4.812320	0.349896	1.027792
CH_3	C_1	-0.48757	-0.86268	-0.05890	3.428020	1.377688	0.000000

* $\rho_k(N_0)$ represents the electronic population (Mulliken) on atom k for the N_0 electron system.

Finally we check the reactivity descriptors of monomers **M1**, **M2** and **M3**. These descriptors for the hydrogen atoms H_{13} and H_{16} (H_{22} and H_{24} for the monomer **M3**) of the monomers are tabulated in Table 4.8. There is no big difference between local descriptors of these two hydrogen atoms except atoms of monomer in **M2**. We have to take into account the activation barriers in order to calculate rate constants of polymerization reaction so we choose H_{13} (H_{22} for monomer **M3**) according to the activation barriers of hydrogen abstraction reaction by using methyl radical.

4.1.6 Chain transfer Reaction for M1, M2 and M3

After determination of the more labile hydrogen atom on the monomers for chain transfer reaction, the radical derivatives of the monomers are used to model this reaction. Figures 4.25-4.27 illustrate the hydrogen abstraction transition states of the monomers.

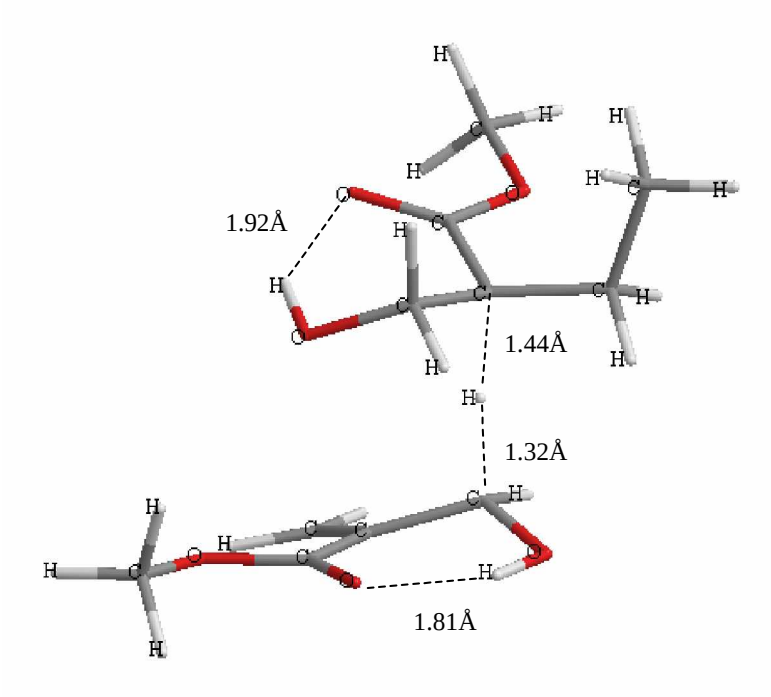

Figure 4.25. H-abstraction transition state for **M1**

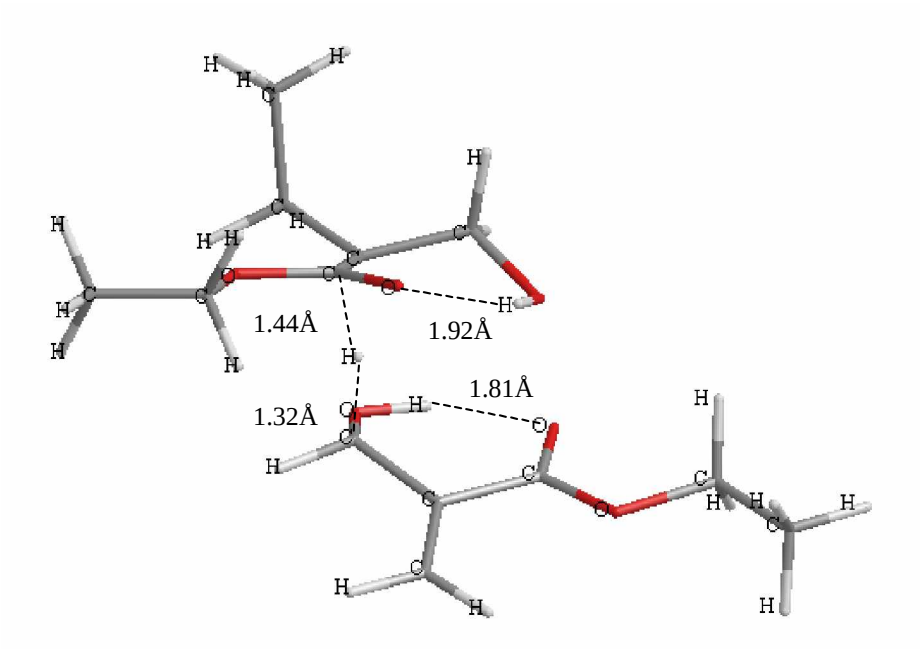

Figure 4.26. H-abstraction transition state for **M2**

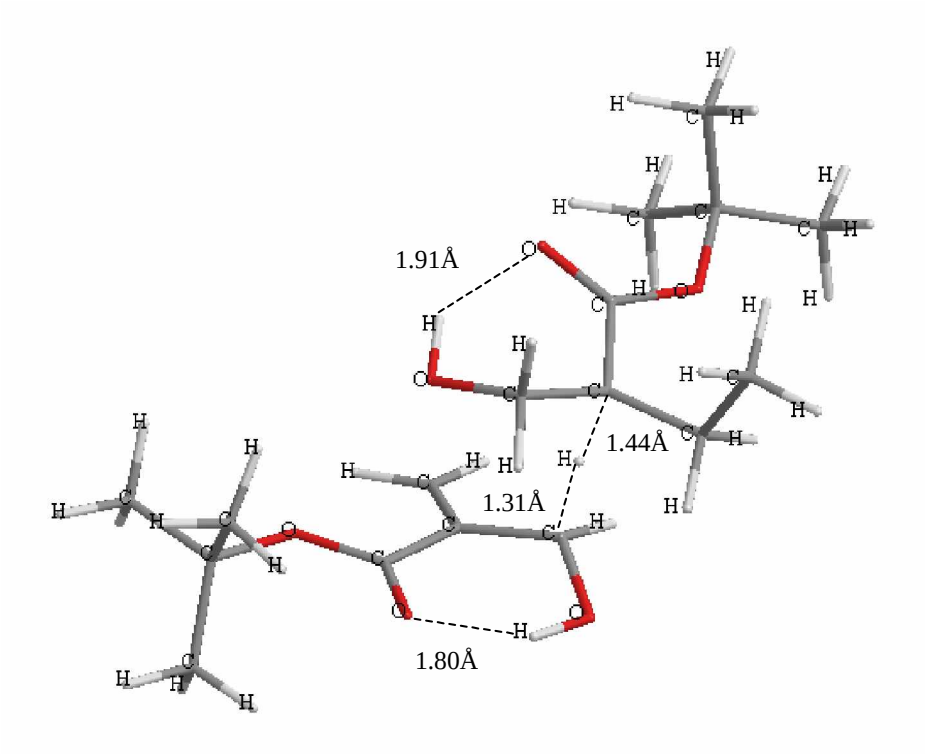

Figure 4.27. H-abstraction transition state for **M3**

4.1.7 Lability of hydrogen atoms on M1, M2 and M3 for modeling disproportionation reaction

The disproportionation reaction occurs between the atom which is on the radical center and the neighbour atom abstracting the other radical center (Figure 4.28).

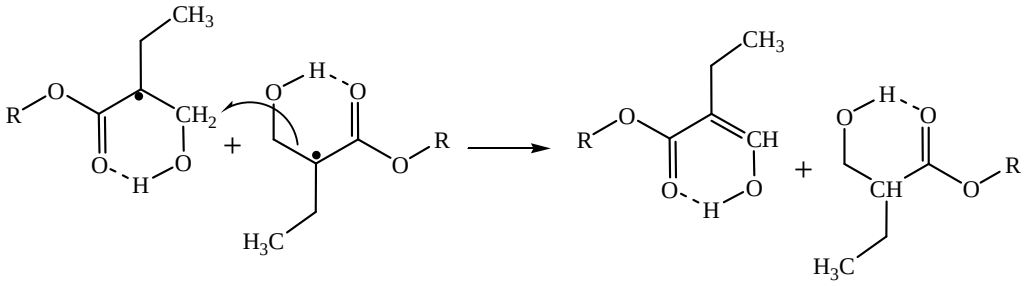

Figure 4.28. Schematic representation of the disproportionation reaction

There are four possible hydrogen atoms on the radical derivatives of alkyl α-hydroxymethyl acrylates. Figures 4.29-4.31 show the Mulliken charges of the labile hydrogen atoms of **M1R**, **M2R** and **M3R**.

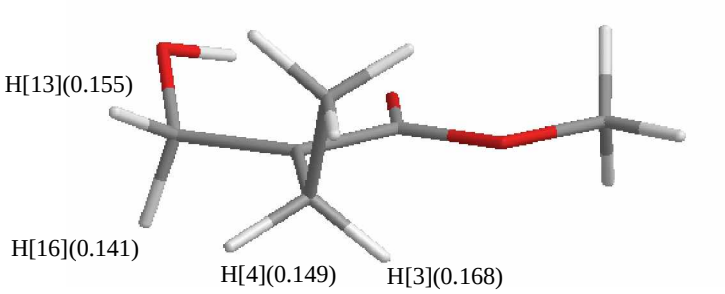

Figure 4.29. Mulliken charges of the labile hydrogen atoms on the radical **M1R**

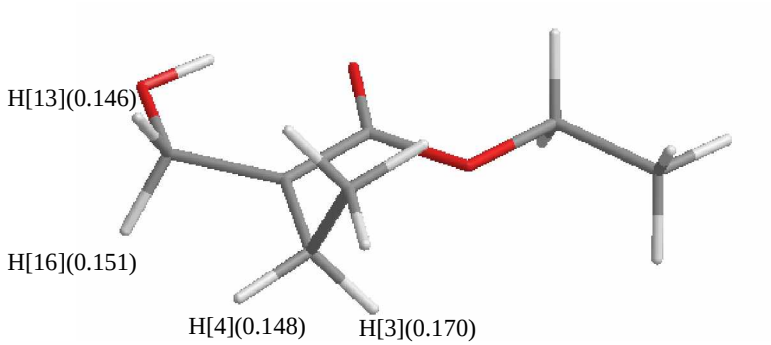

Figure 4.30. Mulliken charges of the labile hydrogen atoms on the radical **M2R**

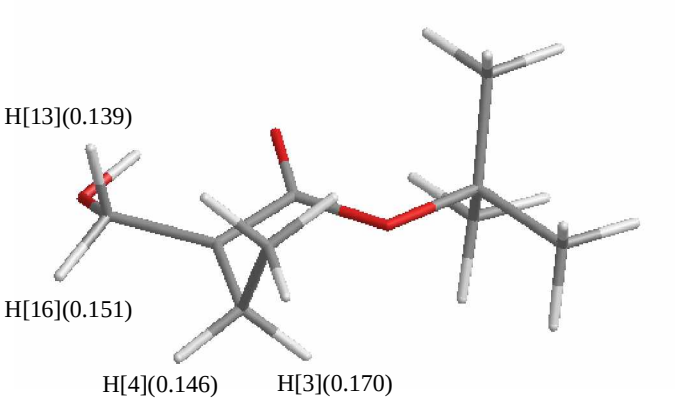

Figure 4.31. Mulliken charges of the labile hydrogen atoms on the radical **M3R**

Mulliken charges indicate that the most labile hydrogen atom on the radical derivatives of the monomers is H_3. On the other hand, hydrogen abstraction barrier by using methyl radical and reactivity descriptors for **M1R**, **M2R** and **M3R** show the most labile hydrogen atom to be H_{16} (Tables 4.9 and 4.10). Figures 4.32–4.34 illustrate hydrogen abstraction transition state structures of the radicals **M1R**, **M2R** and **M3R** for the disproportionation reaction.

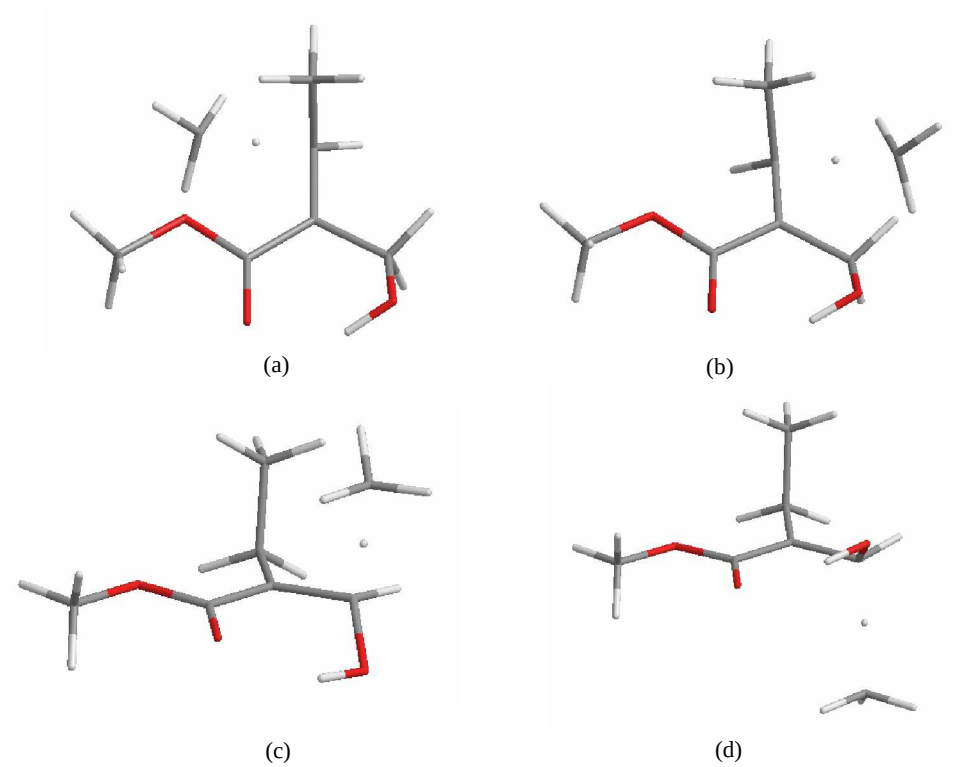

Figure 4.32. Hydrogen abstraction transition state structures of the radical **M1R** for the disproportionation reaction

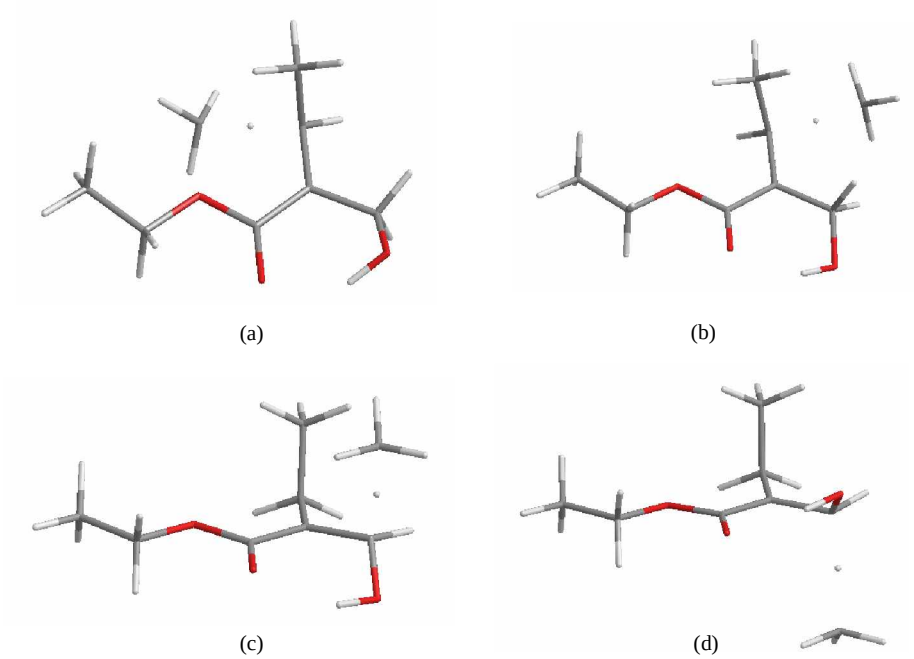

Figure 4.33. Hydrogen abstraction transition state structures of the radical **M2R** for the disproportionation reaction

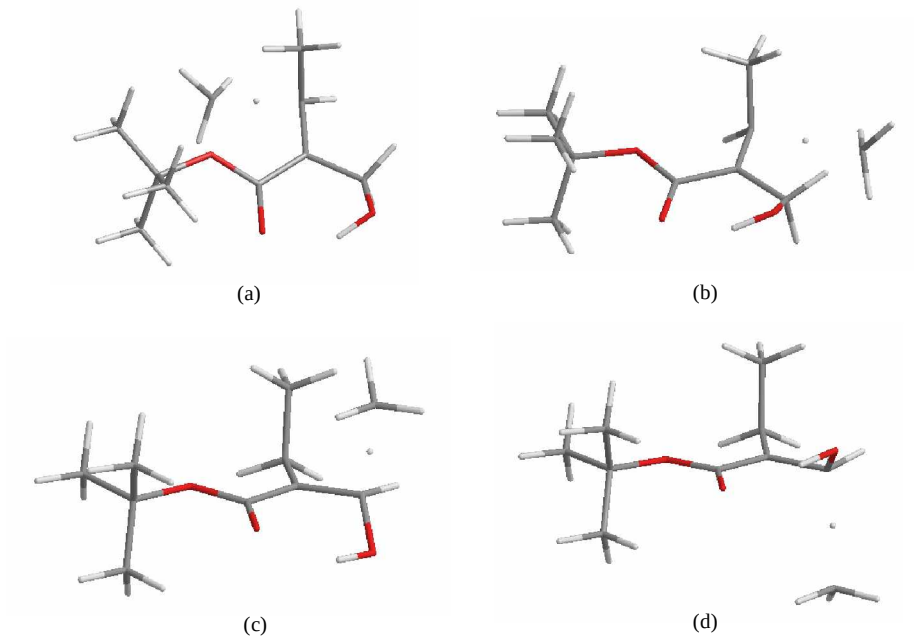

Figure 4.34. Hydrogen abstraction transition state structures of the radical **M3R** for the disproportionation reaction

Table 4.9. Hydrogen abstraction barriers (Ea (kcal/mol)) for **M1R**, **M2R** and **M3R**

	a	**b**	**c**	**d**
M1R	12.07	11.10	9.12	8.92
M2R	11.82	11.20	8.90	8.62
M3R	11.89	10.61	8.52	8.37

Table 4.10. Reactivity descriptors for **M1R**, **M2R** and **M3R**

	k	$\rho_k(N_0)$	$\rho_k(N_o+1)$	$\rho_k(N_o-1)$	S	$s_k^{\,0}$	$s_k^{\,0}(CH_3)-s_k^{\,0}$
M1R	H_3	0.167854	0.097295	0.245259	3.944462	0.291819	1.085869
	H_4	0.148685	0.067688	0.226836	3.944462	0.313877	1.063811
	H_{13}	0.154892	0.067381	0.255869	3.944462	0.371744	1.005944
	H_{16}	0.141455	0.038053	0.274729	3.944462	0.466781	0.910908
M2R	H_3	0.169751	0.097827	0.248465	3.982001	0.299921	1.077768
	H4	0.147861	0.071355	0.215582	3.982001	0.287156	1.090532
	H_{13}	0.146355	0.043542	0.278561	3.982001	0.467923	0.909765
	H_{16}	0.150643	0.047424	0.279225	3.982001	0.461516	0.916172
M3R	H_3	0.166887	0.099652	0.240249	3.993770	0.280756	1.096932
	H_4	0.148497	0.071112	0.222671	3.993770	0.302644	1.075044
	H_{13}	0.155551	0.071132	0.252422	3.993770	0.362015	1.015673
	H_{16}	0.141529	0.042536	0.268075	3.993770	0.450375	0.927313
CH_3	C_1	-0.48757	-0.86268	-0.05890	3.428020	1.377688	0.000000

* $\rho_k(N_0)$ represents the electronic population (Mulliken) on atom k for the N_0 electron system.

As a result of these calculations, H_{16} is determined as the most labile hydrogen atom in order to model the disproportionation reaction.

4.1.8 Disproportionation reaction for M1, M2 and M3

We locate transition state structures after determination which hydrogen atom is the most labile on radicals of alkyl α-hydroxymethylacrylates. Figures 4.35-4.37 show the disproportionation transition state structures for **M1**, **M2**, and **M3**.

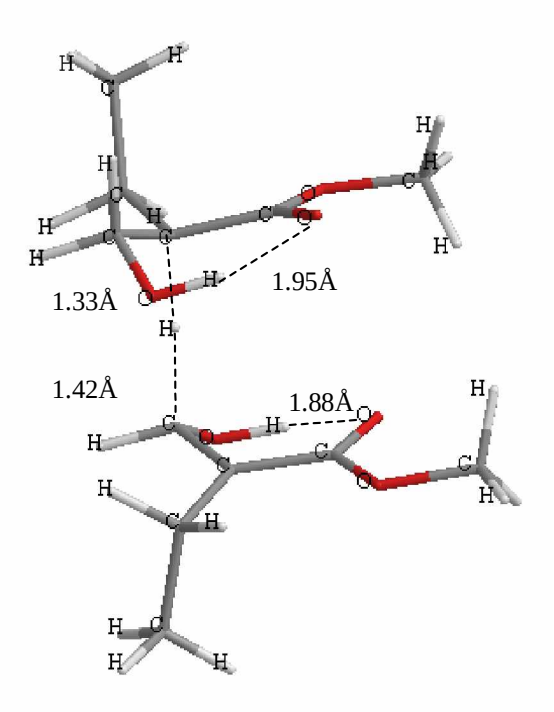

Figure 4.35. Disproportionation transition state for **M1**

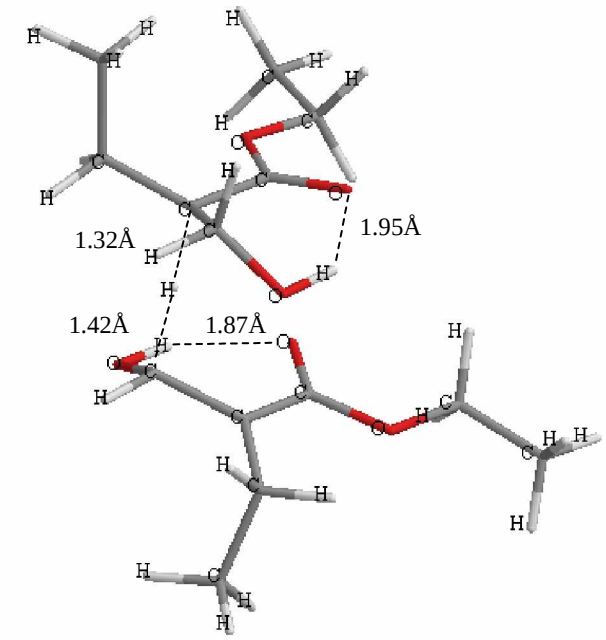

Figure 4.36. Disproportionation transition state for **M2**

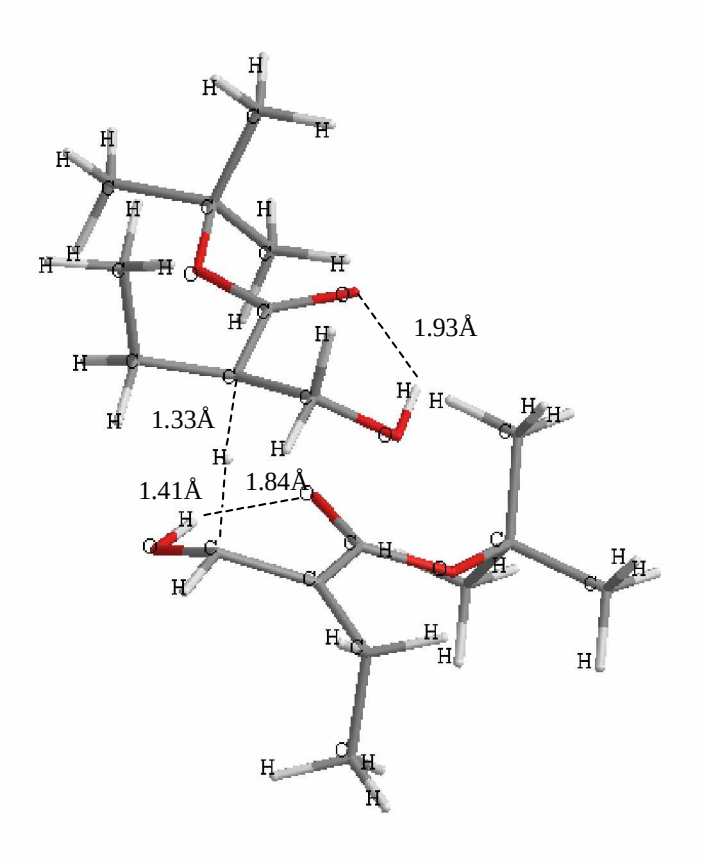

Figure 4.37. Disproportionation transition state for **M3**

Activation barriers for the addition, chain transfer and disproportionation reactions are tabulated in Table 4.11. We can see the steric effect on the activation barriers of those reactions except the monomer **M2**. The activation barriers for the three reactions of **M2** are in the undesired order. While the value of E_{a1} and E_{a2} for **M2** are higher than those of **M3**, the value of E_{a3} of **M2** is lower than that of **M1**. Energy barriers for the propagation reaction for the three monomers are lower than the energy barriers of chain transfer reaction and disproportionation reaction. These results give higher propagation rate constant than chain transfer and disproportionation rate constants. The polimerization rate constants which are calculated according to the Transition State Theory are given in Table 4.12.

Table 4.11. Activation barriers with electronic and ZPE (kcal/mol) for addition, chain transfer and disproportionation reactions

	Reactants	**E_{a1}**	**E_{a2}**	**E_{a3}**
M1	0.00	2.65	4.48	8.87
M2	0.00	3.21	5.03	8.66
M3	0.00	3.12	4.84	9.66

E_{a1} = Addition barrier

E_{a2} = Hydrogen abstraction barrier for chain transfer reaction

E_{a3} = Hydrogen abstraction barrier for disproportionation reaction

Table 4.12. Rate constants for **M1**, **M2**, and **M3**

Monomer	**k_p** **(M^{-1} s^{-1})**	**k_{ct}** **(M^{-1} s^{-1})**	**k_d** **(M^{-1} s^{-1})**	**$k_p/k_d^{1/2}$**
M1	3.91E+01	4.58E+00	4.96E-03	5.56E+02
M2	1.06E+01	8.03E-01	1.02E-02	1.04E+02
M3	5.89E+00	7.24E-01	6.06E-04	2.39E+02

The rates of propagation reactions of **M1**, **M2** and **M3** show a decrease in the order **M1**> **M2**> **M3**, but this trend does not mimic the experimental rate quantitatively. The steric effect can be seen clearly in this order while the size of the sterically hindered group increases, the rate constant k_p of the monomers decrease. This trend is similar with the experimental findings. When the k_p and k_{ct} rate constants are compared, it is seen that k_p is 10 times higher than k_{ct}. It means that although the chain transfer reaction produces a new active radical, it does not enhance the propagation reaction. The size of bulky groups has also an effect on disproportionation reaction. The value of disproportionation rate constant k_d decreases while the size of substituent increases except for **M2**. The kinetic parameter $k_p/k_d^{½}$ shows a qualitative trend with the experimental results but the $k_p/k_d^{½}$ value of **M3** is higher than the value of **M2**. This result is not in agreement with experimental findings. Although the kinetic ratio $k_p/k_{ct}^{½}$ mimics the experimental polymerization rates of monomers we can not consider this ratio as the rate of polymerization because chain transfer reaction does not terminate the propagation reaction.

4.2. Hetero atom effect on the polymerization rate.

In this part, the effect of the hetero atoms on the rate of polymerization is investigated. Methyl α-acetoxymethylacrylate (**M4**) and dimethyl itaconate-methacrylic acid (**M5**) are modeled for this purpose (Table 4.13). Although the main difference between the two monomers is the position of the hetero atom – the number of heavy atoms being the same- the rate of polymerization of **M5** is nearly 30 times higher than that of **M4** (Table 4.14). The reasons that affect the rate of polymerization are investigated in this study.

Table 4.13. Structures of methyl α-acetoxymethylacrylate and dimethyl itaconate-methacrylic acid

No	Structure	Name
M4	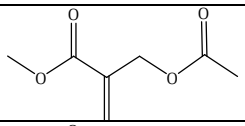	Methyl α-acetoxymethylacrylate
M5	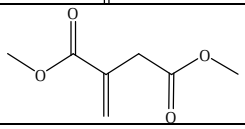	Dimethyl itaconate-methacrylic acid

Table 4.14. Photopolymerization results for **M4** and **M5**

Monomer	Rp ($mol\ L^{-1}\ s^{-1}$)	Dipole (Debye)	Reference
M4	2.42E-01	1.88	[12]
M5	8.67E-03	1.46	[12]

4.2.1. 3D-Structures of M4 and M5

The numbering system of the atoms of the radical derivatives of the methyl α-acetoxymethyl acrylate and dimethyl itaconate-methacrylic acid are shown in Figures 4.38 and 4.39. The various conformers of monomers **M4** and **M5** are modeled by using the quantum mechanical methods (Figures 4.40-4.47). As can be seen in Table 4.16, monomer **M4** prefers to be in a planar structure while monomer **M5** prefers to be in a nonplanar structure. Another difference between the most stable conformers of these monomers is

that the substituents around C_6-C_8 (C_5-C_1 for **M5**) prefer to be in the syn position in monomer **M4** and anti in monomer **M5**. All the dihedrals of the most stable conformer of monomers **M4** and **M5** are given in Table 4.15.

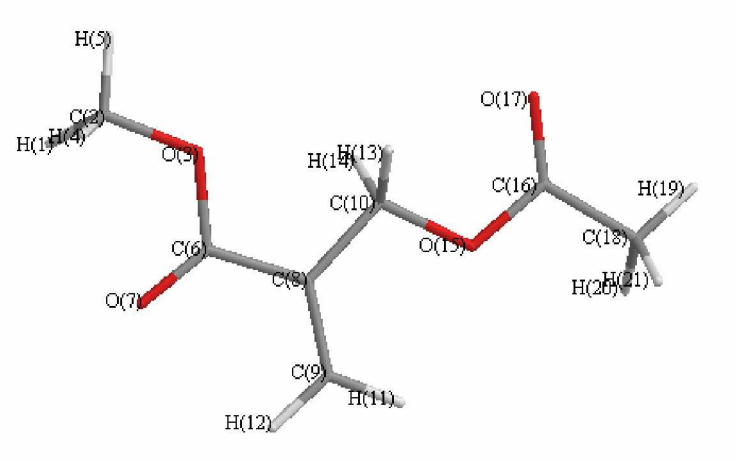

Figure 4.38. Numbering system used for **M4**

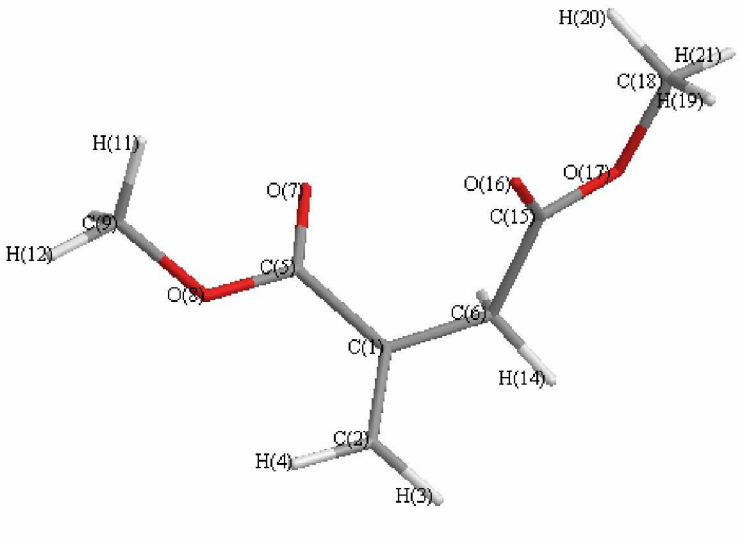

Figure 4.39. Numbering system used for **M5**

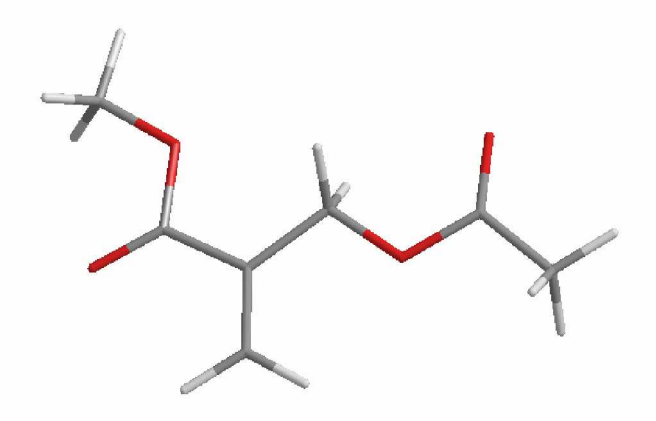

Figure 4.40.The syn planar structure of **M4**

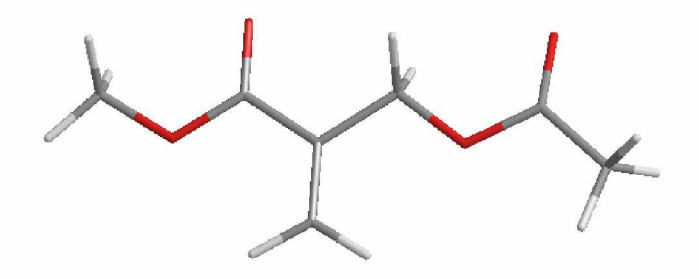

Figure 4.41. The anti planar structure of **M4**

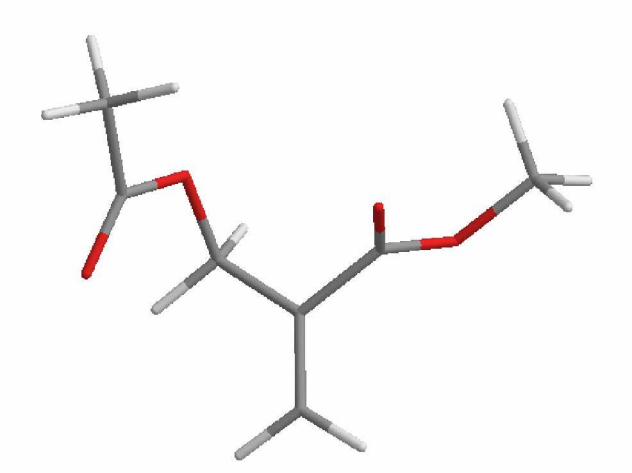

Figure 4.42. The non-planar structure of **M4**

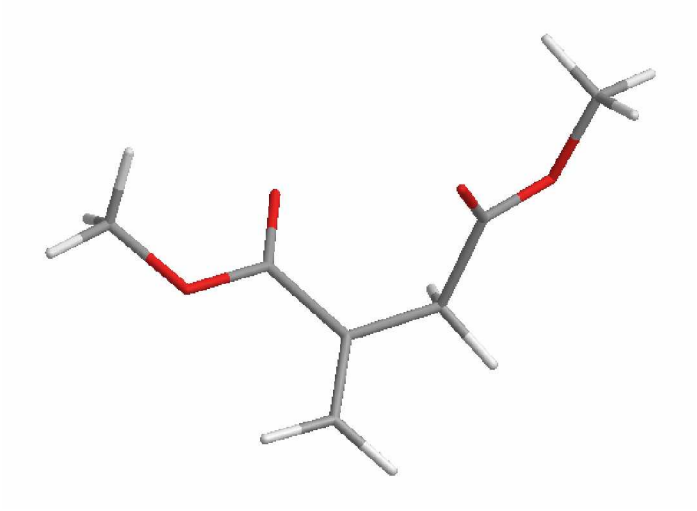

Figure 4.43. The anti non-planar structure (a) of **M5**

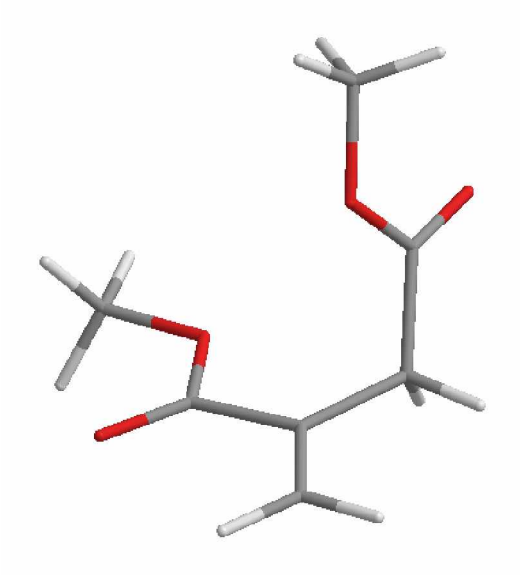

Figure 4.44. The syn non-planar structure (a) of **M5**

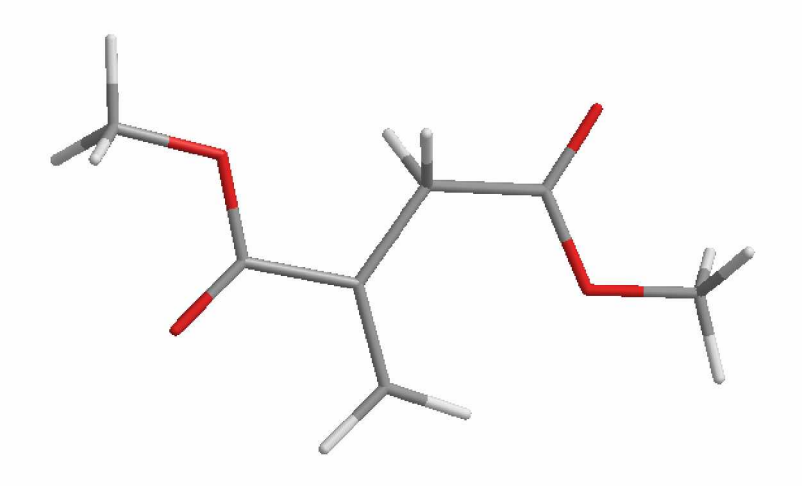

Figure 4.45. The syn planar structure of **M5**

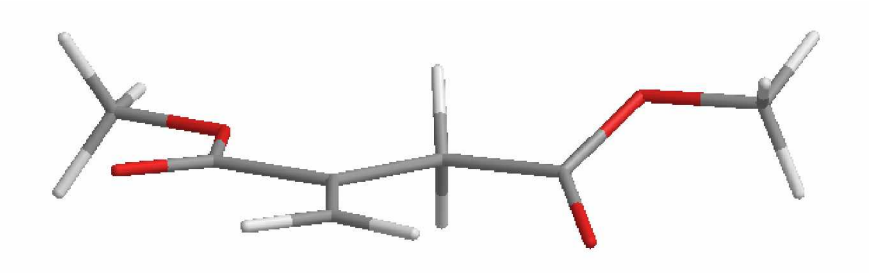

Figure 4.46. The syn non-planar structure (b) of **M5**

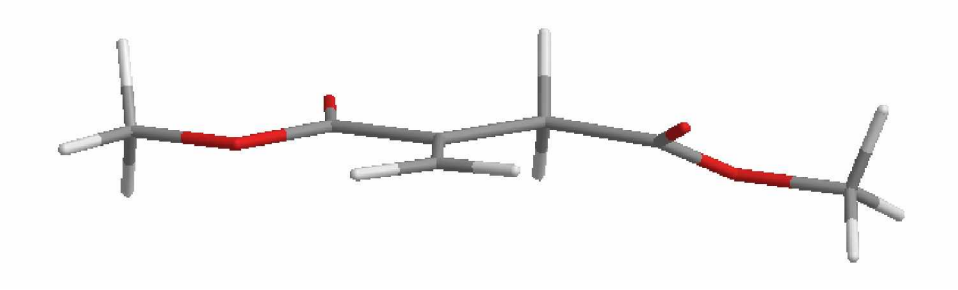

Figure 4.47. The anti non-planar structure (b) of **M5**

Table 4.15. Internal coordinates of monomers **M4** and **M5**.

Internal coordinates	M4	M5
$C_9C_8C_6O_7$ ($C_2C_1C_5O_7$)*	-0.11	-172.28
$H_5C_2O_3C_6$ ($H_{12}C_9O_8C_5$)*	179.97	-179.35
$C_2O_3C_6O_7$ ($C_9O_8C_5O_7$)*	0.09	-0.36
$C_9C_8C_{10}O_{15}$ ($C_2C_1C_6C_{15}$)*	0.07	-114.92
$C_8C_{10}O_{15}C_{16}$ ($C_1C_6C_{15}O_{16}$)*	179.97	17.92
$C_{10}O_{15}C_{16}O_{17}$ ($O_{16}C_{15}O_{17}C_{18}$)*	0.03	-0.50
$O_{17}C_{16}C_{18}H_{19}$ ($C_{15}O_{17}C_{18}H_{21}$)*	-0.04	179.96

* The numbering system used for **M5**

Table 4.16. Relative energies (kcal/mol) for the conformers of **M4** and **M5**

Monomer	M4	M5
syn planar [anti non-planar (a)]*	0.00	0.00
anti planar [syn non-planar (a)]*	0.16	0.65
Non-planar [syn planar]*	6.34	4.24
[syn non-planar (b)]*	-	1.40
[anti non-planar (b)]*	-	0.82

*Conformer for monomer M5

According to the conformer search reasults, the most stable geometies of monomers **M4** and **M5** are different from each other.

4.2.2 3D-structures of the radical derivatives of M4 and M5

The numbering system used in the radical derivatives of the methyl α-acetoxymethyl acrylate (**M4**) and dimethyl itaconate-methacrylic acid (**M5**) is shown in Figures 4.48 and 4.49. All the dihedral angles of the radical derivatives of monomers **M4** and **M5** are given in Table 4.17. While the radical derivative of monomer **M4** preserves its planarity except for the methyl moiety ($C_{23}C_9C_8C_6$ = -96.31), the radical derivative of **M5** is not planar. The carbonyl group on the α-carbon of monomer **M5** prefers to be out of

plane of the C-C double bond plane by 98.15º and the methyl group is out of plane by $C_{23}C_2C_1C_5$ = -82.26º.

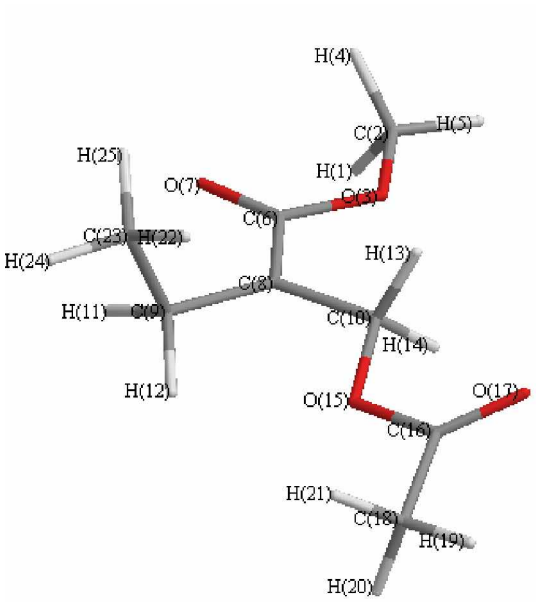

Figure 4.48. Numbering system used for **M4R**

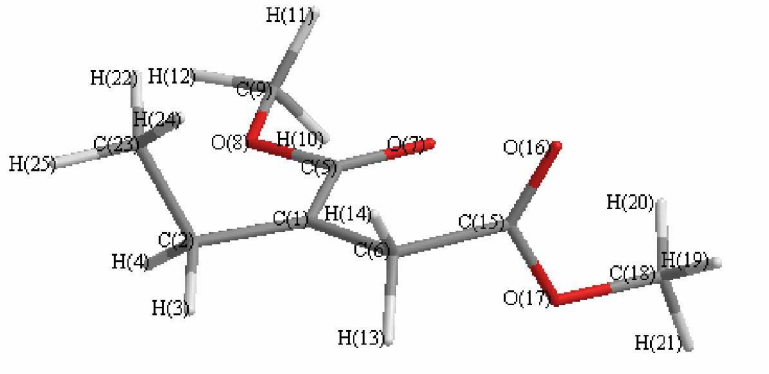

Figure 4.49. Numbering system used for **M5R**

Table 4.17. Internal coordinates for the radicals **M4R** and **M5R**

Internal Coordinates	**M4R**	**M5R**
$C_{23}C_9C_8C_6$ ($C_{23}C_2C_1C_5$)*	-96.31	-82.26
$C_2O_3C_6O_7$ ($C_9O_8C_5O_7$)*	0.04	0.06
$O_7C_6C_8C_9$ ($O_7C_5C_1C_2$)*	-1.16	177.92
$C_9C_8C_{10}O_{15}$ ($C_2C_1C_6C_{15}$)*	0.06	-175.52
$C_8C_{10}O_{15}C_{16}$ ($C_1C_6C_{15}O_{16}$)*	178.03	98.15
$C_{10}O_{15}C_{16}O_{17}$ ($O_{16}C_{15}O_{17}C_{18}$)*	-0.17	-9.00
$O_{17}C_{16}C_{18}H_{19}$ ($C_{15}O_{17}C_{18}H_{21}$)*	-0.85	178.82

* The numbering system used for **M5R**

4.2.3 Propagation reaction of M4 and M5

After the conformer search has been carried out for radicals and monomers, we model the propagation reaction of **M4** and **M5**. The most stable conformers of monomers and their radical derivatives are used to locate transition states structures. Figures 4.50 and 4.51 illustrate the radical addition to the monomers.

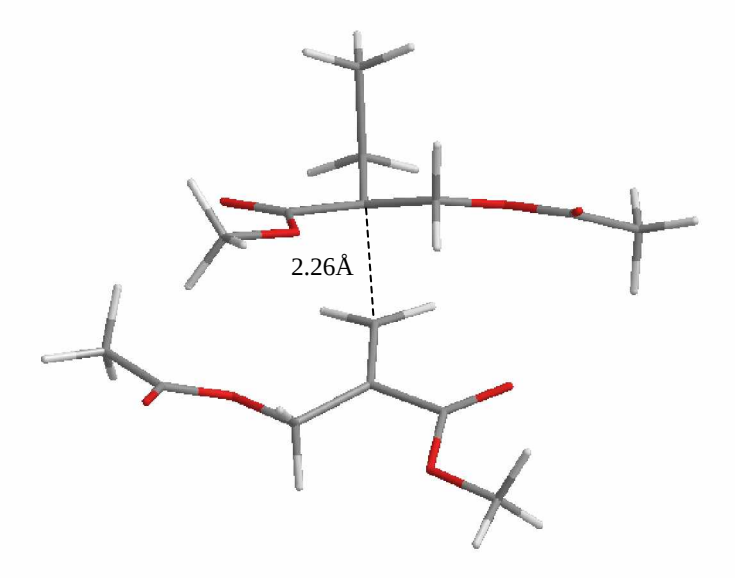

Figure 4.50. Radical addition to **M4**

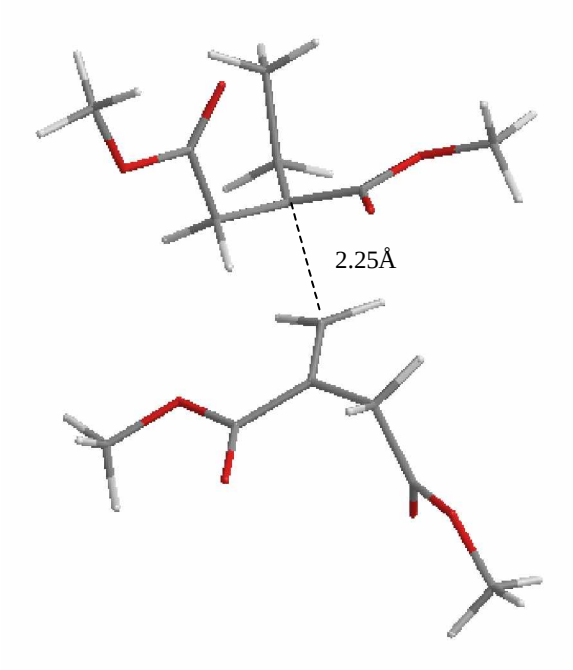

Figure 4.51. Radical addition to **M5**

4.2.4 Lability of hydrogen atoms on M4 and M5

The Mulliken charges of the labile hydrogen atoms on the monomer **M4** are given in Figure 4.52. According to the Mulliken charges of this monomer H_{20} and H_{21} are expected to be more labile because they are more positively charged. On the other hand, hydrogen atoms on the α-carbon atom of monomer **M4** can be abstracted easily because energy barriers for the abstraction reaction of these hydrogen atoms are the lowest one (Table 4.18). Figures 4.53 shows hydrogen abstraction reaction transition states by using methyl radical for **M4**.

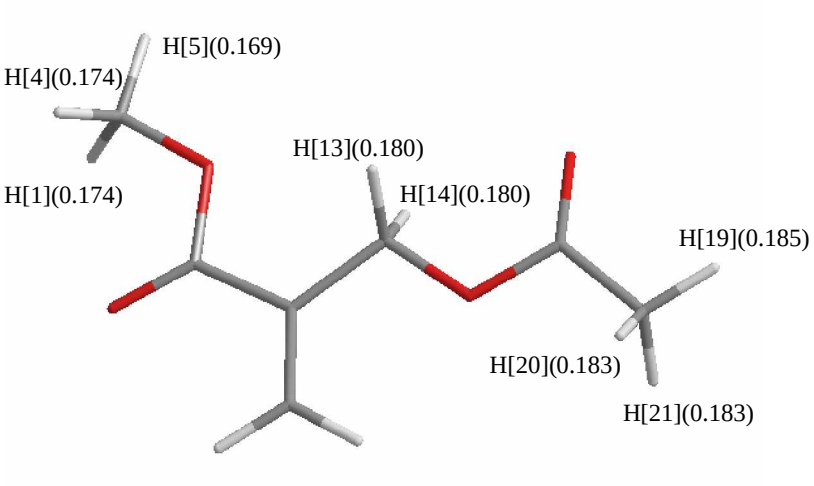

Figure 4.52. Mulliken charges of the labile hydrogen atoms for **M4**

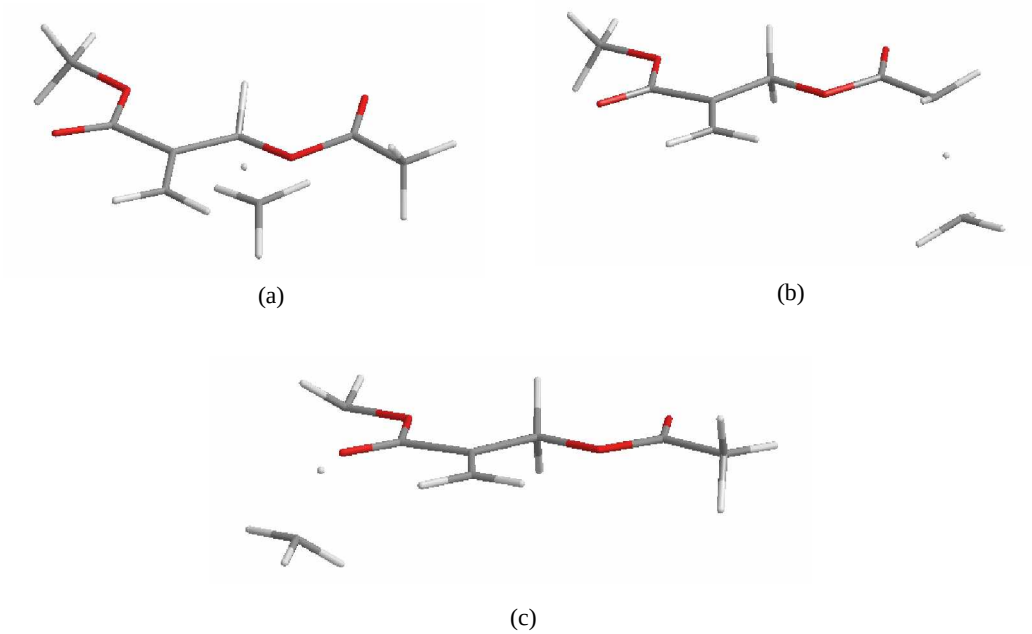

Figure 4.53. Hydrogen abstraction transition state structures for **M4**

Table 4.18. Hydrogen abstraction barriers (Ea (kcal/mol)) for **M4**

	a	**b**	**c**
Ea	6.01	9.21	10.17

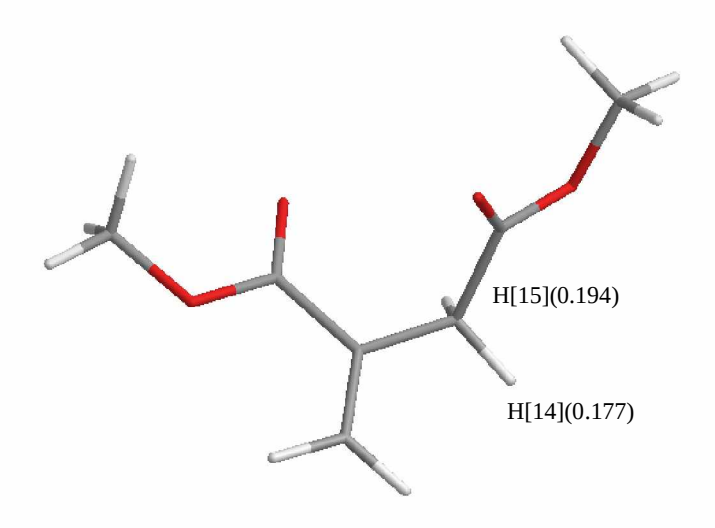

Figure 4.54. Mulliken charges of the labile hydrogen atoms for **M5**

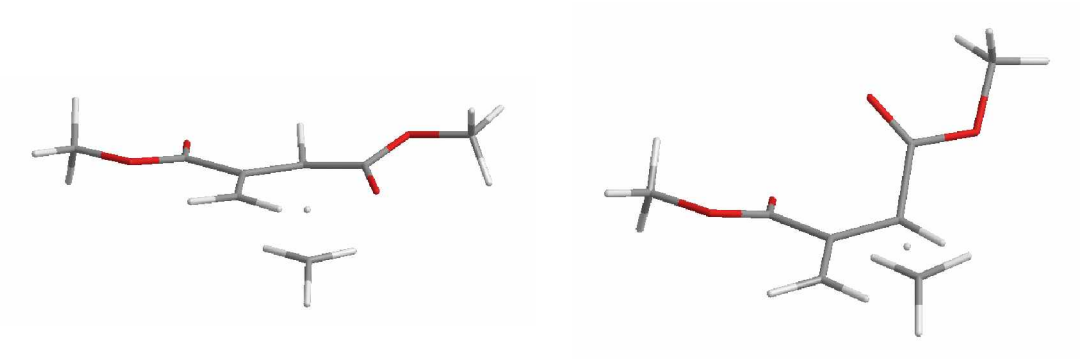

(a) (b)

Figure 4.55. Hydrogen abstraction transition state structures for **M5**

Table 4.19. Hydrogen abstraction barriers (Ea (kcal/mol)) for **M5**

	a	**b**
Ea	5.19	6.40

Table 4.20. Reactivity descriptors for **M4** and **M5**

	k	$\rho_k(N_0)$	$\rho_k(N_o+1)$	$\rho_k(N_o-1)$	S	$s_k^{\,0}$	$s_k^{\,0}(CH_3)-s_k^{\,0}$
M4	H_{13}	0.180172	0.128366	0.244204	4.363954	0.252756	1.124932
	H_{14}	0.180181	0.128379	0.237280	4.363954	0.237619	1.140069
M5	H_{14}	0.196915	0.142227	0.277129	4.435770	0.299197	1.078491
	H_{15}	0.177486	0.117342	0.252313	4.435770	0.299350	1.078338
CH_3	C_1	-0.48757	-0.86268	-0.058900	3.428020	1.377688	0.000000

* $\rho_k(N_0)$ represents the electronic population (Mulliken) on atom k for the N_0 electron system.

The Mulliken charges of two hydrogen atoms H_{14} and H_{15} of monomer **M5** are displayed in Figure 4.54. The chain transfer reaction of these monomers is modeled by using a methyl radical (Figure 4.55). According to the Mulliken charges, the most labile hydrogen atom is H_{15}. This result is also in good agreement with the activation barrier for abstraction reactions of these hydrogen atoms because the abstraction barrier of H_{15} is the lowest one. Finally, we calculate the electronic population on the possible labile hydrogen atoms of monomers **M4** and **M5**. There is no way to distinguish the hydrogen atoms which can be taken into account to model chain transfer reaction in terms of reactivity descriptors in both monomers. Therefore, we decide to choose the most labile hydrogen atoms in both monomers. Both H_{13} and H_{14} are the most labile atoms on monomer **M4** because of symmetry according to the monomer planarity and H_{15} for monomer **M5**.

4.2.5 Chain transfer Reactions for M4 and M5

We try to locate the hydrogen abstraction transition states by using radical derivatives of monomer after checking the lability of hydrogen atoms. Figures 4.56 and 4.57 show the transition states for chain transfer reactions of monomers **M4** and **M5**.

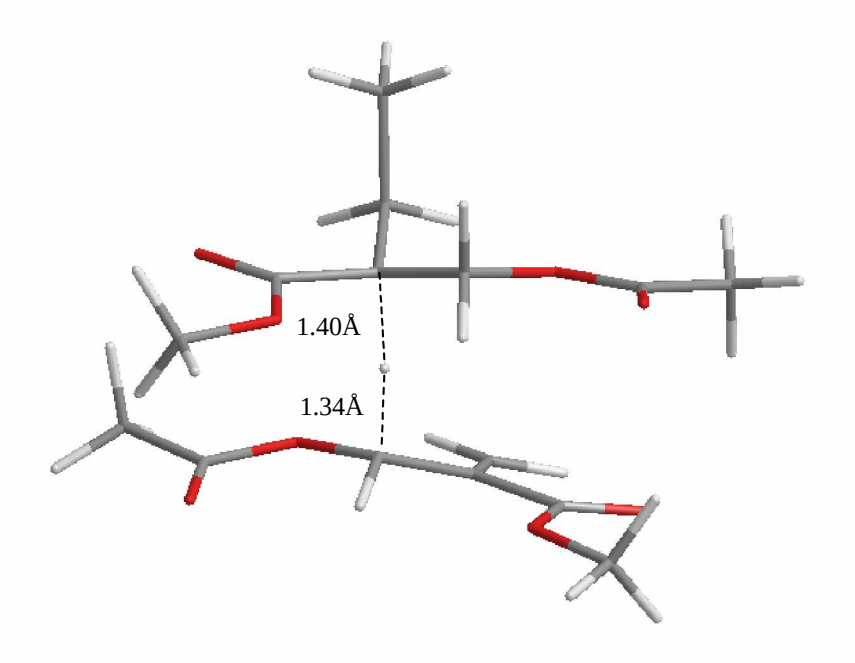

Figure 4.56. H-abstraction transition state for **M4**

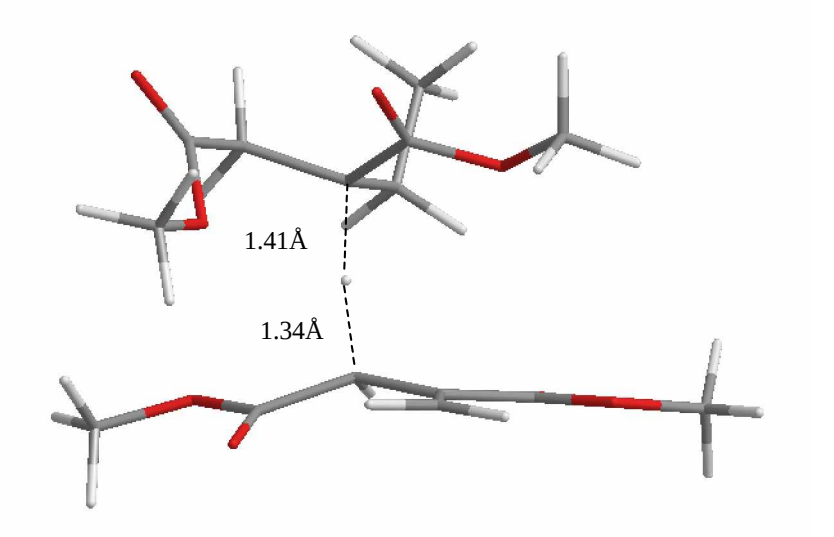

Figure 4.57. H-abstraction transition state for **M5**

4.2.6 Lability of hydrogen atoms on M4R and M5R for modeling disproportionation reaction

There are some hydrogen atoms which are labile for disproportionation reaction on the radicals **M4R** and **M5R**. Mulliken charges of those hydrogen atoms are given in Figures 4.58 and 4.59. According to these charges H_{13} and H_{14} should be more labile for both radicals because they are positively charged. Furthermore, the lability of the hydrogen atoms is also checked by using a methyl radical. Figures 4.60 and 4.61 show hydrogen abstraction transition state structures for the radicals **M4R** and **M5R**. According to the hydrogen abstraction activation barriers, H_{14} is the most labile hydrogen atom on both radicals (Table 4.21). The reactivity descriptors of radicals **M4R** and **M5R** give similar results with the Mulliken charges. H_{13} and H_{14} should be more labile in terms of these descriptors (Table 4.22).

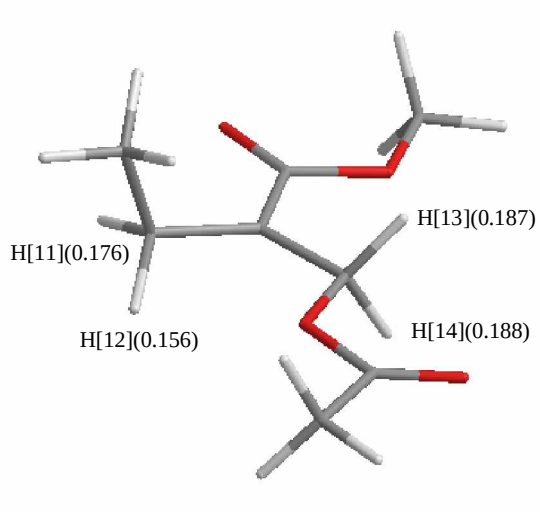

Figure 4.58. Mulliken charges of the labile hydrogen atoms on the radical **M4R**

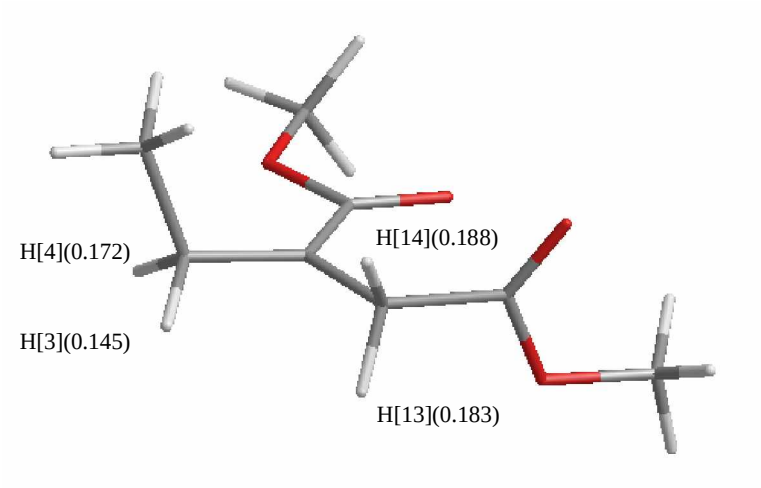

Figure 4.59. Mulliken charges of the labile hydrogen atoms on the radical **M5R**

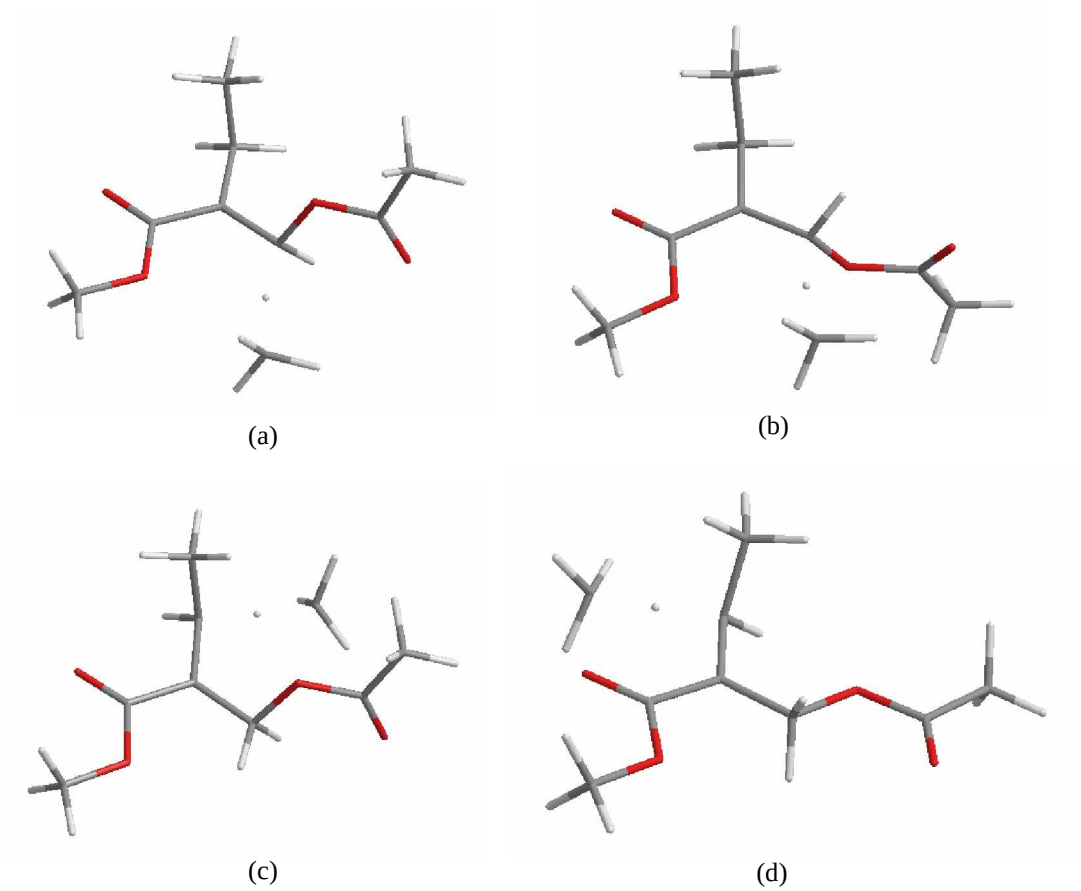

Figure 4.60. Hydrogen abstraction transition state structures of the radical **M4R** for the disproportionation reaction

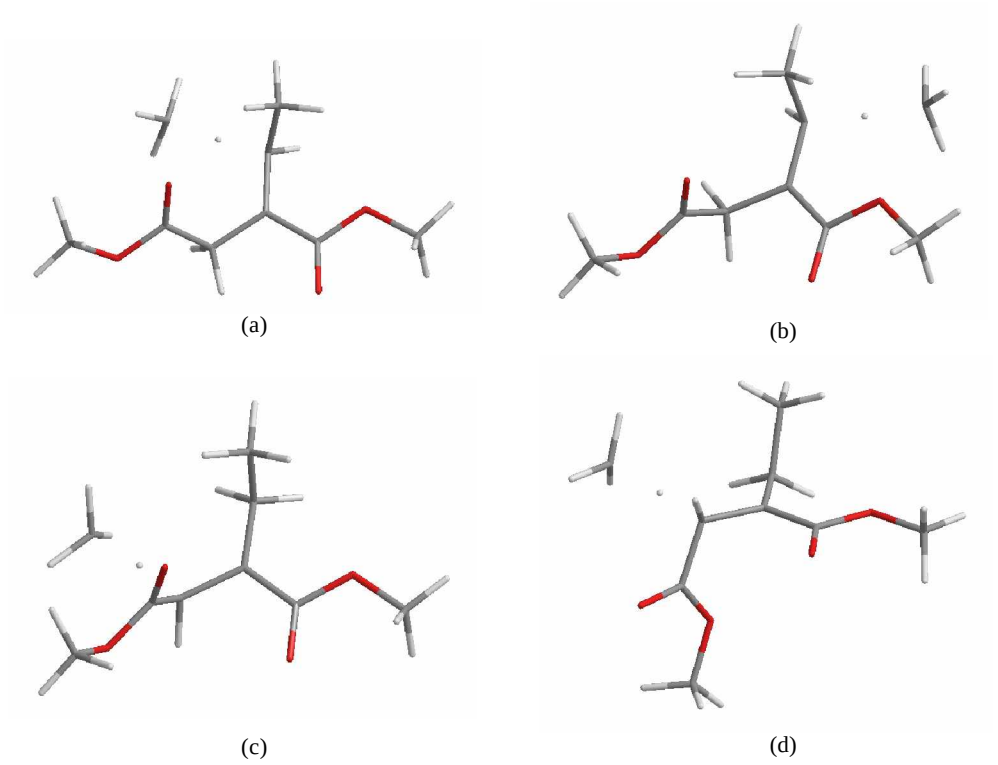

Figure 4.61. Hydrogen abstraction transition state structures of the radical **M5R** for the disproportionation

Table 4.21. Hydrogen abstraction barriers (Ea (kcal/mol)) for M**4R** and **M5R**

	a	**b**	**c**	**d**
M4R	11.72	11.67	11.97	12.41
M5R	7.88	9.97	6.68	7.23

Table 4.22. Reactivity descriptors for **M4R** and **M5R**

	k	$\rho_k(N_0)$	$\rho_k(N_o+1)$	$\rho_k(N_o-1)$	S	$s_k^{\,0}$	$s_k^{\,0}(CH_3)-s_k^{\,0}$
M4R	H_{11}	0.151968	0.066039	0.235935	4.479083	0.380489	0.997199
	H_{12}	0.173870	0.109359	0.248073	4.479083	0.310656	1.067032
	H_{13}	0.188480	0.102927	0.285661	4.479083	0.409240	0.968448
	H_{14}	0.187602	0.115448	0.275352	4.479083	0.358112	1.019576
M5R	H_3	0.145183	0.065067	0.223268	4.169272	0.329791	1.047897
	H_4	0.171565	0.102679	0.250389	4.169272	0.307922	1.069766
	H_{13}	0.182627	0.086349	0.289044	4.169272	0.422545	0.955143
	H_{14}	0.188020	0.098951	0.281903	4.169272	0.381388	0.996300
CH_3	C_1	-0.48757	-0.86268	-0.05890	3.428020	1.377688	0.000000

* $\rho_k(N_0)$ represents the electronic population (Mulliken) on atom k for the N_0 electron system.

4.2.7 Disproportionation reaction for M4 and M5

After having identified which hydrogen atom is more labile for disproportionation reaction, transition states are located to model these reactions. Figures 4.62 and 4.63 show the disproportionation transition state structures for monomers **M4** and **M5**.

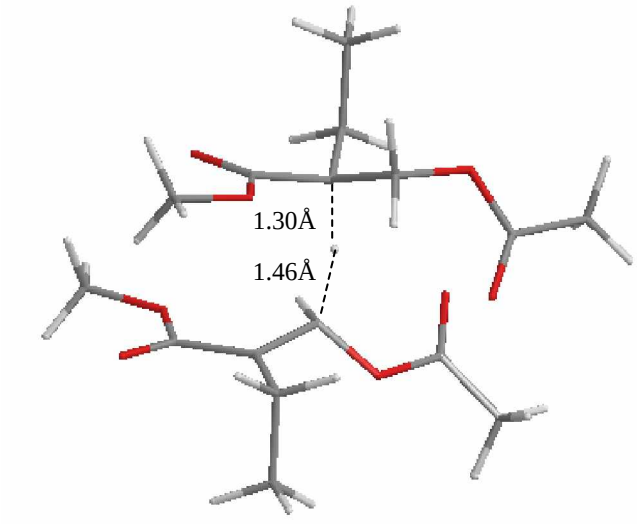

Figure 4.62. Disproportionation transition state for **M4**

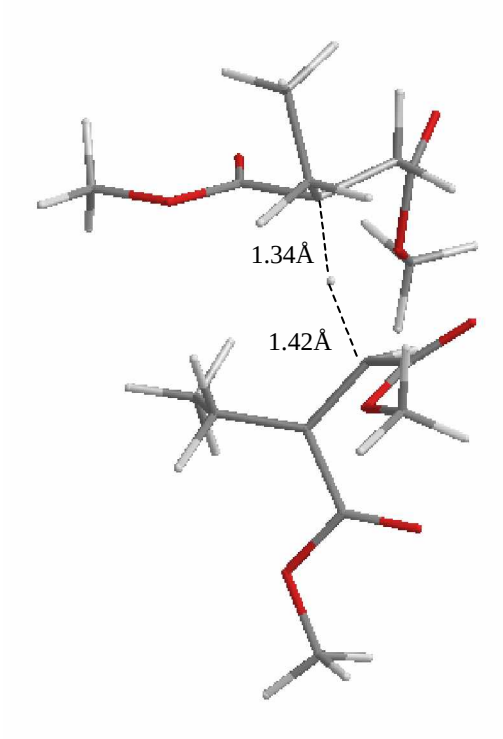

Figure 4.63. Disproportionation transition state for **M5**

Table 4.23. Activation barriers with electronic and ZPE (kcal/mol) for addition, chain transfer and disproportionation reactions

	Reactants	**E_{a1}**	**E_{a2}**	**E_{a3}**
M4	0.00	2.96	9.75	19.05
M5	0.00	4.86	9.84	14.88

E_{a1} = Addition barrier

E_{a2} = Hydrogen abstraction barrier for chain transfer reaction

E_{a3} = Hydrogen abstraction barrier for disproportionation reaction

Activation barriers with electronic and ZPE (kcal/mol) for addition, chain transfer and disproportionation reactions are given in Table 4.23. Activaton barriers of propagation reaction show that monomer **M4** should propagate faster than monomer **M5**. While the activation barriers for the chain transfer reaction of the monomer **M4** and **M5** are similar, the activation barrier of **M4** for the disproportionation reaction is higher than that of **M5**. Therefore, the disproportionation reaction of the monomer **M4** may lead to increase in the

rate of polymerization. Although the activation barriers show this result, the propagation rate constants, k_p, exhibits the inverse trend (Table 4.24).

Table 4.24. Rate constants for **M4** and **M5**

Monomer	$\mathbf{k_p}$ $\mathbf{(M^{-1}s^{-1})}$	$\mathbf{k_{ct}}$ $\mathbf{(M^{-1}s^{-1})}$	$\mathbf{k_d}$ $\mathbf{(M^{-1}s^{-1})}$	$\mathbf{k_p/k_d^{1/2}}$
M4	1.02E+00	1.08E-05	2.53E-12	6.43E+05
M5	6.78E+00	5.99E-05	3.99E-07	1.07E+04

Due to the fact that these monomers have the same pendant group size, we can not attribute this effect to the propagation rate. Because of the electronic effect, the activation barrier of chain transfer reaction for monomer **M5** is expected to be lower than the one for **M4** but the activation barriers for both monomers are nearly similar. The electronic effect is emphasized in the activation barriers for the disproportionation reaction and the rate constant, k_d, for monomers **M4** and **M5**. The allylic hydrogen atoms are strongly affected by the presence of the pendant groups which are attached to the α-C atom of itaconates. At that position the carbonyl moiety of monomer **M5** may stabilize the radicals which are generated by chain transfer and disproportionation reaction. As a result, the calculated ratio $k_p/k_d^{1/2}$ mimics the qualitative trend of the experimental findings.

4.3. The effect of the electron withdrawing and electron donor groups on the polimerizability

Since the calculated trend in the rate constants is in agreement with the experimental data for monomers M1-M3, the same methodology has been applied to the monomers which have the electron-donor group $N(CH_3)_2$, 2-(dimethylamino)ethyl acrylate (**M6**) and the electron withdrawing group CN, 2-(cyano)ethyl acrylate (**M7**). Table 4.25 shows the structure and the name of these monomers. Again for these monomers, the radical which has the methyl radical attached to the C-C double bond is used as the attacking radical to model the propagation, the chain transfer, and the disproportionation reactions. The experimental photopolymerization behavior of 2-(dimethylamino)ethyl acrylate and 2-(cyano)ethyl acrylate is shown in Table 4.26.

Table 4.25 2-(substituted)ethyl acrylate monomer modeled.

No	Structure	Name
M6	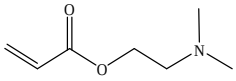	2-(dimethylamino)ethyl acrylate (DMAEA)
M7	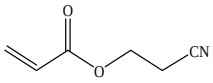	2-(cyano)ethyl acrylate (CEA)

Table 4.26 Photopolymerization results for monomers **M6** and **M7**

Monomer	R_p (mol L^{-1} s^{-1})	Dipole (Debye)	Reference
M6	1.04	2.01	[13]
M7	13.91	3.70	[13]

4.3.1. 3D-Structures of M6 and M7

The numbering system used for the monomers 2-(dimethylamino)ethyl acrylate (**M6**) and 2-(cyano)ethyl acrylate (**M7**) is shown in Figures 4.64 and 4.65.

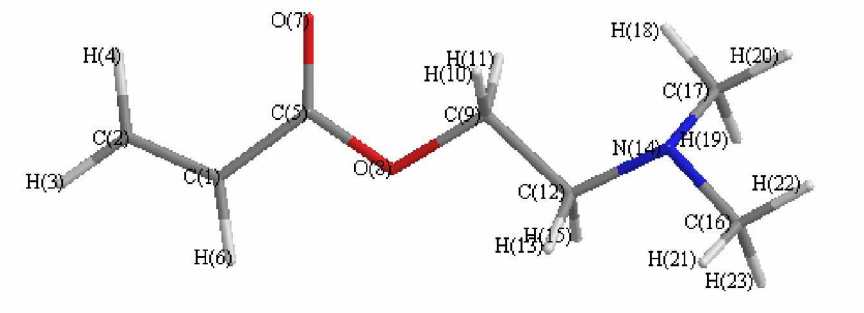

Figure 4.64. Numbering system used for **M6**

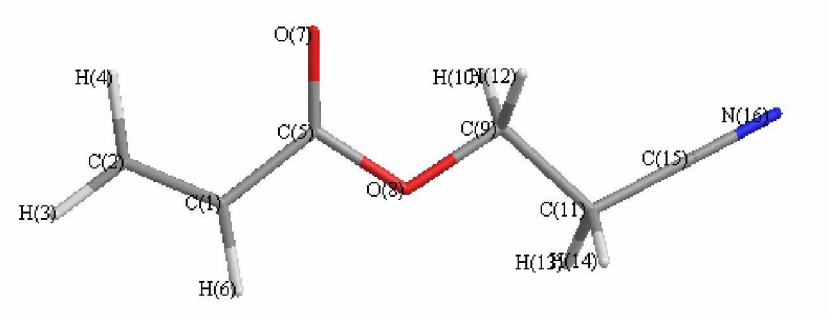

Figure 4.65. Numbering system used for **M7**

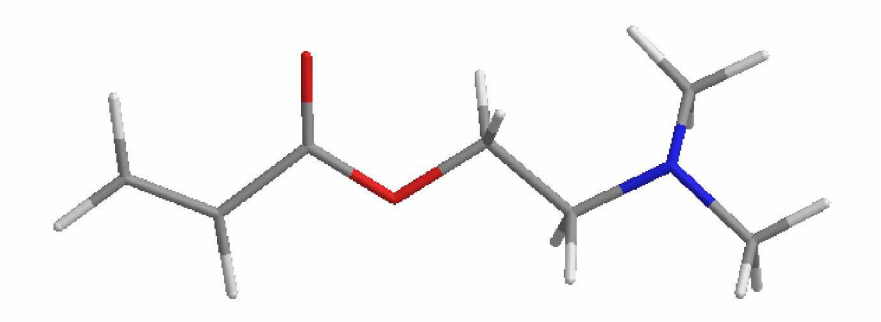

Figure 4.66. The syn structure of **M6**

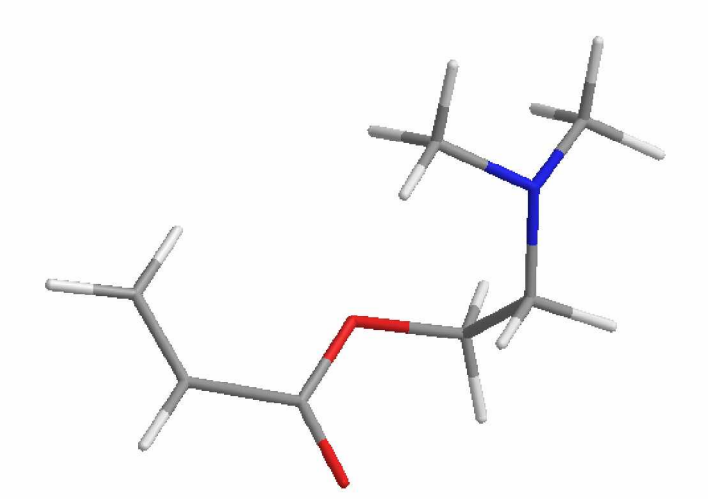

Figure 4.67. The anti structure of **M7**

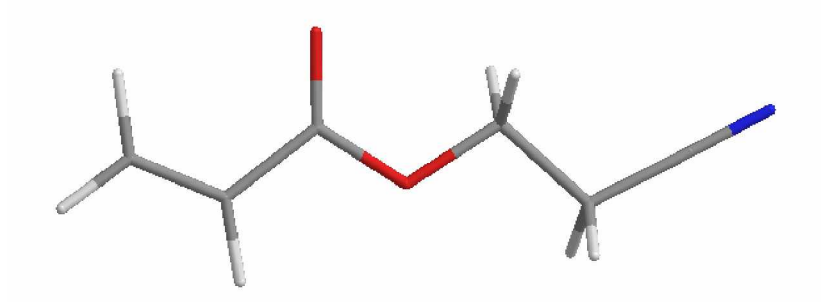

Figure 4.68. The planar structure of **M7**

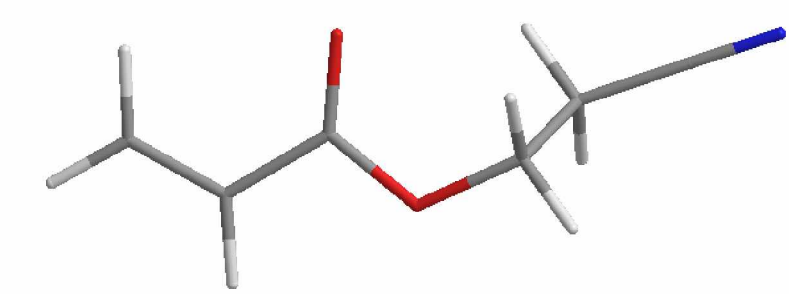

Figure 4.69. The syn structure of **M7**

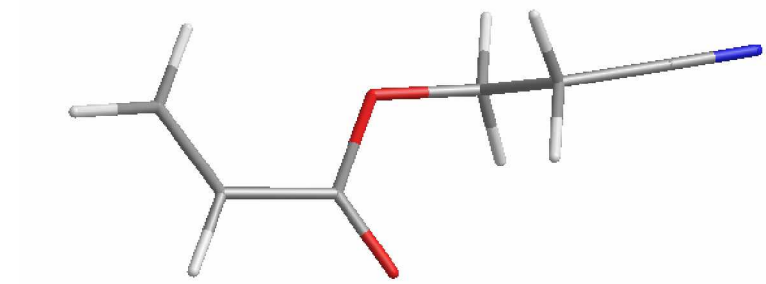

Figure 4.70. The anti structure of **M7**

Based on B3LYP/6-31G* calculations, for both monomers, the syn conformer with respect to the C_1-C_5 bond is more stable than the anti conformer (Table 4.27). Various conformers of **M6** and **M7** are illustrated in Figures 4.66-4.70.

Table 4.27. Relative energies (kcal/mol) of the conformers of **M6** and **M7**

Monomer	M6	M7
syn	0.00	0.00
anti	1.39	0.70
planar	-	0.31

Although in general the acrylate monomers prefer to have planar structures, **M7** prefers to have a nonplanar structure (Figure 4.69) as indicated by the dihedral angle $C_5O_8C_9C_{11}$ which is -81.10º (Table 4.28).

Table 4.28. Internal coordinates of monomers **M6** and **M7**

Internal Coordinates	M6	M7
$C_2C_1C_5O_7$	-0.01	0.13
$C_1C_5O_8C_9$	-179.93	-178.2
$C_5O_8C_9C_{12}(C_5O_8C_9C_{11})^*$	-174.7	-81.1
$O_8C_9C_{12}N_{14}(O_8C_9C_{11}C_{15})^*$	-175.91	-173.68
$C_9C_{12}N_{14}C_{16}$	160	-

* The numbering system used for **M7**

4.3.2 3D-structures of the radical derivatives of M6 and M7

The numbering system in the radical derivatives of the 2-(dimethylamino)ethyl acrylate (**M6**) and 2-(cyano)ethyl acrylate (**M7**) is shown in Figures 4.71 and 4.72. All the dihedral angles of the radical derivatives of monomers M6 and M7 are given in Table 4.29.

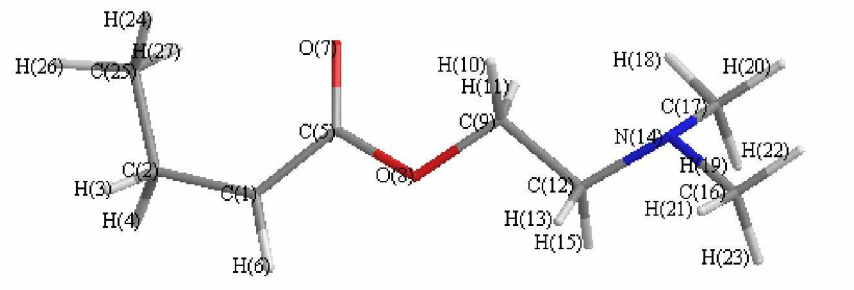

Figure 4.71. Numbering system used for **M6R**

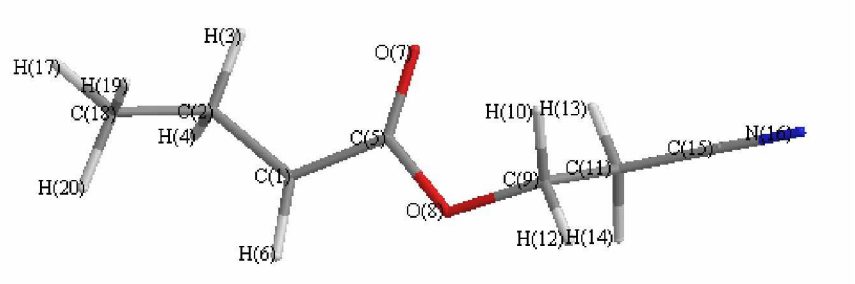

Figure 4.72. Numbering system used for **M7R**

Table 4.29. Internal coordinates of radicals **M6R** and **M7R**

Internal Coordinates	**M6R**	**M7R**
$C_2C_1C_5O_7$	-0.26	-0.19
$C_1C_5O_8C_9$	-179.49	-177.65
$C_5O_8C_9C_{12}$ ($C_5O_8C_9C_{11}$)*	-176.2	-80.73
$O_8C_9C_{12}N_{14}$ ($O_8C_9C_{11}C_{15}$)*	-175.2	-173.73
$C_9C_{12}N_{14}C_{16}$ ($C_9C_{11}C_{15}N_{16}$)*	160.87	10.65
$C_{25}C_2C_1C_5$ ($C_{18}C_2C_1C_5$)*	-121.23	-121.85

* The numbering system used for **M7R**

When we compare 3D structures of the radical derivatives **M6R** and **M7R** with their monomer analogs **M6** and **M7**, there is no main difference except for the presence of the methyl group which is attached to the C-C double bond. Again **M6R** prefers to be planar except for the location of the methyl group which is out of plane by -121.23º ($C_{25}C_2C_1C_5$ = –121.23º). The radical derivative of monomer **M7**, **M7R** is similar in terms of the non-planarity of the methyl group ($C_{18}C_2C_1C_5$ = –121.85º). On the other hand, the cyano moiety prefers to be out of plane ($C_9C_{11}C_{15}N_{16}$ = 10.65º) like its monomer anolog.

4.3.3 Propagation reaction of M6 and M7

The radical derivatives of monomers **M6** and **M7** are used to model the transition states for the propagation reaction. Each radical attacks the less substituted C of the C-C double bond of monomers.

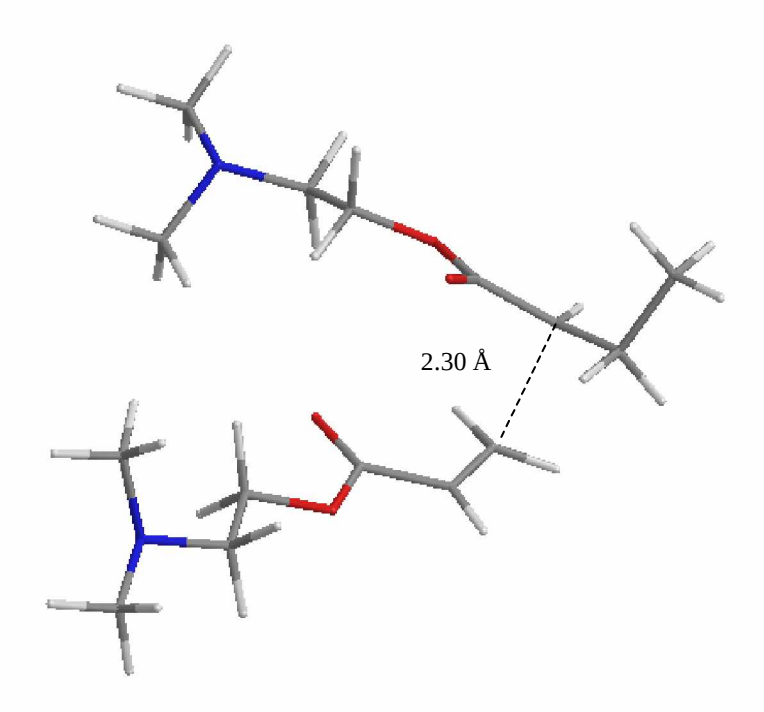

Figure 4.73. Radical addition to **M6**

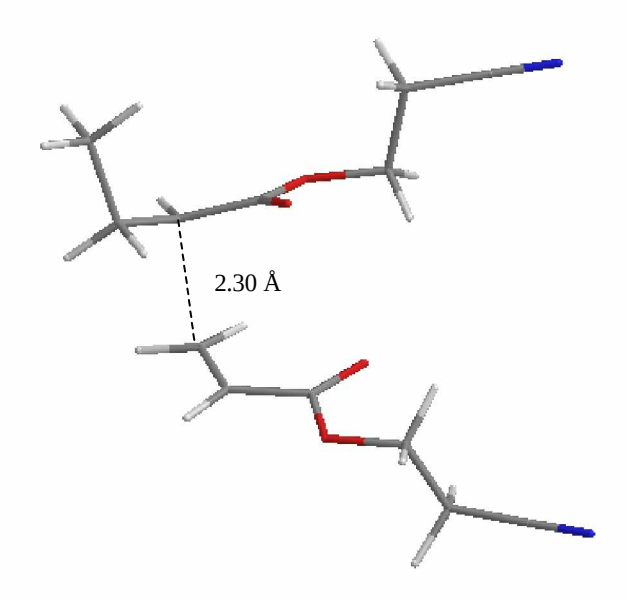

Figure 4.74. Radical addition to **M7**

4.3.4 Lability of hydrogen atoms on M6 and M7

There are some possibilities to model the chain transfer reactions for **M6** and **M7**. Therefore the lability of hydrogen atoms is checked by using a methyl radical. Figure 4.75 shows the Mulliken charges on the active hydrogen atoms for monomer **M6**.

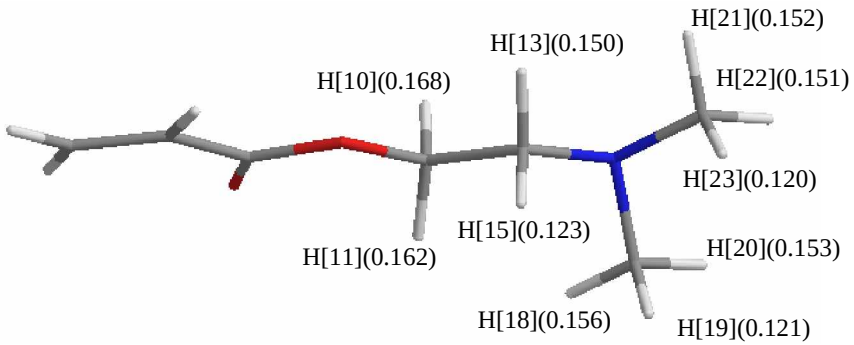

Figure 4.75. Mulliken charges of the labile hydrogen atoms for **M6**

According to the Mulliken charges H_{10} and H_{11} would be expected to more labile because these hydrogen atoms have more positive charges. On the other hand, hydrogen

abstraction barriers show that H_{13} should be abstracted easily because its energy barrier is the lowest one (Table 4.30). Abstraction reaction transition state of H_{13} is given in Figure 4.77. (d).

The Mulliken charges of the labile hydrogen atoms on the monomer **M7** are given in Figure 4.76. When we check the Mulliken charges of labile hydrogen atoms, we can say that H_{13} and H_{14} should be more labile than H_{10} and H_{12}.

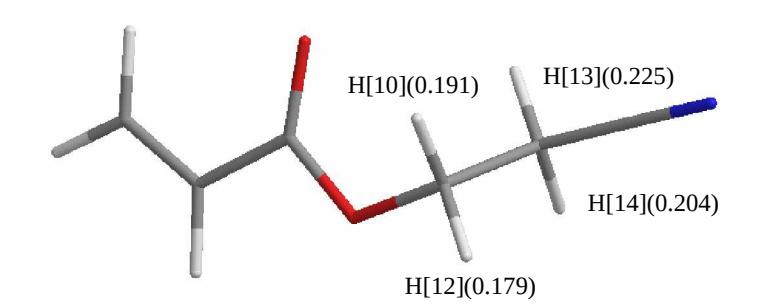

Figure 4.76. Mulliken charges of the labile hydrogen atoms for **M7**

This observation is in agreement with the energy barriers for abstraction reactions of these labile hydrogen atoms. Hydrogen abstraction transition states are illustrated in Figure 4.78. Activation barriers for monomer **M7** show us the most labile hydrogen atoms to be H_{13} and H_{14}.

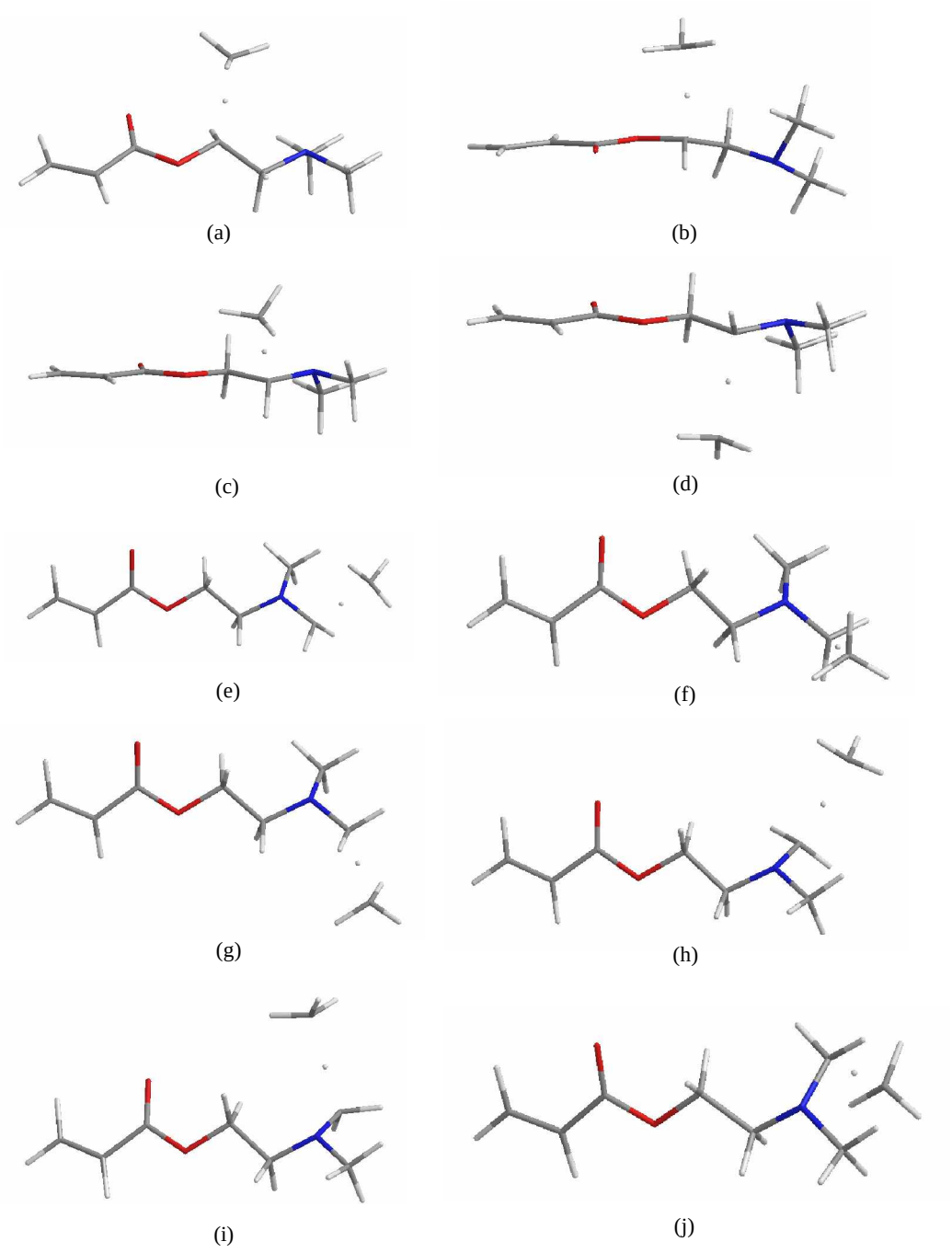

Figure 4.77. Hydrogen abstraction transition state structures for **M6**

Table 4.30. Hydrogen abstraction barriers (Ea (kcal/mol)) for **M6**

	a	**b**	**c**	**d**	**e**	**f**	**g**	**h**	**i**	**j**
E_a	8.76	9.65	9.88	6.60	9.95	10.12	7.05	10.10	10.14	7.26

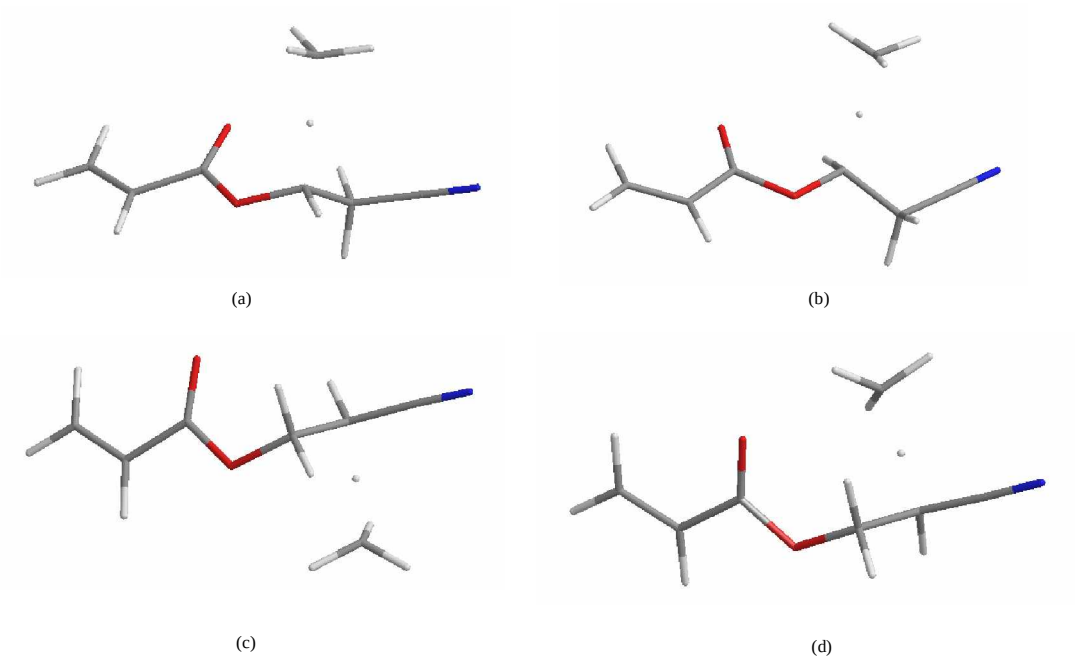

Figure 4.78. Hydrogen abstraction transition state structures for **M7**

Table 4.31. Hydrogen abstraction barriers (Ea (kcal/mol)) for **M7**

	a	**b**	**c**	**d**
Ea	9.92	9.04	7.18	7.43

Table 4.32. Reactivity descriptors for **M6** and **M7**

	k	$\rho_k(N_0)$	$\rho_k(N_o+1)$	$\rho_k(N_o-1)$	S	$s_k^{\,0}$	$s_k^{\,0}(CH_3)-s_k^{\,0}$
M6	H_{10}	0.168054	0.118681	0.204133	5.728689	0.244764	1.132924
	H_{11}	0.162352	0.122204	0.195446	5.728689	0.209790	1.167898
	H_{13}	0.149956	0.131377	0.224266	5.728689	0.266066	1.111622
	H_{15}	0.123358	0.106667	0.236365	5.728689	0.371500	1.006188
	H_{18}	0.155789	0.163892	0.235985	5.728689	0.206499	1.171189
	H_{19}	0.120579	0.101712	0.242214	5.728689	0.402446	0.975242
	H_{20}	0.152940	0.122418	0.235886	5.728689	0.325011	1.052677
	H_{21}	0.151511	0.141436	0.235396	5.728689	0.269134	1.108554
	H_{22}	0.150670	0.124124	0.234555	5.728689	0.316312	1.061376
	H_{23}	0.120095	0.100722	0.243896	5.728689	0.410100	0.967588
M7	H_{10}	0.190836	0.152015	0.234894	4.337454	0.179741	1.197947
	H_{12}	0.178621	0.116241	0.249731	4.337454	0.289506	1.088182
	H_{13}	0.225468	0.221022	0.256029	4.337454	0.075921	1.301767
	H_{14}	0.203713	0.174057	0.256175	4.337454	0.178091	1.199597
CH_3	C_1	-0.48757	-0.86268	-0.05890	3.428020	1.377688	0.000000

* $\rho_k(N_0)$ represents the electronic population (Mulliken) on atom k for the N_0 electron system.

The electron population analysis is carried out in order to understand which hydrogen atom is more labile. H_{15}, H_{19}, and H_{23} are labile hydrogen atoms for monomer **M6**. This result is in agreement with the hydrogen abstraction activation barriers, therefore the most labile hydrogen atom H_{15} is chosen because its activation barrier is the lowest one. For monomer **M7**, there is a contradiction between the evaluation of the Mulliken charges on the labile hydrogen atoms and the activation barriers for abstraction reaction of these hydrogen atoms, however we consider the activation barriers.

4.3.5 Chain transfer Reaction for M6 and M7

After having decided on the identity of the most labile hydrogen, in monomers **M6** and **M7**, we located the transition state structures for the chain transfer reactions for these monomers. Figures 4.79 and 4.80 show hydrogen abstraction transition states for **M6** and **M7**.

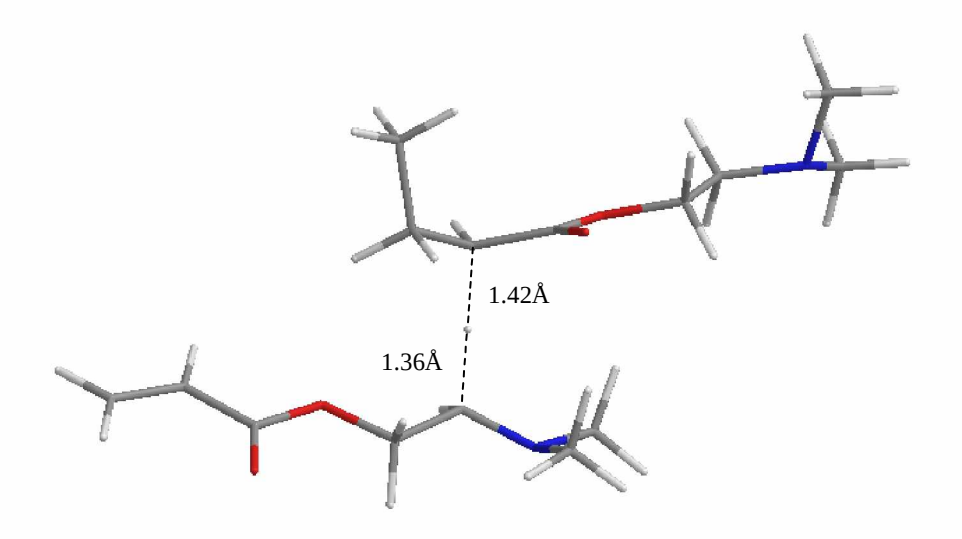

Figure 4.79. H-abstraction transition state for **M6**

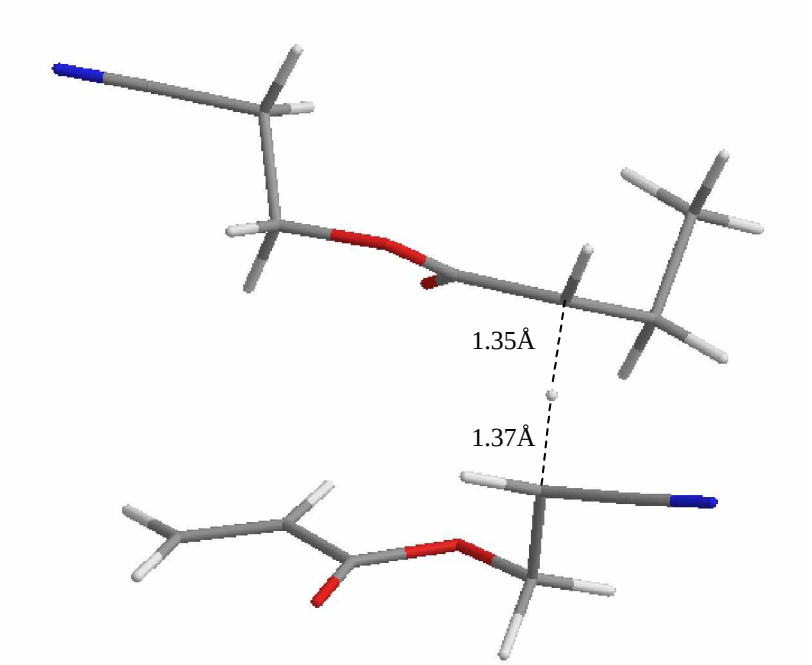

Figure 4.80. H-abstraction transition state for **M7**

4.3.6 Lability of hydrogen atoms on M6R and M7R for modeling the disproportionation reaction

We have used the same procedure in order to understand which hydrogen atom is more labile and have modeled the disproportionation reaction. Based on the Mulliken charges (Figures 4.81 and 4.82), H_4 (for radical **M6R)** and H_3 (for radical **M7R)** these tend to be more labile than the other hydrogen atoms.

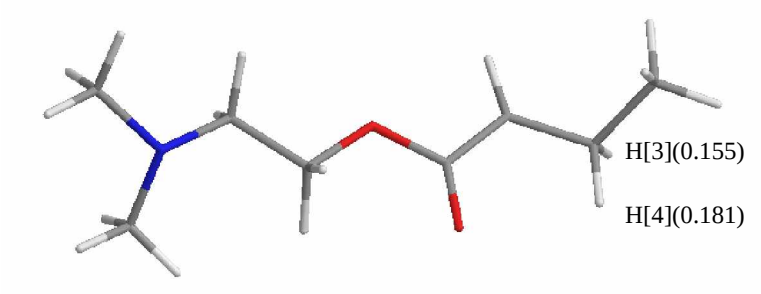

Figure 4.81. Mulliken charges of the labile hydrogen atoms on the radical **M6R**

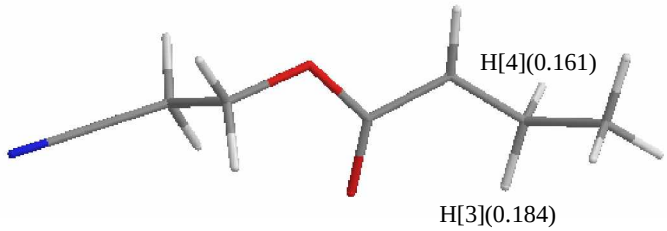

Figure 4.82. Mulliken charges of the labile hydrogen atoms on the radical **M7R**

Then, we take into account the activation barriers of hydrogen abstraction reaction by using methyl radical. H_3 for radical **M6R** and H_4 in radical **M7R** are labile hydrogen atoms (Table 4.33) according to the activation barriers for hydrogen abstraction reaction. Figures 4.83 and 4.84 illustrate hydrogen abstraction transition state structures for the radicals **M6R** and **M7R**.

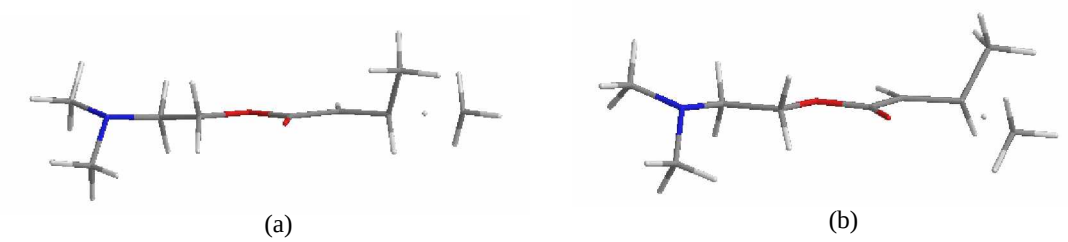

(a) (b)

Figure 4.83. Hydrogen abstraction transition state structures for **M6R** for the disproportionation reaction

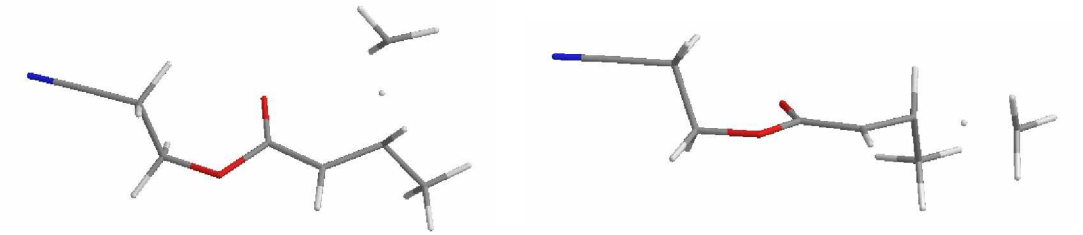

(a) (b)

Figure 4.84. Hydrogen abstraction transition state structures for **M7R** for the disproportionation reaction

Table 4.33. Hydrogen abstraction barriers (Ea (kcal/mol)) for **M6R** and **M7R**

	a	**b**
M6R	10.94	11.89
M7R	11.85	10.96

Finally we look at the reactivity descriptors of radicals. H3 for radical **M6R** and H4 for radical **M7R** are more labile hydrogen atoms according to the electron population analysis. This result also is good agreement with the hydrogen abstraction activation barriers. Therefore we concentrated on H3 for radical **M6R** and H4 for radical **M7R** in order to model the disproportionation reactions.

Table 4.34. Reactivity descriptors for **M6R** and **M7R**

	k	$\rho_k(N_0)$	$\rho_k(N_o+1)$	$\rho_k(N_o-1)$	S	$s_k^{\,0}$	$s_k^{\,0}(CH_3)-s_k^{\,0}$
M6R	H_3	0.155435	0.051687	0.247897	3.738597	0.366775	1.010913
	H_4	0.181162	0.113505	0.239873	3.738597	0.236220	1.141468
M7R	H_3	0.183602	0.117200	0.260594	3.723285	0.266948	1.110740
	H_4	0.161093	0.058403	0.281868	3.723285	0.416012	0.961676
CH_3	C_1	-0.48757	-0.86268	-0.05890	3.428020	1.377688	0.000000

* $\rho_k(N_0)$ represents the electronic population (Mulliken) on atom k for the N_0 electron system.

4.3.7 Disproportionation reaction for M6 and M7

We use two radicals which are the radical derivatives of monomer **M6** and **M7** as we did earlier for monomers **M1**-**M3** in order to model the disproportionation reaction. The radical center attacks the other radical's hydrogen atoms on the C atom which is in the vicinity of the radical center. Figures 4.85 and 4.86 show transition state structures for disproportionation reaction of monomer **M6** and **M7**.

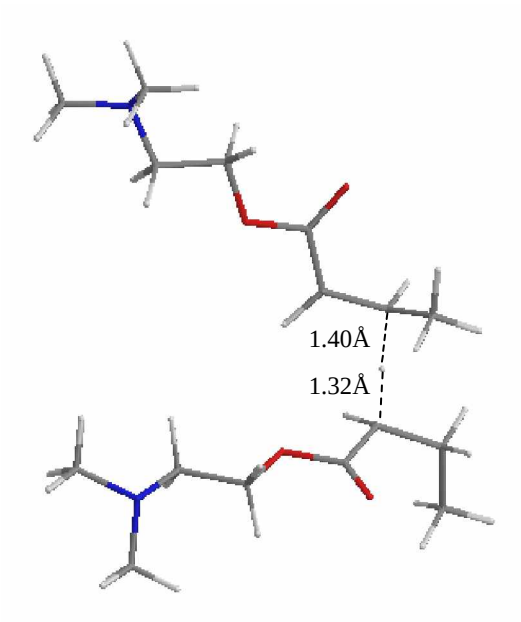

Figure 4.85. Disproportionation transition state for **M6**

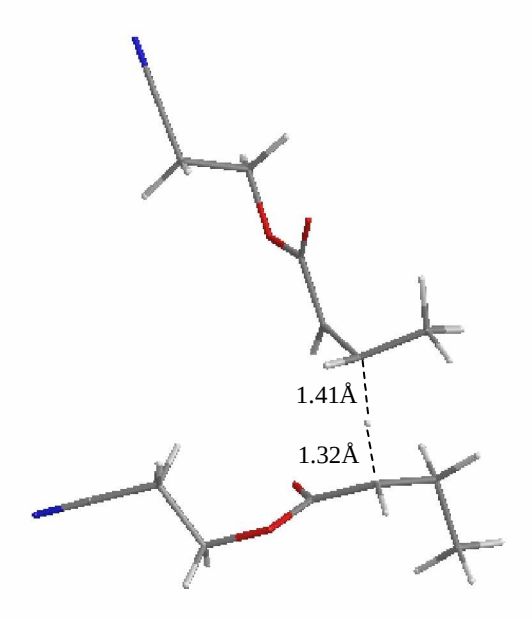

Figure 4.86. Disproportionation transition state for **M7**

The energetics for 2-(dimethylamino)ethyl acrylate (**M6**) and 2-(cyano)ethyl acrylate (**M7**) radical addition reactions, hydrogen abstraction reactions and disproportionation reactions are listed in Table 4.35.

Table 4.35. Activation barriers with electronic and ZPE (kcal/mol) for addition, chain transfer and disproportionation reactions

	Reactants	**E_{a1}**	**E_{a2}**	**E_{a3}**
M6	0.00	2.04	7.80	12.75
M7	0.00	4.42	13.27	17.98

E_{a1} = Addition barrier

E_{a2} = Hydrogen abstraction barrier for chain transfer reaction

E_{a3} = Hydrogen abstraction barrier for disproportionation reaction

The activation barrier for the propagation reaction of the monomer **M6** is lower than that of **M7**. This result should enhance the propagation reaction of the monomer **M6**. **M7** having the highest hydrogen abstraction barrier for both chain transfer (13.27

kcal/mol) and disproportionation reactions (17.54 kcal/mol) must cause an increase in the rate of polymerization. This result can be seen in Table 4.36.

Table 4.36. Rate constants for **M6** and **M7**

Monomer	**k_p ($M^{-1} s^{-1}$)**	**k_{ct} ($M^{-1} s^{-1}$)**	**k_d ($M^{-1} s^{-1}$)**	**$k_p/k_d^{1/2}$**
M6	2.96E+02	0.48E+00	2.41E-04	1.91E+04
M7	1.12E+00	1.16E-06	2.03E-09	2.48E+04

The experimental results show that the polymerization rate of **M7** is nearly 7 times higher than the polymerization rate of **M6** (Table 4.26). If we compare the k_p rate constants of **M6** and **M7**, it can be seen that the k_p rate constant of **M6** is nearly 200 times higher than **M7** (Table 4.36). Therefore we can say that the monomer **M6** is more reactive than **M7**. We may also say that the electron drawing group on the side chain of acrylate decreases the efficiency of chain transfer and disproportionation reaction because the activation barriers for those reactions of the monomer **M7** are higher than those of **M6**. In addition to this, that electron donor moiety on the pendant group of monoacrylate may increases the efficiency of radical propagation since the three activation barriers of **M6** are lower than **M7**. The rate constants k_{ct} and k_d can be used to explain why monomer **M6** has the lower the rate of polymerization than monomer **M7**.

As a result, the ratio $k_p/k_d^{1/2}$ shows the same qualitative trend with experimental results therefore this parameter can be considered the rate of polymerization for predicting in this class of compounds.

4.4 The cyclic group effect on the polymerization rate.

In this study, the effect of a cyclic group on the polymerization rate is investigated. 2,3-epoxypropyl acrylate (**M8**) has an epoxy moiety as a cyclic group. On the other hand, 2-(methoxy)ethyl acrylate (**M9**) has a linear pendant group. Although the main difference is just the cyclic group- the position and the number of heavy atoms being the same -(Table 4.37), the rate of polymerization of **M8** is nearly 2 times higher than that of **M9** and is worth to be investigated.

Table 4.37. Structures of 2,3-epoxypropyl acrylate and 2-(methoxy)ethyl acrylate

No	Structure	Name
M8	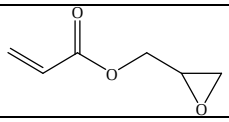	2,3-epoxypropyl acrylate
M9	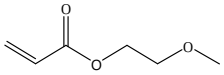	2-(methoxy)ethyl acrylate

Table 4.38. Photopolymerization results for monomers **M8** and **M9**

Monomer	Rp ($mol\ L^{-1}\ s^{-1}$)	Dipole (Debye)	Reference
M8	4.11	2.59	[13]
M9	2.67	2.50	[13]

4.4.1 3D-Structures of M8 and M9

The numbering system of the atoms of the radical derivatives of the 2,3-epoxypropyl acrylate and 2-(methoxy)ethyl acrylate are shown in Figures 4.87 and 4.88. The various conformers of monomers **M8** and **M9** are modeled by using the B3LYP/6-31G* methodology. These monomers show the same conformational properties as the other monomers which have been studied before: monomers **M8** and **M9** prefer to be planar. The epoxy group of monomer **M8** prefers to be out of molecule plane with a dihedral angle of 83.12º (Table 4.39). These conformers are given in Figures 4.89– 4.92 and dihedral angles of the most stable conformer of monomer **M8** and **M9** are given in Table 4.39.

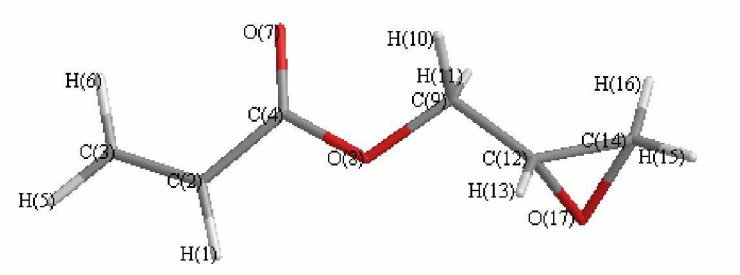

Figure 4.87. Numbering system used for **M8**

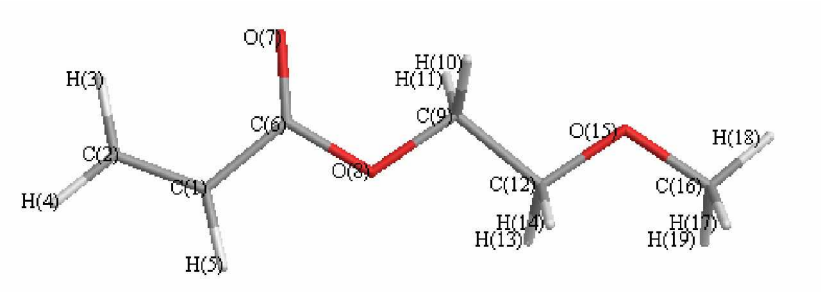

Figure 4.88. Numbering system used for **M9**

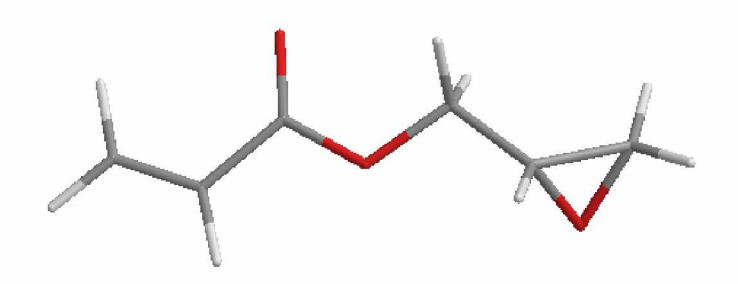

Figure 4.89. The syn structure of **M8**

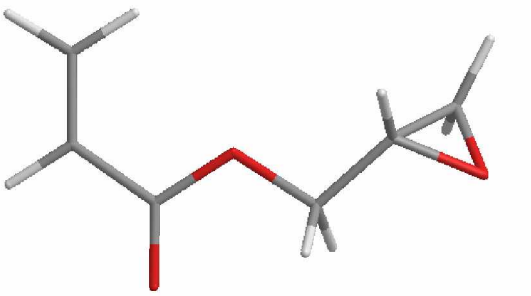

Figure 4.90. The anti structure of **M8**

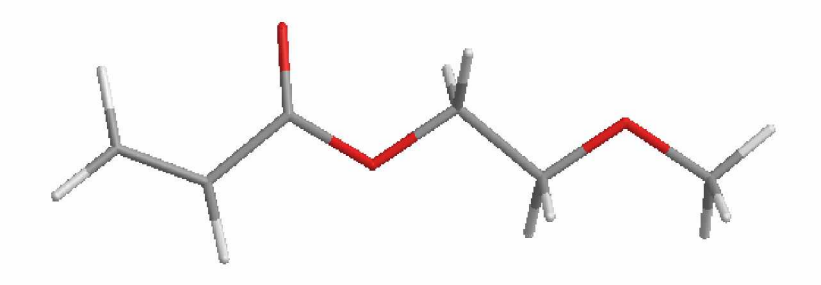

Figure 4.91. The syn structure of **M9**

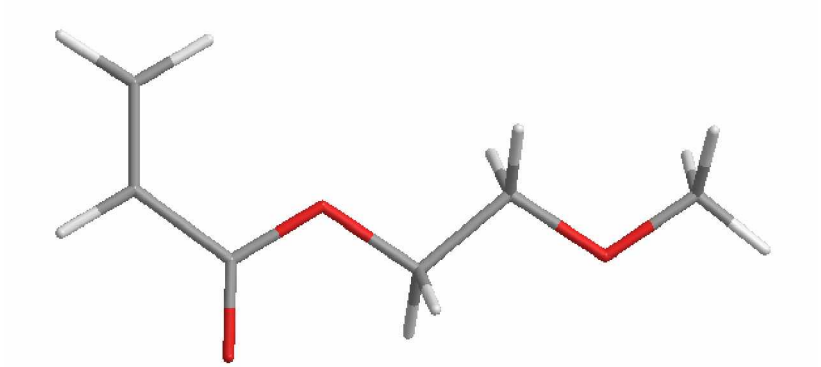

Figure 4.92. The anti structure of **M9**

Table 4.39. Internal coordinates of monomers **M8** and **M9**.

Internal coordinates	**M8**	**M9**
$C_3C_2C_4O_7$ $(C_2C_1C_6O_7)^*$	-0.10	0.08
$C_2C_4O_8C_9$ $(C_1C_6O_8C_9)^*$	179.65	-179.95
$C_4O_8C_9C_{12}$ $(C_6O_8C_9C_{12})^*$	176.22	180.00
$O_8C_9C_{12}O_{17}$ $(O_8C_9C_{12}O_{15})^*$	83.12	179.98
$O_8C_9C_{12}C_{14}$ $(C_9C_{12}O_{15}C_{16})^*$	151.48	-179.98

* The numbering system used for **M9**

Table 4.40. Relative energies (kcal/mol) of the conformers of **M8** and **M9**

Monomer	M8	M9
syn	0.00	0.00
anti	1.08	0.73

As a result, we understand that the most stable conformer of monomer **M8** and **M9** prefers the syn position as in the case of **M6** and **M7** (Table 4.40).

4.4.2 3D-structures of the radical derivatives of M8 and M9

Radical derivatives of monomer **M8** and **M9** are generated by attacking the methyl radical to the less substituted C of the C-C double bond of the monomer. The numbering system in the radical derivatives of the 2,3-epoxypropyl acrylate and 2-(methoxy)ethyl acrylate is shown in Figures 4.93 and 4.94. The generated methyl moiety of these radicals prefers to be out of the radical plane by 122.36º and 123.05º in **M8R** and **M9R**, respectively (Table 4.41). The epoxy group of **M8R** prefers to be out of the radical plane $O_8C_9C_{12}O_{17}$ = 83.50º like its monomer analog. All the dihedral angles of the radical derivative of monomers M8 and M9 are given in Table 4.41.

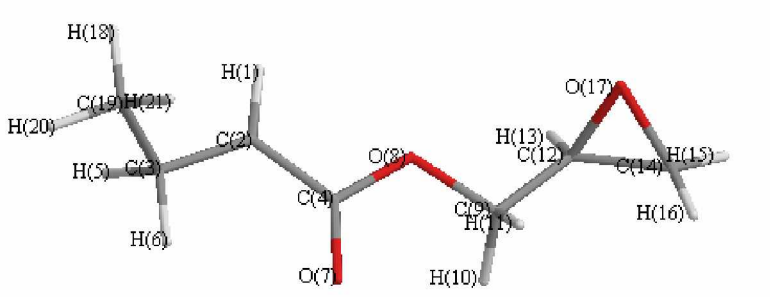

Figure 4.93. Numbering system used for **M8R**

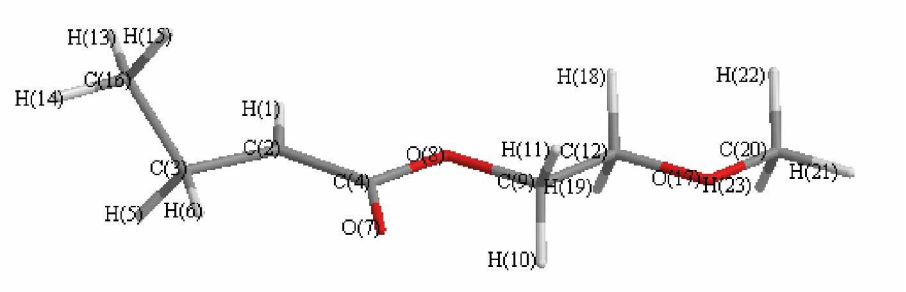

Figure 4.94. Numbering system used for **M9R**

Table 4.41. Internal coordinates for **M8R** and **M9R**.

Internal coordinates	**M8R**	**M9R**
$C_3C_2C_4O_7$	-0.01	0.23
$C_2C_4O_8C_9$	179.43	-179.99
$C_4O_8C_9C_{12}$	176.36	-179.32
$O_8C_9C_{12}O_{17}$	83.50	-179.81
$O_8C_9C_{12}C_{14}$ ($C_9C_{12}O_{17}C_{20}$)*	151.89	179.97
$C_{19}C_3C_2C_4$ ($C_{16}C_3C_2C_4$)*	122.36	123.05

* The numbering system used for **M9R**

4.4.3 Propagation reaction of M8 and M9

When the most stable conformers of monomers and radical derivatives of monomers are calculated, the propagation reaction transition states of monomer **M8** and **M9** are located. Figures 4.95 and 4.96 show the radical addition transition states to those monomers. We observe that the pendant group of monomers is not identical in the transition state geometry. While the epoxy groups look at each other at the transition state of monomer **M8**, the methoxy group prefers to be far away from each other at the transition state of monomer **M9**. The hydrogen bonds between H_{13} on the monomer **M8** and O_{17} on the radical **M8R**, H_{13} and H_{15} on the radical **M8R** and O_{17} on the monomer **M8** stabilizes that transition state geometry (Figure 4.95).

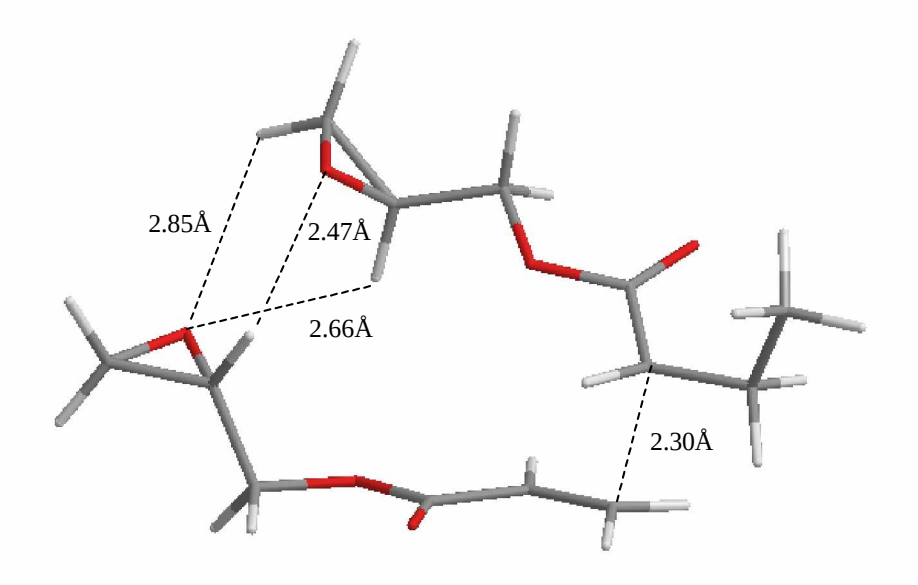

Figure 4.95. Radical addition to **M8**

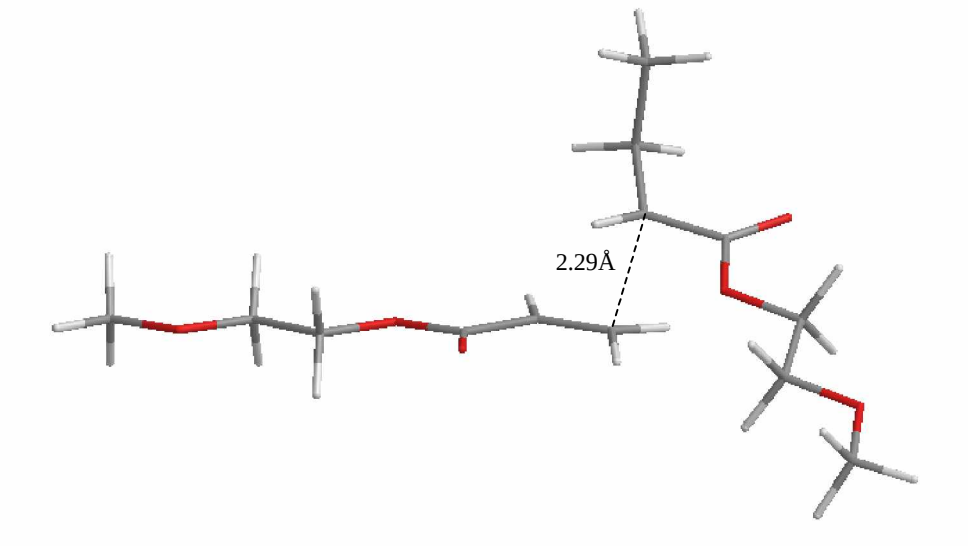

Figure 4.96. Radical addition to **M9**

4.4.4 Lability of hydrogen atoms on M8 and M9

Because there are hydrogen atoms which can be abstracted during the chain transfer reaction, the lability of these hydrogen atoms is checked by using a methyl radical. Mulliken charges of labile hydrogen atoms on the monomer **M8** and **M9** are given in Figures 4.97 and 4.98. According to the Mulliken, H_{10} and H_{11} for monomer **M8** and **M9** should be more labile because they are more positively charged. On the other hand, by using methyl radical, hydrogen abstraction reaction barriers show that H_{10} is more labile atom on monomer **M8** (Table 4.42) bacause it has the lowest activation barrier to chain transfer reaction. Figures 4.98 shows hydrogen abstraction reaction transition states by using methyl radical for **M8**.

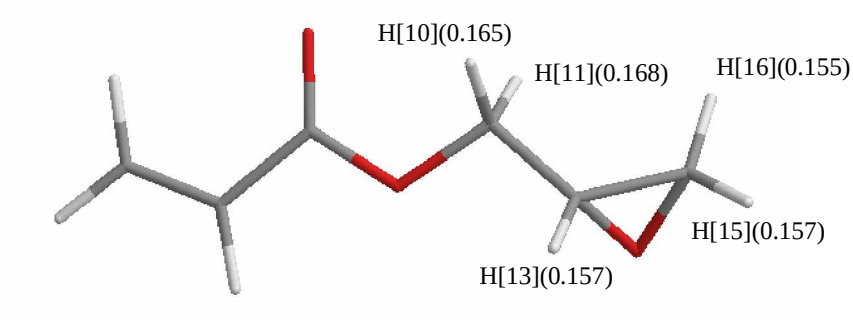

Figure 4.97. Mulliken charges of the labile hydrogen atoms on the monomer **M8**

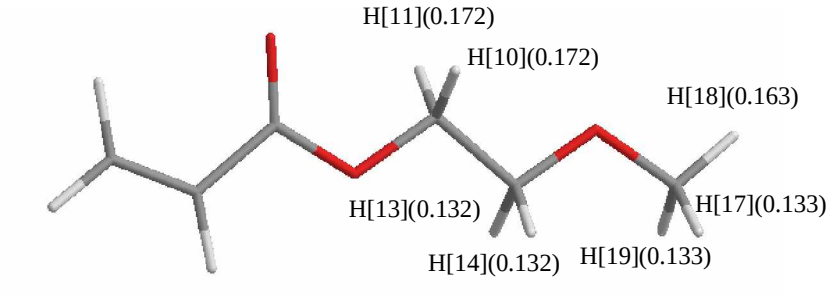

Figure 4.98. Mulliken charges of the labile hydrogen atoms on the monomer **M9**

On the other hand, by using the methyl radical, hydrogen abstraction reaction barriers show that H_{10} is the more labile atom on monomer **M8** (Table 4.42) because it has

the lowest activation barrier to chain transfer reaction. Figures 4.99 shows hydrogen abstraction reaction transition states for **M8**.

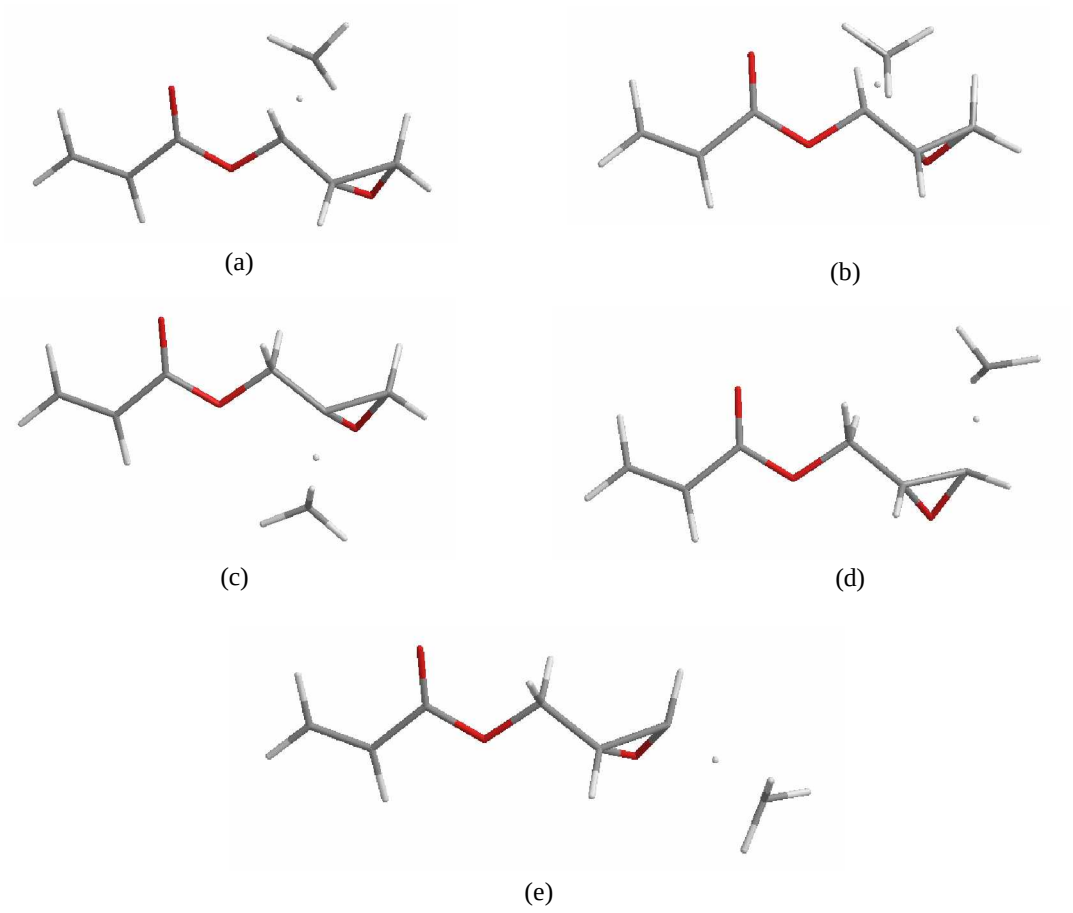

Figure 4.99. Hydrogen abstraction transition state structures for **M8**

Table 4.42. Hydrogen abstraction barriers (Ea (kcal/mol)) for **M8**

	a	**b**	**c**	**d**	**e**
Ea	8.89	8.06	10.04	10.81	10.45

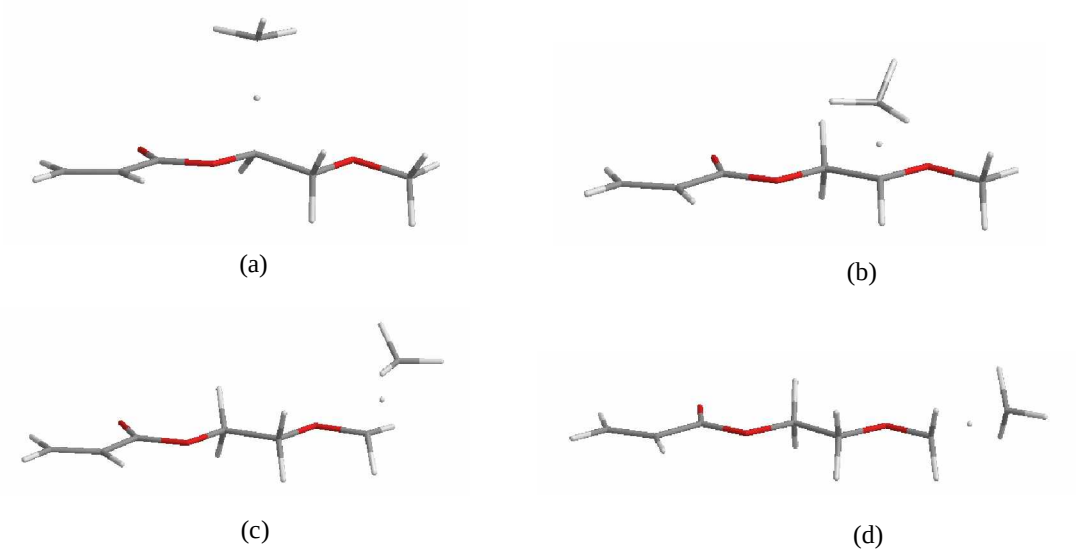

Figure 4.100. Hydrogen abstraction transition state structures for **M9**

Table 4.43. Hydrogen abstraction barriers (Ea (kcal/mol)) for **M9**

	a	**b**	**c**	**d**
Ea	8.84	8.03	9.11	11.49

M9 has symmetry with respect to the plane in the monomer. Therefore only half of the hydrogens are considered while checking the lability of the hydrogen atoms (Figure 4.100). The energy barriers for hydrogen abstractions by using methyl radical show that the most labile hydrogen atoms are H_{13} and H_{14} because these hydrogen atoms have the lowest energy barriers to the hydrogen abstraction reaction (Table 4.43). Figure 4.100 shows the hydrogen abstraction transition states by using a methyl radical. Finally we look at reactivity descriptors for monomer **M8** and **M9** but there is no important difference between descriptors. Therefore we define the most labile hydrogen atoms according to the hydrogen abstraction activation barriers. H_{10}, H_{13} and H_{14} are determined as the most labile hydrogen atoms for **M8** and **M9** respectively.

Table 4.44. Reactivity descriptors for **M8** and **M9**

	k	$\rho_k(N_0)$	$\rho_k(N_o+1)$	$\rho_k(N_o-1)$	S	$s_k^{\,0}$	$s_k^{\,0}(CH_3)-s_k^{\,0}$
M8	H_{10}	0.165491	0.116666	0.227899	4.382697	0.243750	1.133938
	H_{11}	0.168489	0.118197	0.213979	4.382697	0.209891	1.167797
	H_{13}	0.157180	0.130218	0.240954	4.382697	0.242661	1.135027
	H_{15}	0.157425	0.116608	0.252787	4.382697	0.298416	1.079272
	H_{16}	0.115127	0.132890	0.235526	4.382697	0.224911	1.152777
M9	H_{10}	0.171777	0.123244	0.216112	4.612546	0.214179	1.163509
	H_{11}	0.171775	0.123242	0.216495	4.612546	0.215067	1.162621
	H_{13}	0.131568	0.111684	0.222863	4.612546	0.256409	1.121279
	H_{14}	0.131565	0.111681	0.220876	4.612546	0.251833	1.125855
	H_{17}	0.133097	0.115231	0.224419	4.612546	0.251817	1.125871
	H_{18}	0.162664	0.134895	0.239287	4.612546	0.240756	1.136932
	H_{19}	0.133100	0.111523	0.225368	4.612546	0.262557	1.115131
CH_3	C_1	-0.48757	-0.86268	-0.05890	3.428020	1.377688	0.000000

* $\rho_k(N_0)$ represents the electronic population (Mulliken) on atom k for the N_0 electron system.

4.4.5 Chain transfer Reaction for M8 and M9

After checking which hydrogen atoms are more labile, on monomers **M8** and **M9** we locate transition state structures for the chain transfer reaction of these monomers. Figures 4.101 and 4.102 illustrate hydrogen abstraction transition states for monomer **M8** and **M9**.

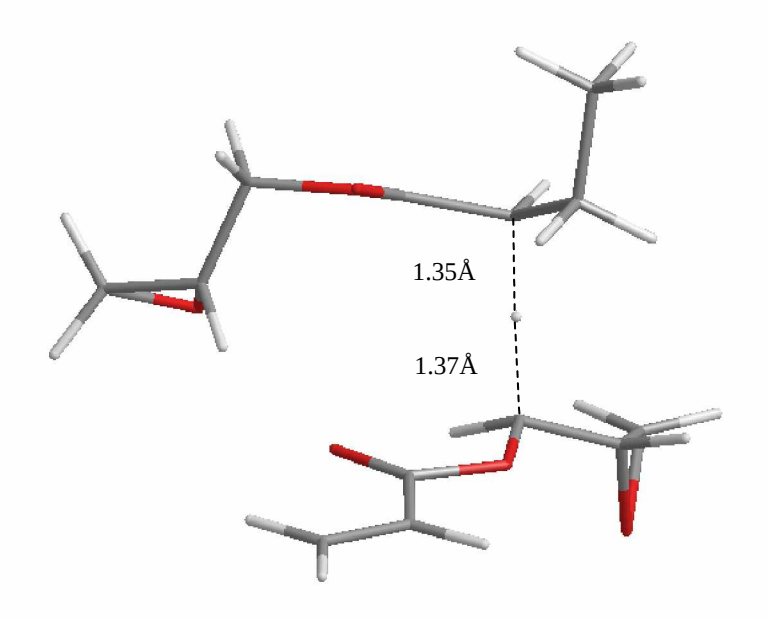

Figure 4.101. H-abstraction transition state for **M8**

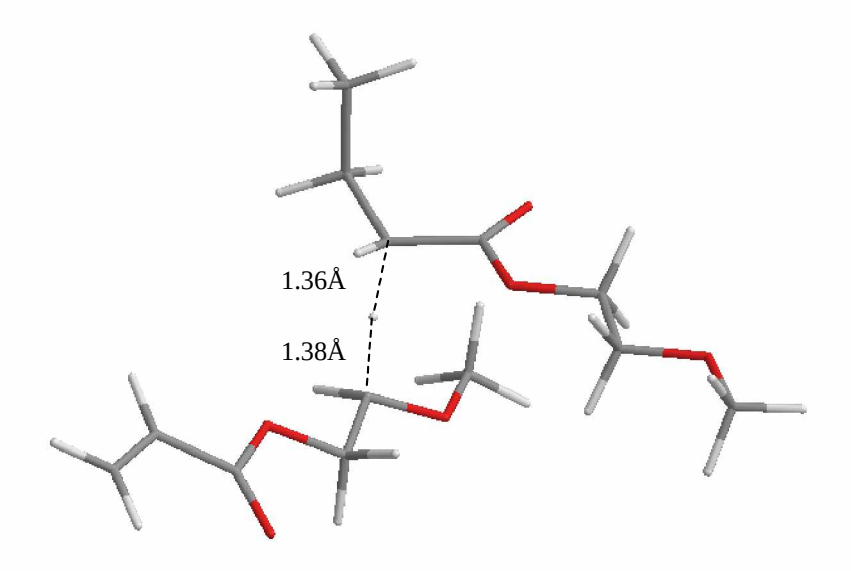

Figure 4.102. H-abstraction transition state for **M9**

5.4.6 Lability of hydrogen atoms on M8R and M9R for modeling disproportionation reaction

Mulliken charges of the labile hydrogen atoms on radical **M8R** and **M9R** are given in Figures 4.103 and 4.104. The most labile hydrogen atom is H_6 for both radical **M8R** and **M9R** according to that charges.

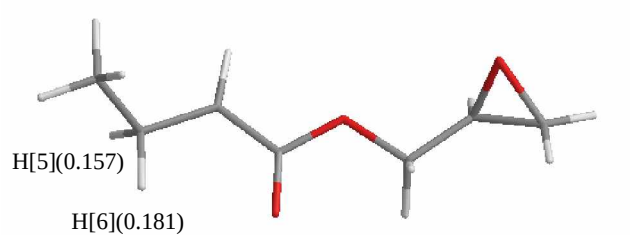

Figure 4.103. Mulliken charges of the labile hydrogen atoms on the radical **M8R**

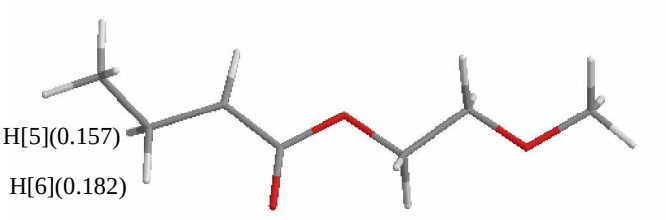

Figure 4.104. Mulliken charges of the labile hydrogen atoms on the radical **M9R**

Hydrogen abstraction energy barriers show that the most labile hydrogen atom is H_5 because its energy barrier is lowest one (Table 4.45). Figures 5.105 and 5.106 illustrate hydrogen abstraction transition state structures of the radicals **M8R** and **M9R**.

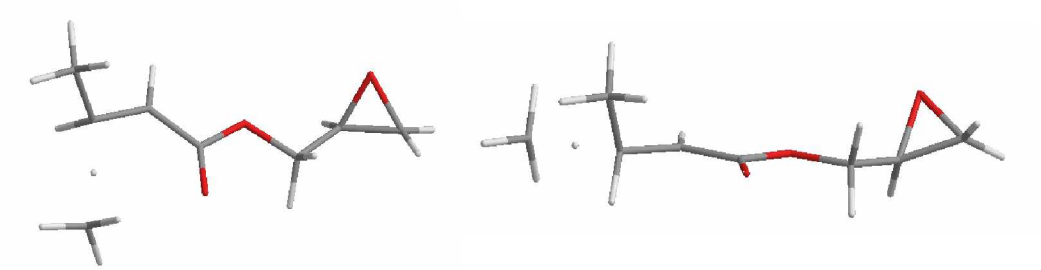

(a) (b)

Figure 4.105. Hydrogen abstraction transition state structures of the radical **M8R** for the disproportionation reaction

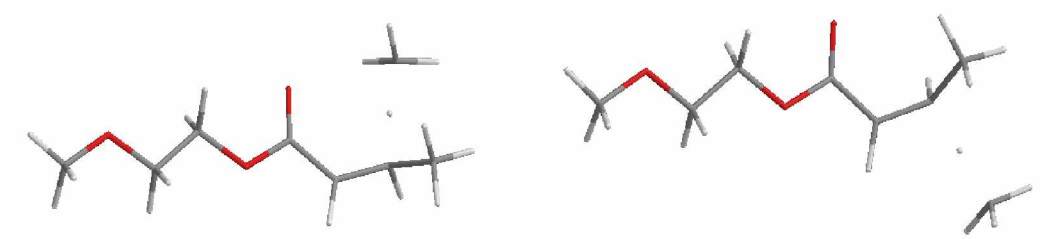

(a) (b)

Figure 4.106. Hydrogen abstraction transition state structures of the radical **M8R** for the disproportionation reaction

Table 4.45. Hydrogen abstraction barriers (Ea (kcal/mol)) for **M8R** and **M9R**

	a	**b**
M8R	11.86	10.92
M9R	11.83	10.90

Table 4.46. Reactivity descriptors for **M8R** and **M9R**

	k	$\rho_k(N_0)$	$\rho_k(N_o+1)$	$\rho_k(N_o-1)$	S	$s_k^{\,0}$	$s_k^{\,0}(CH_3)-s_k^{\,0}$
M8R	H_5	0.156950	0.052807	0.273443	3.612717	0.398548	0.979140
	H_6	0.181042	0.113311	0.255350	3.612717	0.256573	1.121115
M9R	H_5	0.174217	0.098361	0.254616	3.608240	0.281903	1.095785
	H_6	0.147818	0.054179	0.239097	3.608240	0.333614	1.044074
CH_3	C_1	-0.487570	-0.862680	-0.058900	3.428020	1.377688	0.000000

* $\rho_k(N_0)$ represents the electronic population (Mulliken) on atom k for the N_0 electron system.

The reactivity descriptors of the hydrogen atoms on radical **M8R** and **M9R** show that the most labile hydrogen atom is H_5 for **M8R** but there is no essential difference between hydrogen atoms of radical **M9R**.We consider H_5 as the most labile hydrogen atom both for radical **M8R** and **M9R** based on hydrogen abstraction barriers.

4.4.7 Disproportionation reaction for M8 and M9

After determination which hydrogen atom is the most labile one for disproportionation reaction, we try to locate transition state structures to model these reactions. Figure 4.106 and 4.107 show disproportionation transition states for monomers **M8** and **M9**.

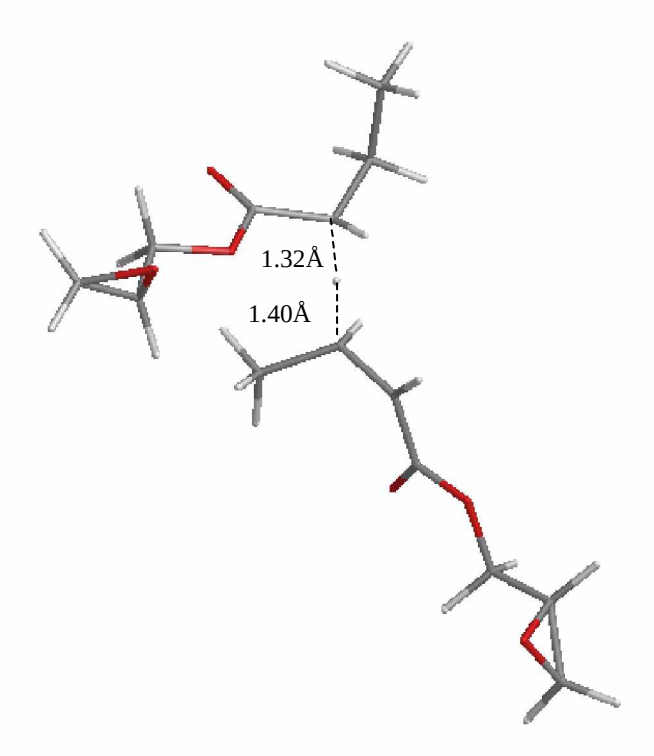

Figure 4.107. Disproportionation transition state for **M8**

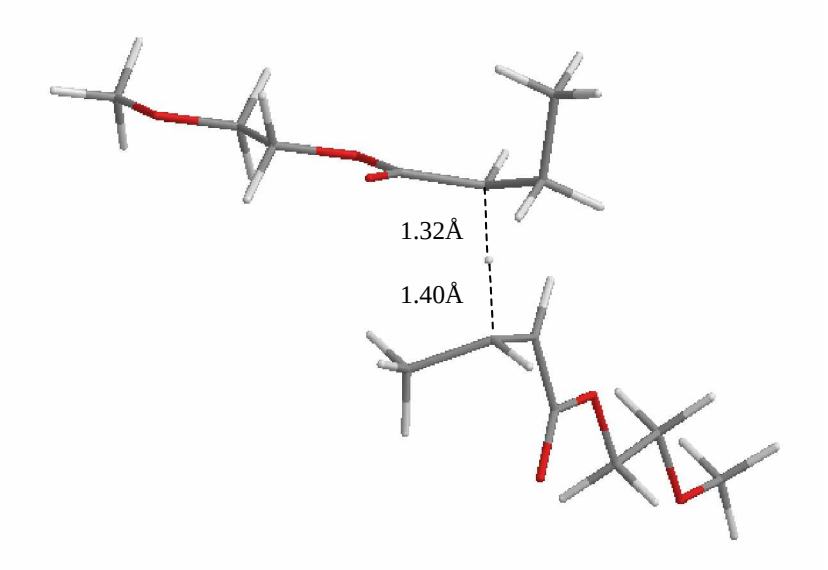

Figure 4.108. Disproportionation transition state for **M9**

The energetics for 2,3-epoxypropyl acrylate (**M8**) and 2-(methoxy)ethyl acrylate (**M9**) radical addition reactions, hydrogen abstraction reactions and disproportionation reactions are listed in Table 4.47.

Table 4.47. Activation barriers with electronic and ZPE (kcal/mol) for addition, chain transfer and disproportionation reactions

	Reactants	**E_{a1}**	**E_{a2}**	**E_{a3}**
M8	0.00	2.62	13.20	17.53
M9	0.00	4.83	11.77	17.41

E_{a1} = Addition barrier

E_{a2} = Hydrogen abstraction barrier for chain transfer reaction

E_{a3} = Hydrogen abstraction barrier for disproportionation reaction

According to the activation barriers of reactions for monomer **M8** and **M9**, we can see that **M8** having the highest hydrogen abstraction barrier for both chain transfer (13.20 kcal/mol) and disproportionation (17.53 kcal/mol) reactions leads to increase in the rate of polymerization. Although the difference between these monomers is just having a cyclic

pendant group analog for **M9** it causes an increase in the energy barrier for chain transfer and disproportionation reactions.

Table 4.48. Rate constants for **M8** and **M9**

Monomer	k_p ($M^{-1} s^{-1}$)	k_{ct} ($M^{-1} s^{-1}$)	k_d ($M^{-1} s^{-1}$)	$k_p/k_d^{1/2}$
M8	1.42E+00	1.68E-06	1.79E-09	3.35E+04
M9	3.39E+00	3.84E-05	3.07E-09	6.11E+04

Although the activation barrier for addition reaction of monomer **M9** is higher than the activation barrier of monomer **M8**, the propagation rate constant of **M9** also is higher than **M8** (Table 4.48).

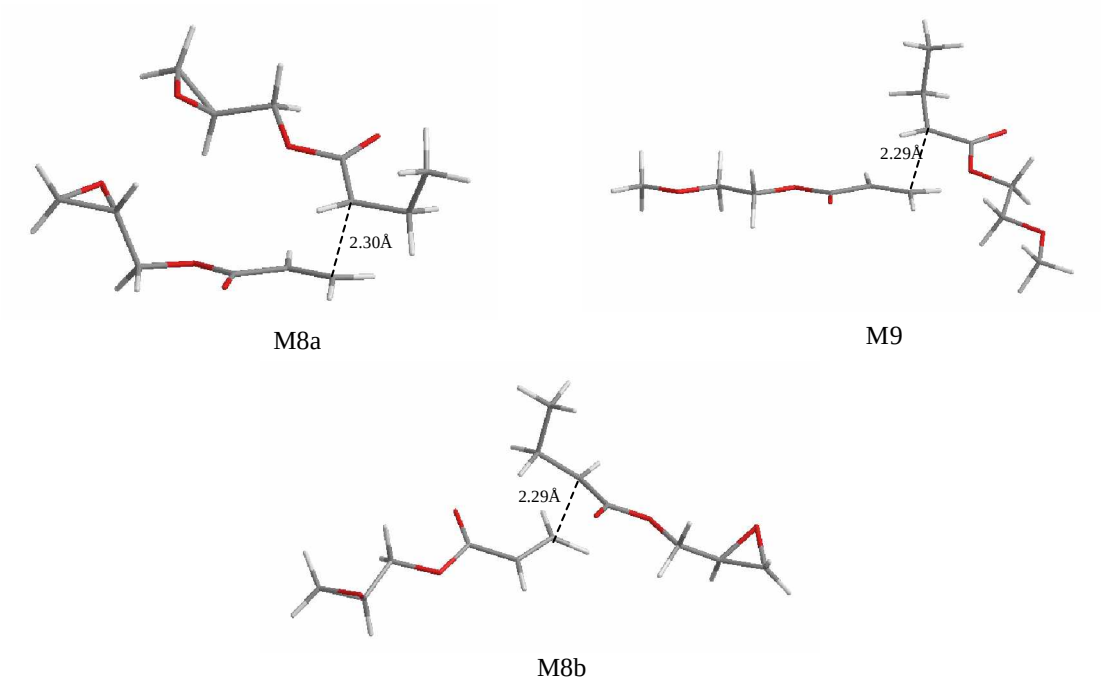

Figure 4.109. Transition state structures of propagation reaction of **M8** and **M9** with a different transition state structure of **M8**.

Table 4.49. Rate constants for **M8** and **M9**

Monomer	k_p ($M^{-1} s^{-1}$)	k_{ct} ($M^{-1} s^{-1}$)	k_d ($M^{-1} s^{-1}$)	$k_p/k_d^{1/2}$
M8	1.72E+00	1.68E-06	1.79E-09	4.07E+04
M9	3.39E+00	3.84E-05	3.07E-09	6.11E+04

We choose another transition state structure which has a higher entropy of the transition state for the propagation reaction of the monomer **M8** (**M8b** in Figure 4.109). This new transition state geometry causes an increase in the propagation rate of the monomer **M8**. On the other hand, it increases the rate of propagation just 1.2 times than the previous case. The trend in the propagation rate constants does not mimic the experimental rate quantitatively although the entropic effect is taken into account (Table 4.49). Calculated chain transfer rate constant of monomer **M8** is smaller than monomer **M9**. We may say that the cyclic group on the monomer **M8** has a negative effect on the chain transfer reaction. Also the disproportionation rate constants show the same trend with the chain transfer rate constants. The ratio $k_p/k_d^{1/2}$ does not mimic the experimental results for the monomers **M8** and **M9**.

4.5 Relationship between experimental rates and calculated parameters

In this study, the Boltzmann-averaged dipole moment of various conformers of the monomers is calculated according to the formula

$$\mu_{calc} = \sum_j D_j \frac{e^{-\Delta Ej / RT}}{\sum_i e^{-\Delta Ei / RT}} = \sum_j D_j p_j \qquad (4.1)$$

where with D_j is the dipole moment of conformation j, ΔEj is the difference between the energy of conformation j and the energy of the global minimum conformation, T is the absolute temperature, and R is the gas constant; p_j is the probability of finding the molecule in conformation j at the temperature T. T is set to 298.15 K. The summation over j runs over all unique structures. μ_{calc} is the calculated Boltzmann-averaged dipole moment.

The aim of this study is to understand whether the quantum mechanical calculations mimic the experimentally observed polymerization behavior of acrylates in Figures 4.110-4.116. The relationship between the calculated Boltzmann averaged dipoles and the calculated rate of polymerization of monomers are also given in Figures 4.113-4.116.

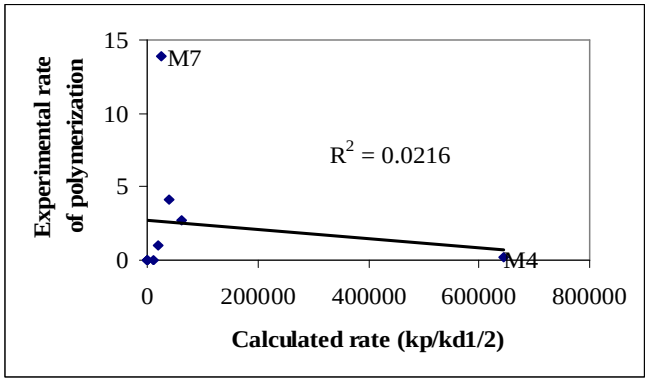

Figure 4.110. The correlation between the calculated rate of polymerization and the maximum rate of photoinitiated polymerization for acrylates.

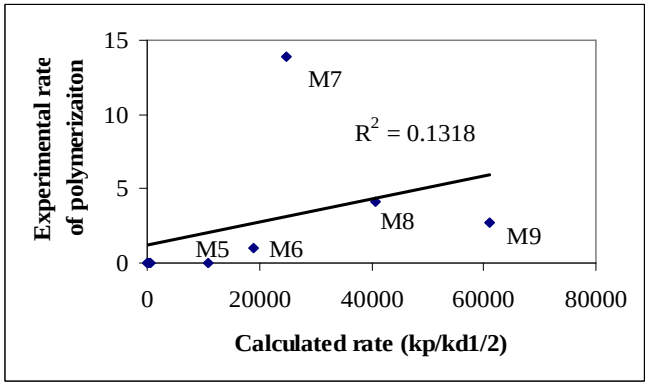

Figure 4.111. The value of **M4** is removed from Figure 4.110

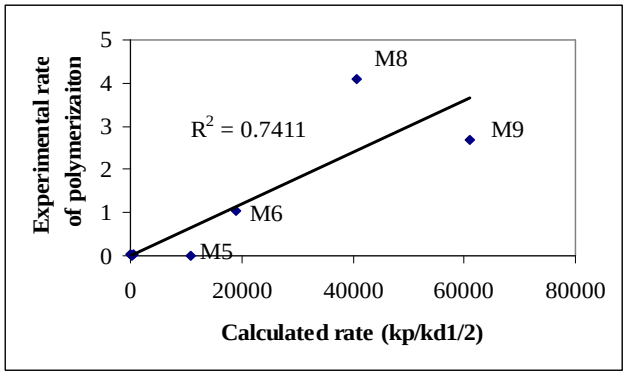

Figure 4.112. The values of **M4** and **M7** are removed from Figure 4.111

Based on Figures 4.110 – 4.112 eventhough there is not a direct relationship between the experimental and calculated rate of polymerization the calculated results show the same qualitative trend with the experimental findings (Figure 4.112).

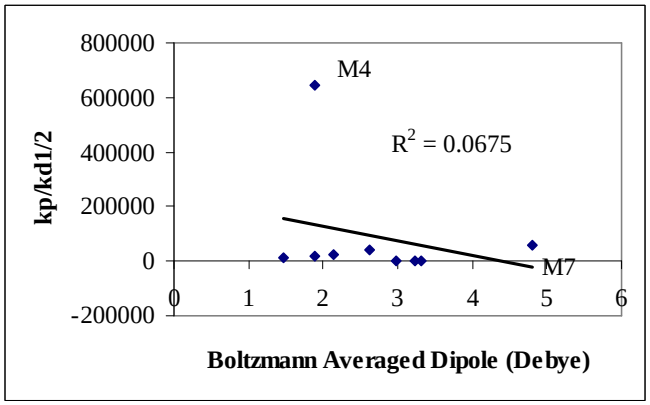

Figure 4.113. The relationship between calculated rate of polymerization and Boltzmann averaged dipole moment of acrylates.

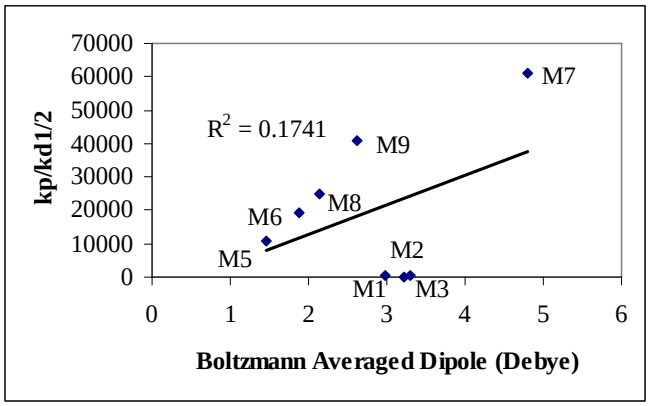

Figure 4.114. The value of **M4** is removed from Figure 4.113

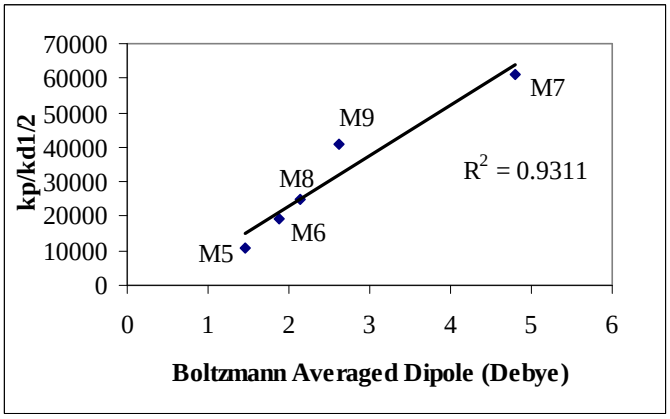

Figure 4.115. The values of **M1**, **M2**, **M3**, and **M4** are removed from Figure 4.114

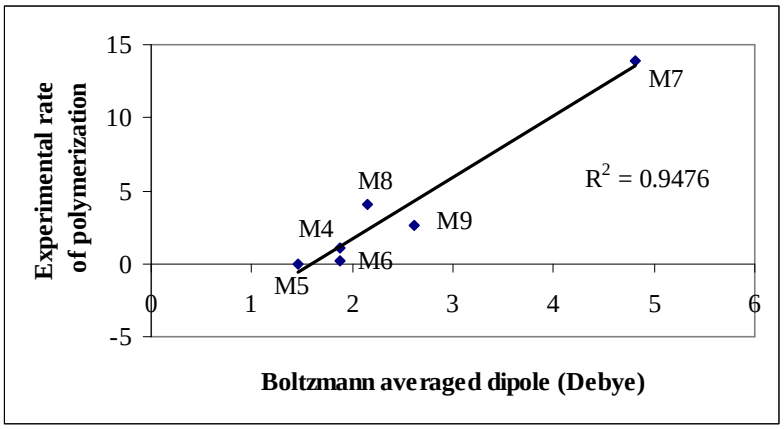

Figure 4.116. The relationship between the experimental rate of polymerization and Boltzmann averaged dipole moment of acrylates

Figure 4.115 illustrates the fact that there is a direct relationship between the Boltzmann averaged dipole moment and the calculated rate of polymerization (kp/kd½) without the monomers **M1**, **M2**, **M3**, and **M4**. Monomers **M1**, **M2**, and **M3** possess hydrogen bonds and do not obey this trend. Those monomers can be considered separately because they are alky α-hydroxymethyl acrylates except for monomer **M4**.

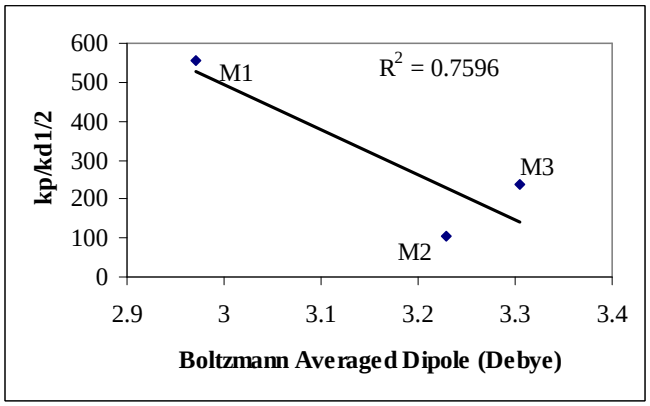

Figure 4.117. The relationship betwen calculated rate of polymerization and Boltzmann averaged dipole of alkyl α-hydroxymethyl acrylates

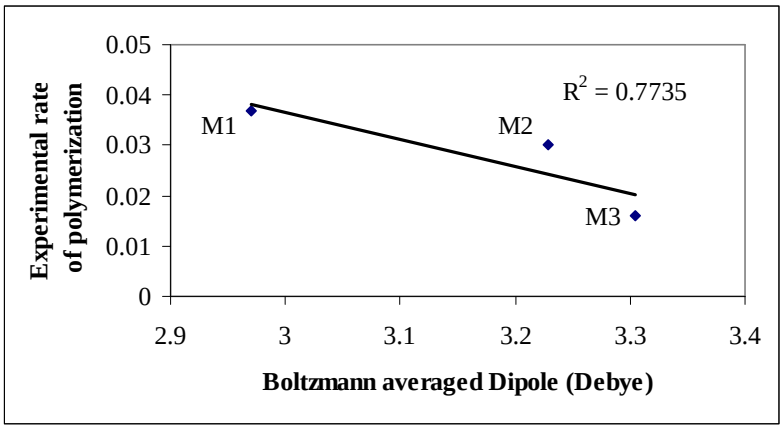

Figure 4.118. The relationship between the experimental rate of polymerization and Boltzmann averaged dipole of alkyl α-hydroxymethyl acrylates

The results for **M1**-**M2** show that there is an inverse relationship between the rate of polymerization and the dipole moment (Figure 4.117).

There is a very remarkable direct relationship between the experimental rate of polymerization and the Boltzmann averaged dipole moment for monomers **M4**-**M9** (Figure 4.116). However the relationship between the experimental rate of polymerization and the Boltzmann averaged dipole moment for **M1**-**M3** is poor due to the presence of H-bonding in the three monomers (Figure 4.118).

5. CONCLUSIONS

In this study, several acrylic monomers are modeled by using the quantum mechanical methods in order to understand the structure reactivity relationship. The polymerization kinetics, Boltzmann averaged dipole moments and local molecular descriptors for the preferential side of attack have been considered.

The propagation reaction is modeled by radical attacking to the least substituted the C-C doule bond of the monomer. The chain transfer reaction is modeled by the α-methylene hydrogen abstraction and the disproportionation reaction is modeled by the α-methylene hydrogen abstraction of the radical. The rate constants k_p, k_{ct}, k_d and $k_p/k_d^{1/2}$ ratio are evaluated in order to obtain quantitative understanding of the reactivity structure relationship. The results show that the rate constant k_p does not mimics alone the experimental rates. The ratio $k_p/k_d^{1/2}$ is used to generate a quantitative picture. In general, this ratio mimics qualitatively the experimentally observed trends. On the other hand, the $k_p/k_d^{1/2}$ ratio of the two monomers **M4** and **M7** does not mimic the experimental results. In this study, the reinitiation reaction is not modeled. After generation of a new radical by the chain transfer reaction, it can be used to model another propagation reaction then, the new rate constant k_p can be evaluated in order to understand the experimentally observed trends.

The dipole moment of acrylate monomers has positive effects on the polymerization rate. An increase in the dipole moment leads to an increase in the rate of polymerization. However, alkyl α-hydroxylmethyl acrylates have the inverse relationship with the dipole moment. An increase in the dipole moment causes a decrease in the rate of polymerization for those monomers.

6. SUGGESTIONS FOR FUTURE WORK

The following suggestions can be made for future work.

- Modeling the reinitiation reaction
- Carrying out the kinetics with a higher basis set (B3LYP/6-311G**) for one set of compounds.
- Assessing the effect of basis set on the kinetics of each step.

REFERENCES

1. Robello, D. R., *Introduction to Polymer Chemistry*, http://www.chem.rochester.edu/~chem421/frpolym.htm, 2002.

2. Beuermann, S. and M. Buback, "Rate Coefficients of Free Radical Polymerization Deduced from Pulsed Laser Experiments", *Prog. Polym. Sci.,* 27, 191-254, 2002.

3. Fernández-Garcia, M., M. Fernández-Sanz and E. L. Madruga, "A Kinetic Study of Butyl Acrylate Free Radical Polymerization in Benzene Solution", *Macromol. Chem. Phys.*, 201, 1840-1845, 2000.

4. Decker, C.; Moussa, K. "Real-time Kinetic Study of Laser-induced Polymerization" *Macromolecules,* 22, 4455-4462, 1989.

5. Decker, C.; Moussa, K. "A New Class of Highly Reactive Acrylic Monomers, 2. Light-induced Copolymerization with Difunctional Oligomers", *Makromol. Chem.*, 192, 507-522, 1991.

6. Moussa, K.; Decker, C. "Light-induced Polymerization of New Highly Reactive Acrylic Monomers", *J. Polym. Sci., Polym. Chem.*, 31, 2197-2203, 1993.

7. Decker, C.; Moussa, K., "A New Class of Highly Reactive Acrylic Monomers, 1. Light-induced Polymerization", *Makromol. Chem. Rapid Commun*., 11, 159-167, 1990.

8. Decker, C.; Moussa, K. Photopolymerisation de Monomeres Multifonctionnels—V. Resines Polyurethannes-acrylates, *Eur. Polym. J.*, 27, 881-889, 1991.

9. Decker, C. "High-speed Curing by Laser Irradiation", Nucl. Instrum. Methods Phys. Ress. B, 151, 22-28, 1999.

10. T. J. Smith et al., “Crosslinking Kinetics of Methyl and Ethyl (α-hydroxymethyl)acrylates: Effect of Crosslinker Type and Functionality”, *Polyme*r, 44, 6211-6216, 2000.

11. Avci, D. / Communication.

12. B. Yamada, B. and S. Kobatake, “Radical Polymerization, Co-Polymerization, and Chain Transfer of α-Substituted Acrylic Esters”, *Prog. Polym. Sci*., 19, 1089-1131, 1994.

13. Jansen, J. F. G. A., A. A. Dias, M. Dorschu and B. Coussens, “Fast Monomers: Factors Affecting the Inherent Reactivity of Acrylate Monomers in Photoinitiated Acrylate Polymerization”, *Macromolecules*, 36, 3861-3873, 2003.

14. Fernandez-Monreal, M. C., R. Cervo and E. L. Madruga, “Free-Radical Homopolymerization and Copolymerization of Ethyl α-hydroxymethylmethacrylate in Tetrahydrofuran”, *J. Polym. Sci., Part A: Polym. Chem*., 30, 2313-2319, 1992.

15. Avci, D., S. H. Kusefoglu, R. D. Thompson and L. J. Mathias, “Ester Derivatives of α-hydroxymethylacrylates: Itaconate Isomers Giving High Molecular Weight Polymers”, *J. Polym. Sci., Part A: Polym. Chem.*, 32, 2937-2945, 1994.

16. B. Yamada, S. Kobatake, “Radical Polymerization, co-Polymerization, and Chain Transfer of α-Substituted Acrylic Esters”, *Prog Polym. Sci*., 19, 1089-1131, 1994.

17. Smith, T. J., B. S. Shemper, J. S. Nobles, A. M. Casanova, C. Ott, L. J. Mathias, “Crosslinking Kinetics of Methyl and Ethyl (α-hydroxymethyl)acrylates: Effect of Crosslinker Type and Functionality”, 44, 6211-6216, 2003.

18. D. Thompson, T. H. Barclay, and L. J. Mathias, “Syntheses, Polymerization, and Characterization of Novel Semifluorinated Methacrylates, Including Novel Liquid-crystalline Materials”, *Polym. Preper. Am. Chem. Soc. Div. Polym. Chem*., 34 (1), 509-520, 1993.

19. B. Yamada, M. Satake, and T. Otsu, “Role of Bulky α-substituent in Free-radical Polymerization and Copolymerization of methyl α-(alkoxymethyl)acrylates”, *Makromol. Chem*., 192, 2713-2722, 1991.

20. B. Yamada, S. Kobatake, and S. Aoki, “Polymerization of 2-(substituted methyl)acrylate Bearing ω-methoxyoligoethyleneoxy Groups as Side Chains to New Low T_g polymer”, *J. Polym. Sci., Part A: Polym. Chem*., 31, 3433-3438, 1993.

21. L. T. Simonida, J. M. Filipović, J. S. Velićković, L. Katsikas, I. G. Popović, “The Polymerization Kinetics of Lower Dialkyl Itaconates”, *Macromol. Chem. Phys*. 200, 2421-2427, 1999.

22. Avcı, D., L. J. Mathias, “Synthesis and Photopolymerizations of new Hydroxyl-containing dimethacrylate crosslinkers”, *Polymer*, 45, 1763-1769, 2004.

23. Jansen, J. F. G. A., Dias, A. A., Dorschu, M., Coussens, B., “Effect of Dipole Moment on the Maximum Rate of Photoinitiated Acrylate Polymerizations”, *Macromolecules*, 35, 7529-7531, 2002.

24. Parr, R. G. and W. Yang, *Density Functional Theory of Atoms and Molecules*, Oxford University Press, New York, 1989.

25. Handy, N. C., “Density Functional Theory”, in: B. O. Roos (ed.), *Lecture Notes in Quantum Chemistry*, Vol. 2, pp. 91-123, Springer-Verlag, Berlin, 1994.

26. Frisch, *et al.*, *Gaussian 98 Revision A.7*, Gaussian, Inc., Pittsburgh PA, 1998.

27. Laidler, K. J., W. L. Hase and J. T. Hynes, “Current Status of Transition-State Theory”, *J. Phys. Chem*., 87, 2664-2682, 1983.

28. Laidler, K. J. and M. C. King, “The Development of Transition State Theory”, *J. Phys. Chem*., 87, 2657-2664, 1983.

29. Pechukas, P., “Transition State Theory”, *Ann. Rev. Phys. Chem*., 32, 159-177, 1981.

30. Pechukas, P., “Recent Developments in Transition State Theory”, *Ber. Bunsen-Ges. Phys. Chem.*, 86, 372-378, 1982.

31. Truhlar, D., B. C. Garrett and S. J. Klippenstein, “Current Status of Transition State Theory”, *J. Phys. Chem*., 100, 12771-12800, 1996.

32. Becke, A. D., “Density Functional Thermochemistry. III. The Role of Exact Exchange”, *J. Chem. Phys.*, Vol. 98, pp. 5648-5652, 1993.

33. Lee, C., W. Yang and R. G. Parr, “Development of Colle-Salvetti Correlation Energy Formula into a Functional of the Electron Density”, *Phys. Rev. B*, Vol. 37, pp. 785-789, 1988.

34. Gonzalez, C., C. Sosa and H. B. Schlegel, “Ab Initio Study of the Addition Reaction of the Methyl Radical to Ethylene and Formaldehyde”, *J. Phys. Chem*., 93, 2435-2440, 1989.

35. Arnaud, R., N. Bugaud, V. Vetere and V. Barone, “Role of Polar and Enthalpic Effects in the Addition of Methyl Radical to Substituted Alkenes: A Density Functional Study Including Solvent Effects”, *J. Am. Chem. Soc*., 120, 5733-5740, 1998.

36. Wong, M. W. and L. Radom, “Radical Addition to Alkenes: Further Assessment of Theoretical Procedures”, *J. Phys. Chem. A*, 102, 2237-2245, 1998.

37. Heuts, J. P. A., R. G. Gilbert and L. Radom, “Determination of Arrhenius Parameters for Propagation in Free-Radical Polymerizations: An Assessment of Ab Initio Procedures”, *J. Phys. Chem*., 100, 18997-19006, 1996.

38. Wong, M. W., A. Pross and L. Radom, “Addition of tert-Butyl Radical to Substituted Alkenes: A Theoretical Study of the Reaction Mechanism”, *J. Am. Chem. Soc*., 116, 11938-11943, 1994.

39. Susnow, R. G., A. M. Dean and W. H. Green Jr, “Hydrogen Abstraction Rates via Density Functional Theory”, *Chem. Phys. Lett*., 312, 262-268, 1999.

40. Parr, R. G. and W. Yang, *Density Functional Theory of Atoms and Molecules*, Oxford University Press, New York, 1989.

41. Handy, N. C., “Density Functional Theory”, in: B. O. Roos (ed.), Lecture Notes in Quantum Chemistry, Vol. 2, pp. 91-123, Springer-Verlag, Berlin, 1994.

42. Leach, A. R., Molecular Modelling Principles and Applications, Prentice Hall, England, 2001.

43. Becke, A. D., “Density-Functional Exchange Energy Approximation with Correct Asymptotic Behavior”, *Phys. Rev. A*., 38, 3098-3103, 1988.

44. Becke, A. D., “A New Mixing of Hartree-Fock and Local Density Functional Theories”, *J. Chem. Phys*., 38, 1372-1377, 1993.

45. Lee, C., W. Yang and R. G. Parr, “Development of Colle-Salvatti Correlation Energy Formula into a Functional of the Electron Density”, *Phys. Rev. B*, 37, 785-789, 1988.

46. Becke, A. D., “Density Functional Thermochemistry. III. The Role of Exact Exchange”, *J. Chem. Phys*., 98, 5648-5652, 1993.

47. Pauling, L. J., “The Nature of the Chemical Bond. IV. The Energy of Single Bonds and the Relative Electronegativity of Atoms”, *J. Am. Chem. Soc*., 54, 3570-3582, 1932.

48. Ficher, H. and L. Radom, “Factors Controlling the Addition of Carbon-Centered Radicals to Alkenes”, *Macromol. Symp*., 182, 1-14, 2002.

49. Pearson, R. G., “Maximum Chemical and Physical Hardness”, *J. Chem. Ed*., 76, 267-275, 1999.

50. Roy, R. K., S. Krishnamurti, P. Geerlings and S. Pal, "Local Softness and Hardness Based Reactivity Descriptors for Predicting Intra- and Intermolecular Reactivity Sequences: Carbonyl Compounds", *J. Phys. Chem. A*, 102, 3740-3755, 1998.

51. Geerlings, P. and F. D. Proft, "HSAB Principle: Applications of Its Global and Local Forms in Organic Chemistry", *Int. J. Quantum Chem*., 80, 227-235, 2000.

52. Avci, D., Mathias LJ, Thigpen K., "Photopolymerization Studies of Alkyl and Aryl Ester Derivatives of Ethyl α-hydroxymethylacrylate", *J Polym Sci, Part A: Polym Chem*, 34(15), 3191-3201, 1996.